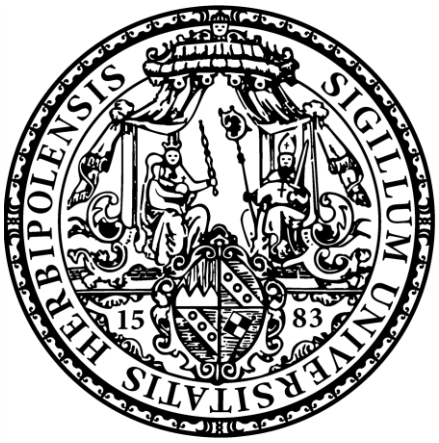

The regulation of T cell metabolism by neutral sphingomyelinase 2

Die Regulation des T-Zell-Metabolismus durch Neutrale Sphingomyelinase 2

Doctoral thesis for a doctoral degree
at the Graduate School of Life Sciences
Julius-Maximilians-Universität Würzburg

Section: Infection and Immunity

submitted by

Maria Nathalia de Lira

From São João de Meriti, Brazil

Würzburg 2020

Submitted on:

……..……..

Office stamp

Members of the Thesis Committee

Chairperson: Prof. Dr. Georg Gasteiger

Primary Supervisor: Dr. Elita Avota

Supervisor (Second): PD Dr. Niklas Beyersdorf

Supervisor (Third): Prof. Dr. Almut Schulze

Date of Public Defence: ……..……

Date of Receipt of Certificates: ……

I dedicate this dissertation to the memory of my loving father Nelson Luis de Lira.
(1959-2015)

“When life gives you lemons, don't make lemonade!

Make life take the lemons back! Get mad!”

Cave Johnson – Portal

Acknowledgments

I would like to express my sincere gratitude to my supervisor Dr. Elita Avota whose advices was outstanding in every step of my time in the lab and outside the lab. I thank you for all the energy you invest in me and the project so we all could succeed together.

I would like to thank Prof. Dr. Sibylle Schneider-Schaulies for opening the door of her lab and welcome me. Thank you for all the advice and critiques that helped me grow as a scientist and human.

I would like to thank my thesis committee members Prof. Dr. Almut Schulze and PD Dr. Niklas Beyersdorf, for all fruitful discussions, all support, motivation, and positive energy.

I also would like to thank Prof. Dr. Jürgen Schneider-Schaulies and Prof. Dr. med. Lars Dölken for being always present and challenge me every day with the burning questions.

My special thanks go to all members of the DFG-Forschergruppe SphingoFOR 2123 for excellent collaboration, discussions, and advice.

I would like to thank Dr. Sudha Janaki Raman for all the help with the seahorse experiments.

I also would like to express my gratitude to all the formers and actual lab members that somehow made my life way funnier and helped in the lab. Anna, Charlene, Claudia, Franziska, Hannah, Marie, Nora, Phillip, Sara, Rebekka, and Yann. Especially, I would like to thank with all my heart to Dr. Shaghayegh Derakhshani for being one of the most amazing people that I met during my Ph.D. journey, transcending from being a lab member and becoming a true friend. Thank you for all the moments, coffees, cakes, and utterly understand me.

I thank all my other Ph.D. students friends, Janice, Lara, Manivel, Sabrina, and Teresa, that shared with me the same anxiety, happiness, and love for science. Also, to all my friends from the immunomodulation course.

I am very thankful for all the friends I made during this time in Germany. I am very much grateful to all my friends from Taekwondo.

I indebted thanks to my lovely Brazilian friends for all support, love, and always remind me that I was never alone, and I will never be. Thank you, Aline, Alyssa, Amauri, Bruno, Daniel, Juliana, and Raphael.

I also thank all support from my family and friends in Brazil.

I thank all my best friends, now so distant but always there when I needed them with love, support, laughter, and memes. Thank you, Daniel, Diego, Fernanda, Gabriela, Giovanni, Guilherme, Leticia, Rebeca, Pedro, Peterson, Rai, and Victor.

I thank my analyst Natalia for helping me find the best version of myself. Mental health is absolutely important.

Last but not least, I thank my mother and my brother for being absolutely supportive, loving, caring, and always believe in me. I thank you for all the sacrifice and energy spent to help me to be where I am right now. An ocean is nothing. There is no distance for love.

Table of Contents

Summary

T cells play an essential role in the immune system. Engaging the T cell receptor (TCR) initiates a cascade of signaling events that activates the T cells. Neutral sphingomyelinase (NSM) is a member of a superfamily of enzymes responsible for the hydrolysis of sphingomyelin into phosphocholine and ceramide. Sphingolipids are essential mediators in signaling cascades involved in apoptosis, proliferation, stress responses, necrosis, inflammation, autophagy, senescence, and differentiation.

Upon specific ablation of NSM2, T cells proved to be hyper-responsive to CD3/CD28 co-stimulation, indicating that the enzyme acts to dampen early overshooting activation of these cells. It remained unclear whether a deregulated metabolic activity supports the hyper-reactivity of NSM2 deficient T cells. This work demonstrates that the ablation of NSM2 activity affects the metabolism of the quiescent $CD4^+$ T cells. These accumulate ATP in mitochondria and increase basal glycolytic activity by increasing the basal glucose uptake and GLUT1 receptor expression, which, altogether, raises intracellular ATP levels and boosts cellular respiration. The increased basal metabolic activity is associated with rapid phosphorylation of S6, a mTORC1 target, as well as enhanced elevation total ATP levels within the first hour after CD3/CD28 costimulation. Increased metabolic activity in resting NSM2 deficient T cells does, however, not support sustained stimulated responses. While elevated under steady-state conditions and elevated early after co-stimulation in NSM2 deficient CD4+ T cells, the mTORC1 pathway regulating mitochondria size, oxidative phosphorylation, and ATP production is impaired after 24 hours of stimulation. Taken together, the absence of NSM2 promotes a hyperactive metabolic state in unstimulated CD4+ T cells yet fails to support sustained T cell responses upon antigenic stimulation without affecting T cell survival.

Zusammenfassung

T-Zellen spielen eine wesentliche Rolle im Immunsystem. Die Aktivierung des T-Zell-Rezeptors (TCR) löst eine Kaskade von Signalereignissen aus, die die T-Zellen aktivieren. Neutrale Sphingomyelinase (NSM) gehört zu einer Superfamilie von Enzymen, die für die Aufspaltung von Sphingomyelin in Phosphocholin und Ceramid verantwortlich sind. Sphingolipide sind wesentliche Mediatoren in Signalkaskaden, die an Apoptose, Proliferation, Stressreaktionen, Nekrose, Entzündung, Autophagie, Seneszenz und Differenzierung beteiligt sind. NSM2-depletierte T-Zellen erwiesen sich als hyper-reaktiv gegenüber CD3/CD28-Kostimulation, was darauf hinweist, dass das Enzym eine überschießende Aktivierung dieser Zellen dämpft. Es blieb unklar, ob die Hyperreaktivität NSM2-defizienter T-Zellen durch eine deregulierte Stoffwechselaktivität unterstützt wird. Diese Arbeit zeigt, dass NSM2-Insuffizienz den Metabolismus ruhender CD4+-T-Zellen beeinflusst: Diese akkumulieren ATP in Mitochondrien und zeigen eine erhöhte basale glykolytische Aktivität, die auf einer erhöhten Glukoseaufnahme und Expression des GLUT1-Rezeptors beruht und mit einer Erhöhung intrazellulärer ATP-Werte und gesteigerten Zellrespiration einhergeht. Aufgrund ihrer bereits erhöhten basalen metabolische Aktivität zeigen NSM2 defiziente T Zellen eine im Vergleich zu Kontrollzellen schnellere, effizientere Aktivierung nach Kostimulation, die sich in Phosphorylierung von S6, eines mTORC1 Targets, sowie erhöhtem ATP Spiegel manifestiert. Dies kann jedoch nicht aufrechterhalten werden: Die mTORC1-Aktivierung, die die Größe der Mitochondrien, die oxidative Phosphorylierung und die ATP-Produktion reguliert, unter stationären Bedingungen in NSM2-defizienten CD4+-T-Zellen erhöht ist, ist nach 24-stündiger Kostimulation beeinträchtigt. Insgesamt scheint die NSM2-Aktivität wesentlich für die Regulation der basalen metabolischen Aktivität ruhender T-Zellen und der Vermeidung

überschiessender Antworten nach Kostimulation zu sein, jedoch ebenso wichtig für die dauerhafte Aufrechterhaltung des Aktivierungssignals zu sein.

.

1. Introduction

1.1. Sphingolipid metabolism

Sphingolipids (SLs) include a class of bioactive lipids found in the cellular membranes and modulate the biophysical properties of membranes [1]. SLs control a broad range of cellular functions: cell cycle, apoptosis, cell migration, and inflammation [2]. SL metabolism is highly compartmentalized within the cell (Fig.1), and different enzymes are involved in the synthesis of various sphingolipids. Concerning the structure, the sphingolipids have a standard 18 carbon amino-alcohol sphingosine (Sph) backbone [3]. The combination of fatty acid with sphingosine gives the necessary building element of all SLs—ceramide (Cer), which is the central hub of SL metabolism.

Formation of Cer can occur via three different pathways within specific organelles [4]: (1) *de novo* synthesis pathway in the endoplasmic reticulum; (2) salvage pathways in lysosomes and (3) catabolic pathway on the cellular membranes.

(1) The synthesis of 3-ketosphinganine by the condensation of L-serine and palmityl-CoA catalyzed by the enzyme serine palmitoyltransferase is the first step of the *de novo* pathway. Next, 3-ketosphinganine is reduced to sphinganine, which is acylated to dihydroceramide. The last step is the oxidation of dihydroceramide to ceramide catalyzed by dihydroceramide desaturase.

(2) In the salvage pathway, acid ceramidase converts released ceramides into Sph.

(3) In the catabolic pathway, sphingomyelin (SM) is hydrolyzed by sphingomyelinases (SMases) resulting in Cer, and phosphocholine formation. Ceramide can also be synthesized in the mitochondria-associated membranes.

Newly synthesized Cer can be further converted into five different lipids: ceramide-1-phosphate (C1P), sphingomyelin (SM), ceramide phosphoethanolamine (CPE), galactosylceramide (Galβ1–10Cer) and glucosylceramide (GlcCer) [5]

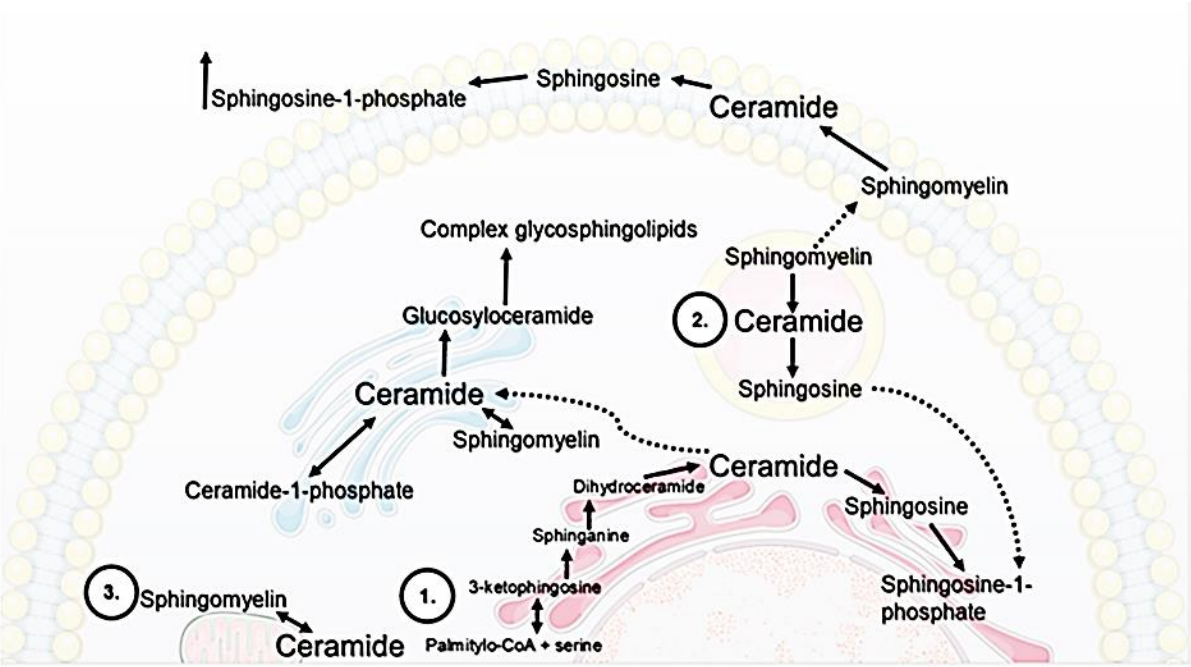

Figure 1. Key pathways of sphingolipid metabolism. (Adapted from Bochénska and Gabig-Cimínska, 2020 [6])

1.2. Characterization of neutral sphingomyelinase 2

Neutral sphingomyelinase 2 (NSM2) is an enzyme that hydrolyzes SM and generates ceramide at neutral pH 7,0. Initially, NSM2 was discovered in the rat brain [7]. Four mammalian neutral sphingomyelinases have been identified [8], [9]. NSM2 is the most studied. It is 655 amino acid protein with a molecular mass of 71 kDa coded by the *SMPD3* gene. NSM2 protein contains two hydrophobic segments at the N-terminus and catalytic site at C-terminus [10] (Fig. 2).

Neutral pH, divalent cations (Mg^{2+} or Mn^{2+}), and interaction with anionic lipids within the plasma membrane are mandatory for NSM2 activity [11].

NSM2 localization to the Golgi organelles was demonstrated in several cell lines [10]. NSM2 was shown to localize to the cytosolic leaflet of the plasma membrane (PM), suggesting the presence of SM pool at the cytosolic leaflet of the PM [12]. In T cells, NSM2 is localized predominantly at the PM [13]. However, the mechanism underlying specific localization of NSM2 and its potential trafficking between multiple intracellular locations is unclear.

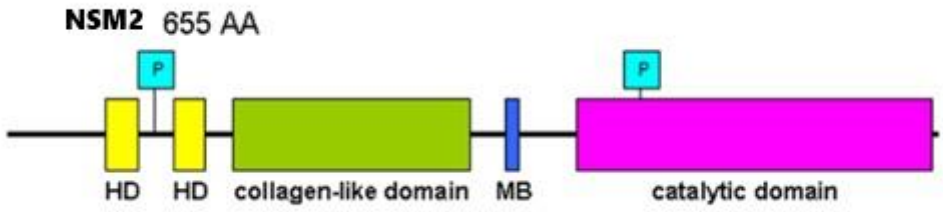

Figure 2. Schematic illustration of domains in human NSM2 (GenBank accession numbers Q9NY59). HD: hydrophobic domain, MB: Mg 2+ binding domains P: Palmitoylation site. (Adapted from Wu *et al*., 2010. [14])

1.2.1. NSM2 as a modulator of cellular growth and stress responses

NSM2 plays a vital role in regulating bone development and formation. In 2005, the NSM2 knock-out mouse was generated and showed characteristic embryonic and juvenile dwarfism phenotype [15]. The published data show that NSM2 knockout animals have impaired production of growth hormones and decreased concentrations of serum insulin-like growth factor leading to the prolonged cell cycle and hypoplasia observed in NSM2 deficient mice. The development of fragilitas ossium was attributed to the mutation of the SMPD3 gene in the *fro/fro* mouse [16]. The phenotype of the fro/fro mouse is characterized by smaller size at birth, multiple fractures in long bones and ribs, with severely impaired mineralization of the bones but healthy cartilage growth.

In addition to its regulatory role in acute stress responses, NSM2 is also implicated in cell growth inhibition and tumorigenesis. Upregulation of NSM2 mRNA and protein caused a cell cycle arrest in the G0/G1 phase with consequent increases in ceramide levels, especially in the very long chain C(24:1) and C(24:0) ceramides in MCF7 cells [17], [18]. A study of primary osteoblasts found that treatment with conditioned medium from a prostate cancer cell line (PC-3) significantly reduced NSM2 expression [19]. Mutations in the *SMPD3* gene were identified in cancer [20]. 5% of acute myeloid leukemias and 6% of acute lymphoid leukemias have mutations in the NSM2 coding gene. NSM2 modulates stress-induced bronchial and lung injury in pulmonary diseases. H_2O_2 induced activation of NSM2 ceramide generation and apoptosis, and Glutathione (GSH) inhibited this phenomenon. Oxidant exposure was also suggested to affect NSM2 localization with oxidant exposure causing trafficking to the PM, whereas in contrast, exposure to GSH resulted in NSM2 trafficking to the nucleus [21]. NSM2 inhibitor GW4869 was shown to inhibit hypoxia-induced pulmonary vasoconstriction *in vivo* [22]. NSM2 is implicated in diverse physiological processes and can be activated for different signals. Consistent with the stimulation of NSM2 activity by cytokines, studies have also shown that NSM2 plays a role in the inflammatory response [23]–[25]. Among the various inflammatory stimuli, tumor necrosis factor - α (TNF-α) is one of the broadest studied activators of NSM2.

Functionally, NSM2 was found to be upstream of the TNF-α-stimulated expression of vascular cell adhesion molecule-1 (VCAM) and intercellular adhesion molecule-1 (ICAM) in lung epithelial cells [26] (Fig. 3).

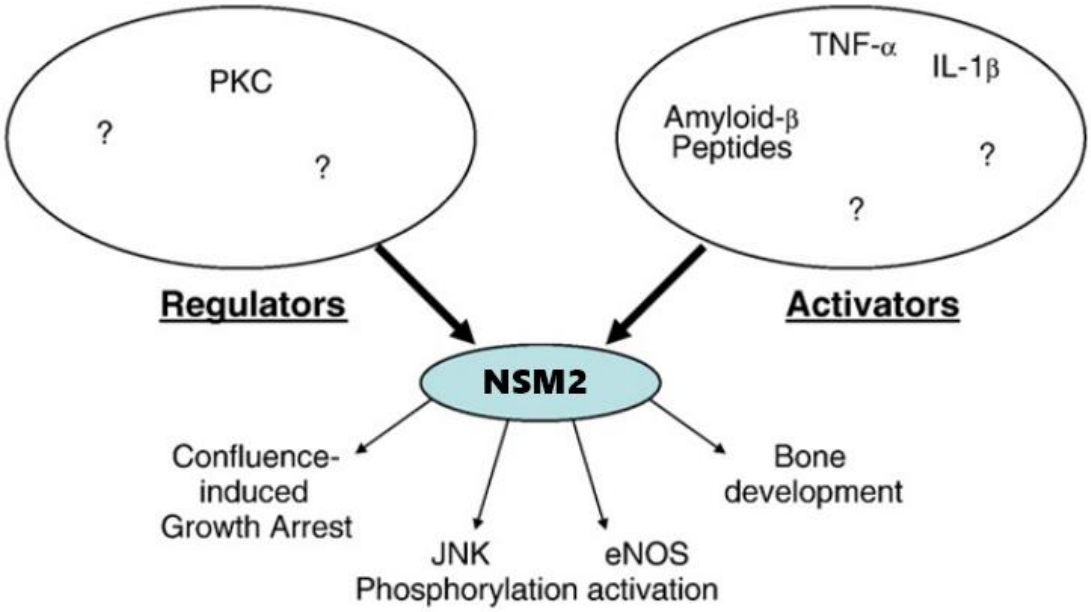

Figure 3. Mechanisms of NSM2 activation and regulation. (Adapted from Clarke and Hannun, 2006 [27])

1.2.2. NSM2 as a regulator of T cell function

NSM2 enzymatic activity is transiently induced by TCR ligation in the presence and absence of CD28 mediated co-stimulation [28]. NSM2 induces the formation of ceramide-rich platforms, which has the potential to modify plasma membrane microdomains and TCR receptor-proximal signaling clusters [29].

Ceramide-rich domains are hydrophobic, which leads to the exclusion of cholesterol from these areas [30], [31], thereby modifying downstream signaling and affecting the outcome of antigen-stimulation [13]. The accumulation of ceramide-rich domains at the plasma membrane leads to the reduction of actin cytoskeleton dynamics, which is important for the spreading and polarization of T cells [32]. NSM2-deficient T cells are strongly dependent on CD28 co-stimulation and are unable to mobilize $Ca2^{+}$ at low antigen doses indicating NSM2 role in TCR signal amplification [33]. NSM2 can be activated by the measles virus (MV) surface interaction with a not yet described

receptor on the cells of hematopoietic origin. Prolonged activation of NSM2 by MV leads to the paralyzed cytoskeleton and is partially responsible for the proliferative inhibition of T cells [34].

1.3. Immunometabolism

Immunometabolism is an emerging field that connects immunology and metabolism. In recent years, advanced technologies allow immunologists to observe the modifications in metabolites and uncover their role in immune response coordination [35]. Immune cells are responsible for controlling and protecting the organism against pathogens [36]. Cell type-specific metabolic profiles affect cell quiescence state, immune activation, and their proliferative capacity [37]. Metabolic pathways must be dynamic to adapt the cell demands for energy and biosynthesis. Metabolic flexibility is crucial to help cells to rapidly adjust to antigenic signals and nutrient availability [38]. The functional specificity of each immune cell subset determines its biochemical profile, which is associated with cell subset specific metabolic phenotypes. For example, T cells, naïve, effector, and memory cells have distinct metabolic profiles that are crucial for their maintenance and function [39].

1.4. Metabolic pathways

A metabolic pathway is, by definition, a step-by-step series of interconnected biochemical reactions that convert a substrate molecule through a series of metabolic intermediates, eventually yielding a final product [40]. Metabolic pathways are very diversified in terms of final products but have an interconnected nature (Fig. 4). That means the products from one pathway can is used as a precursor in a second pathway. T cells are very specialized cells and activate several pathways at the same time, depending on their activation state and subset [41]. T cells coordinate over six major metabolic pathways: glycolysis, oxidative phosphorylation, fatty acid oxidation, fatty acid synthesis, pentose phosphate pathway, and amino acid pathway.

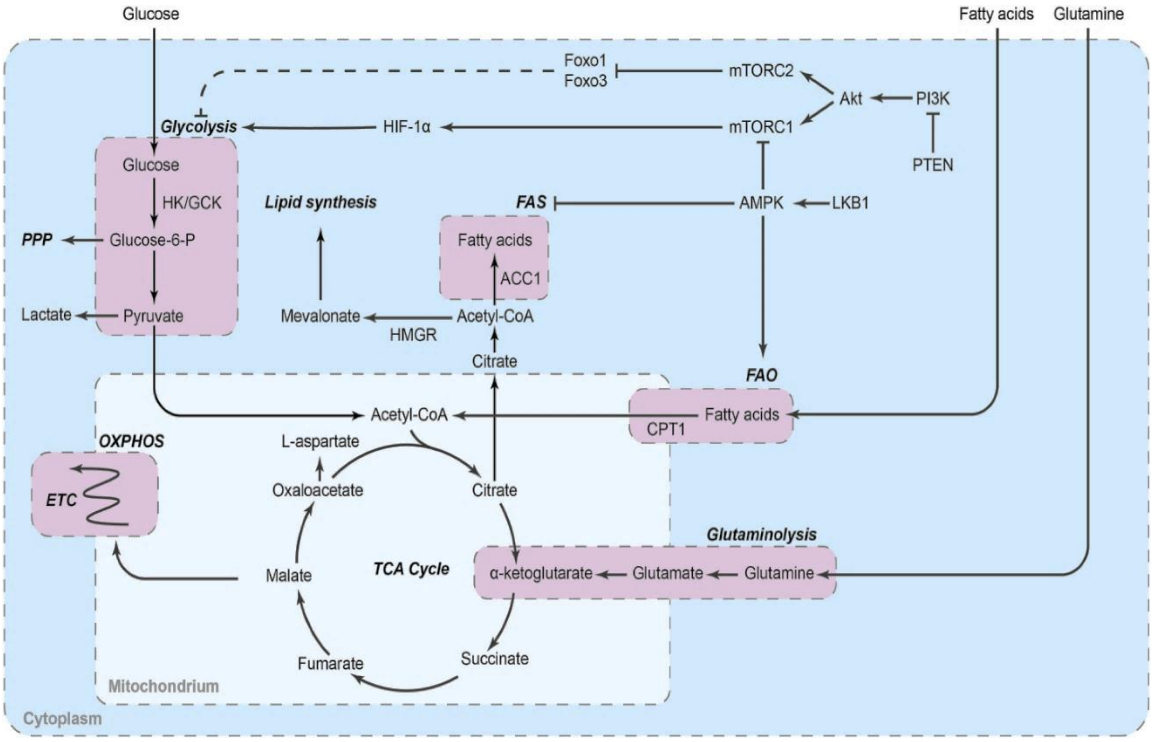

Figure 4. Simplified metabolic pathways in T cells. (Adapted from H. Hashimoto *et al.,* 2020 [42])

1.5. Metabolic profile of quiescent T cells

T cells are critical immune cells and vital to create a proper adaptive immune response. They are highly dynamic in metabolic response to the antigens. Quiescent T cells are mature naïve T cells that had recently emigrated from the thymus or memory T cells that circulate in the blood. They are small in size and are resting in the G_0 phase of the cell cycle. Quiescent T cells (also named resting T cells) have low basal metabolic activity, and little or no expression of activation markers [43], [44]. Up to 95% of the ATP production of quiescent T cells comes from the oxidative phosphorylation (OXPHOS) [45]. The OXPHOS is responsible for producing 30 to 36 ATP molecules from 10 NADH and 2 succinate molecules. OXPHOS is very advantageous in helping cells to build large stores of ATP with less energetic investment. During the quiescent state, T cells need ATP to maintain membrane integrity, protein turnover, and nutrient transport across the membrane [46]. Glucose and mitochondrial metabolism are critical regulators of quiescence. Quiescent T cells relay on mitochondria OXPHOS energy, whereas mitochondrial activity and glucose uptake sharply increase upon activation [47], [48].

Although the cells in the quiescent state are often characterized as “metabolic inactive,” this state needs to be actively maintained to prevent unspecific or autoimmune reactions. Intrinsic signals regulate the survival of quiescent T cells, such as tonic TCR signaling, IL-7, and lysosphingolipid sphingosine-1-phosphate (S1P), which control the quiescence state (Fig. 5) [49], [50].

Tonic TCR signaling in dense lymphoid tissues is responsible for activating transcription factors FOXO1 and FOXO3 and inducing IL-7 receptor-α (IL-7Rα) expression and signaling [51]. The IL-7-IL7R-AKT signaling is responsible for sustaining the basal glycolytic flux by inducing basal GLUT1 expression [52]. Kruppel-like factor 2 (KLF2) belongs to the group of transcription factors highly expressed in

peripheral naïve cells and can actively regulate the quiescence [53]. KLF2 can prevent Jurkat cells from entering the cell cycle; therefore, stopping the proliferation and inhibiting expression of c-myc, an important transcription factor involved in the activation [54], [55]. FOXO and KLF family members together can regulate the expression of molecules that are crucial to the homing of naïve T cells: CC-chemokine receptor 7 (CCR7), S1P, and CD62L [56]. S1P levels in the blood and lymph fluid regulates T cell egress from draining lymph nodes. S1P binding to the sphingosine-phosphate receptor 1 (S1PR1) on the T cell surface suppresses mitophagy to maintain their mitochondrial content and keep the optimal OXPHOS levels [50]. Metabolic quiescence state is also regulated by the tuberous sclerosis complex (TSC) [57]. TSC is responsible for suppressing the mTORC1 activation on naïve T cells and prevent aberrant activation [58]. TSC also inhibits glycolysis forcing the cells to sustain the metabolism through mitochondria/OXPHOS [59].

Summarizing, well-coordinated quiescence supports long-term survival of T cells in the periphery, shapes the activation of naïve, and reactivation of memory cells controlling the expansion and memory phases of the immune response.

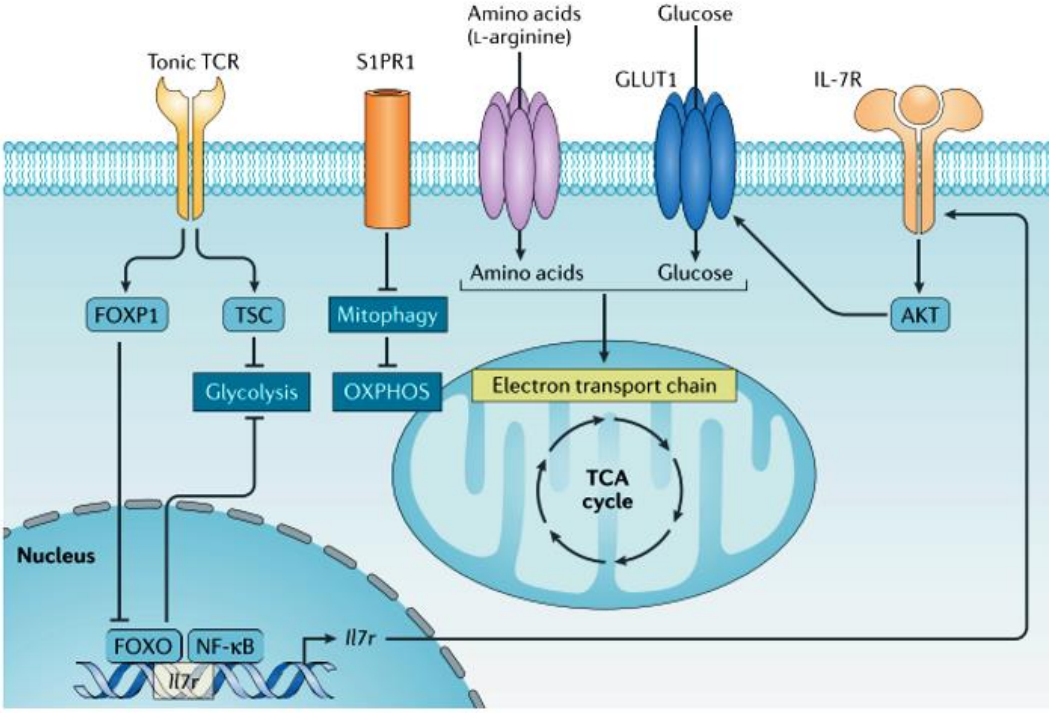

Figure 5. Cell intrinsic mechanism that regulates T cell quiescence (Adapted from Chapman *et al*., 2020 [60])

1.6. Metabolic characteristics of activated T cells

After antigen recognition, T cells undergo an activation process. Cells need to modify their metabolic activity to supply energy that is required for growth, proliferation, and differentiation into T effector (Teff). Teff cells include several T cell types responding to stimulation: regulatory (Treg), helper, and cytotoxic T cells. $CD4^+$ helper (Th) cells stimulate macrophages, B cells, and killer T cells to mount appropriate immune response [61], [62]. T cells endure a process called the metabolic switch or metabolic reprogramming to meet the new energetic requirements upon activation [63].

During the metabolic switch, the main source for ATP production is changed from OXPHOS to glycolysis, even in the presence of oxygen. The aerobic glycolysis, also known as the “Warburg effect” was first characterized by Otto Warburg in cancer cells.[64], [65]. Generally, glycolysis seems to be less beneficial in comparison to OXPHOS regarding the ATP yield: 4 ATP and 36 ATP molecules produced, respectively. Glucose metabolism is important to trigger proper proliferation [66].

In the absence of glucose, T cells do not proliferate, even if high levels of glutamine added to the cell culture. Several studies suggest that T cells increase the glycolytic metabolism to increase the availability of glycolytic precursors for biosynthetic reactions [37], [67], [68]. Some glycolytic intermediates are used to generate precursors for protein, nucleotide, and lipid synthesis [69].

Another reason to prefer glycolysis over OXPHOS is to avoid the increase in the intracellular ROS concentration that can lead to apoptosis [70]. During activation, T cells upregulate OXPHOS about 2-fold, while the glycolysis is up-regulated up to 5 times.[71], [72]. The differentiation and effector functions of inflammatory Th1, Th2, and Th17 cells relies on the engagement of aerobic glycolysis. Memory T cell and Treg functionality depend on fatty acid oxidation (FAO) pathways (Fig. 6).

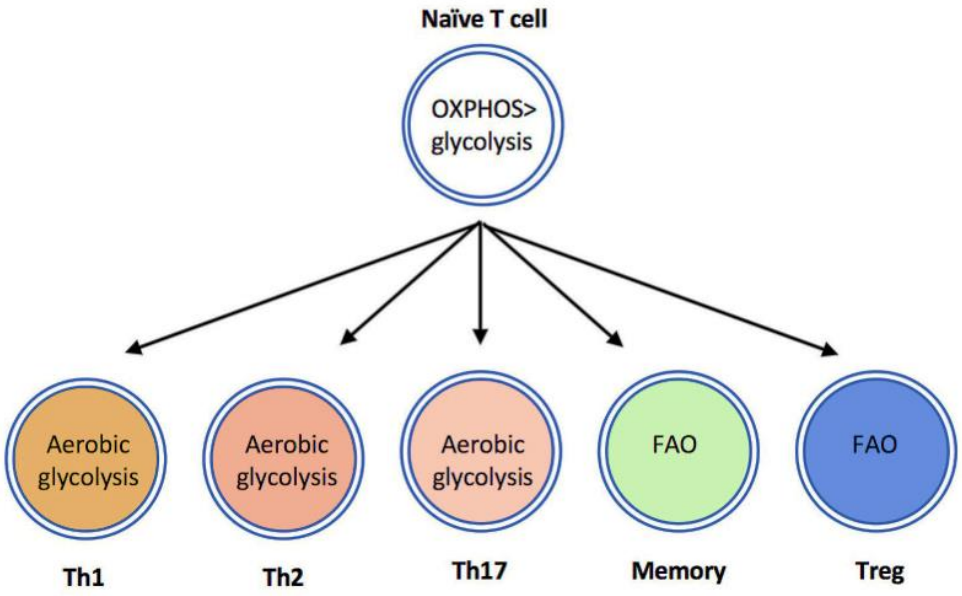

Figure 6. CD4+ T cell subsets use distinct metabolic programs. (Adapted from Salmond, 2018 [73])

1.7. Signaling pathways in metabolic reprogramming

Metabolic reprogramming is initiated by the early signaling events in T cell activation. T cell activation is dependent on two signals: (1) interaction of the antigenic peptide with the TCR and (2) interaction of co-stimulatory molecules and their ligands, i.e., CD28 and CD80/CD86 [74]. Both signals are cooperating in an increase in nutrient uptake, especially glucose. After TCR engaging and co-stimulation with CD28, T cells induce activation of phosphatidylinositol 3'-kinase (PI3K)-AKT signal pathway. This pathway is responsible for upregulating the expression and trafficking of GLUT1 to the cell surface [75], [76]. AKT signaling increases glycolysis by inducing hexokinase activity [77] and phosphorylating phosphofructokinase-2 (PFK-2) [78], two vital enzymes in the glycolytic pathway. Downstream of TCR/CD28, there are several canonical regulators of T cell metabolism upon T cell activation, among the most important ones are kinases: mechanistic target of rapamycin (mTOR) and AMP-activated kinase (AMPK).

mTOR is an evolutionarily conserved serine/threonine kinase that coordinates nutrient sensing and activation [79]. mTOR exists in two independent complexes (Fig. 7). Rapamycin and nutrient-sensitive mTORC1 complex are composed of mTOR, the regulatory-associated protein of mTOR (RAPTOR), mammalian lethal with SEC13 protein 8 (MLST8) and proline-rich Akt substrate (PRAS) 1 and endogenous regulator DEP domain-containing mTOR-interacting protein (DEPTOR). mTORC2 complex is insensitive to acute inhibition by rapamycin and contains mTOR, rapamycin-insensitive companion of mTOR (RICTOR), GβL, and mammalian stress-activated protein kinase interacting protein 1 (mSIN1) [58]. Key downstream targets of mTORC1 include the translational regulators 4E-binding proteins (4E-BPs) and ribosomal protein S6 kinases (S6Ks). The existence of two mTOR complexes allows the regulation of the same protein by different stimuli. While mTORC1 responds to nutrient availability, mTORC2 is stimulated by cytokines and growth factors [80]. In addition to the upregulation of glycolytic metabolism, T cell activation increase the uptake and hydrolysis of amino acids through the amino acid transporter SLC7A5 and glutamine transporter SLC1A5 that in turn, sustain mTORC1 activation [81]. Precisely regulated mTOR activation is mandatory for the cells to reach the maximum of its metabolic capacity and coordinate the cell fate. TCR stimulation can lead to asymmetric division of mTORC1 activity in mother and daughter cells. In such a way, daughter cells with high mTORC1 activation have elevated glycolytic flux and generate effector T cells, and T cells with lower mTORC1 activity differentiate in memory cells [82].

AMPK can affect mTORC1 activation by phosphorylation of TSC2 and RAPTOR to inhibit mTOR signaling [83]. AMPK itself is activated when the cellular AMP/ATP ratio increases in response to nutrient starvation [84]. In contrast to mTOR, studies demonstrated that AMPK is not important to control cell differentiation in normal nutrient conditions [85]. The lack of AMPK was not vital to interrupt the cells to acquire

an effector phenotype. Still, it is crucial to help the cells to adapt to a different environment; for example, in a highly hypoxic and glucose deprived tumor microenvironment, cells that lack AMPK have increased cell death rates [86], [87].

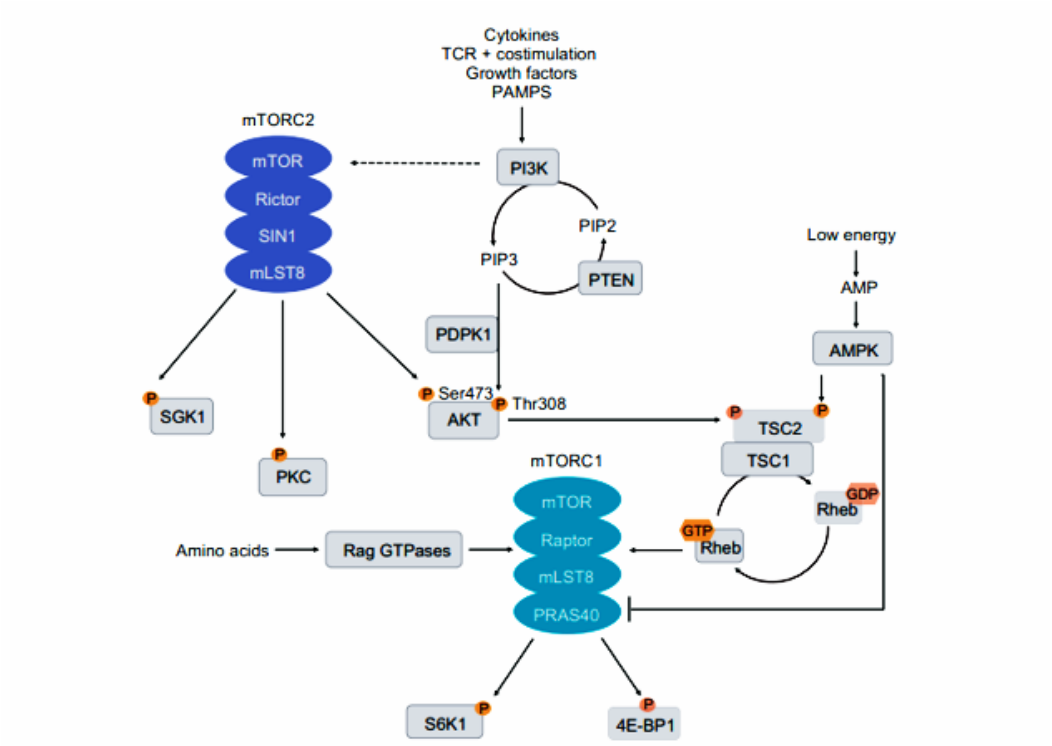

Figure 7. The mTOR pathway. (Adapted from Linke *et al.,* 2017 [88])

1.8. Mitochondria – the powerhouse of the (T) cell

Mitochondria are well known as the cellular “powerhouse” [89]. Mitochondria are the primary source for ATP biosynthesis; however, the role of mitochondria in the immune responses and coordination of T cell activation extends beyond the ATP production. For example, mitochondria are crucial to the generation of fatty acids, Ca^{2+} homeostasis, iron metabolism, regulating innate immunity, and apoptotic cell death [90]–[92]. They are the organelles with a double membrane. The outer mitochondrial membrane (OMM) contains proteins mitofusin1 and 2 (Mfn-1 and Mfn-2) regulating mitochondrial dynamics, [93], [94], the anti-apoptotic proteins, such as B-cell lymphoma 2 (BCL-2) [95], mitochondrial antiviral signaling protein (MAVS) [96] and mitochondrial voltage-dependent anion channel (VDAC) proteins [97], [98]. The inner mitochondrial membrane (IMM) contains a different pool of membrane transporters and is less permeable than the OMM. Electron Transport Chain (ETC) proteins sit in the IMM. They are responsible for transferring electrons provided by NADH and $FADH_2$ to oxygen, while generating differential membrane potential ($\Delta\Psi m$) across the mitochondrial inner membrane, leading to a gradient utilized to produce ATP.

The mitochondrial matrix is enclosed by the IMM and contains ribosomes, nucleotides, soluble enzymes, and the mitochondrial DNA (mtDNA) necessary for replication, DNA repair, recombination, and transcription [99].

The tricarboxylic acid (TCA), commonly known as the Krebs cycle or citric acid cycle, takes place in the mitochondria matrix and its metabolites can also be used for the production of cholesterol, nucleotides, and amino acids [100]. Taken together, mitochondria bridge nutrient metabolism to fulfill the bioenergetic demands of the cell through the coordination of the TCA cycle and ETC (Fig. 8).

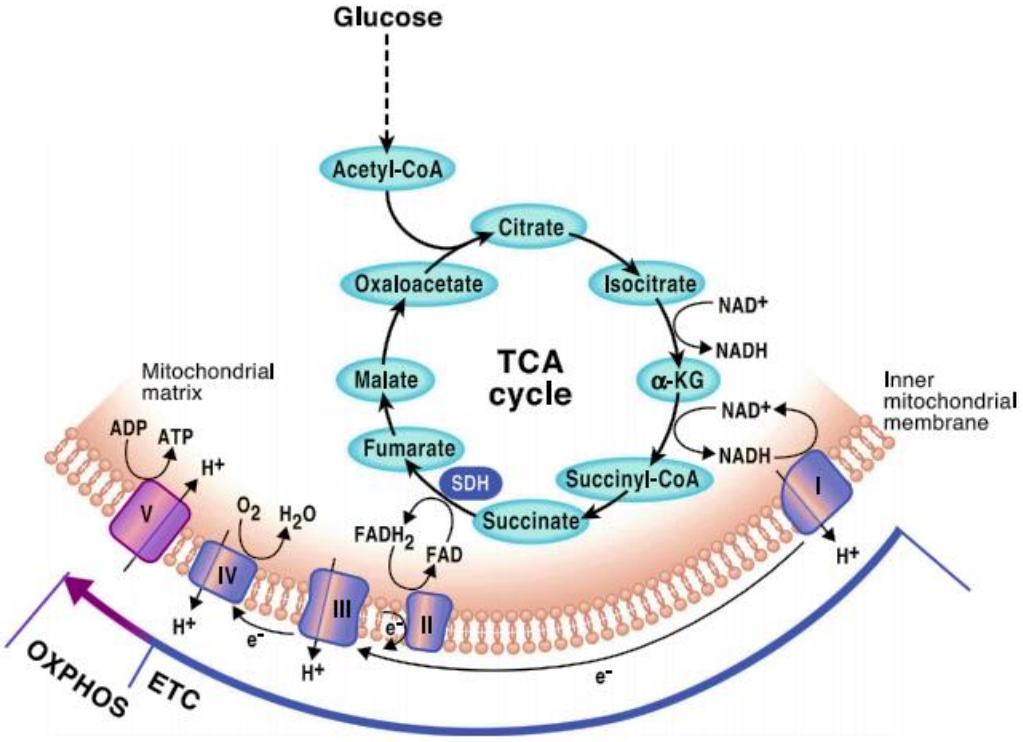

Figure 8. The TCA cycle and OXPHOS are tightly coordinated. (Adapted from Martinez-Reyes *et al.*, 2020 [101])

1.8.1. The role of mitochondrial dynamics in T cell activation

Mitochondria are highly dynamic organelles that undergo continuous fission and fusion. The constant turnover through mitochondrial biogenesis and mitophagy to maintain mitochondrial morphology, homeostasis, and inheritance. The four major proteins involved in mitochondrial dynamics are members of dynamin-like guanosine triphosphatases (GTPases), which include: Mfn1 and 2, optic atrophy 1 (Opa1) and dynamin-related protein 1 (Drp1) [102]. Mfn1 and Mfn2 are localized to the OMM, and Opa1 is localized to the IMM. The binding of two mitochondria mediates mitochondrial fusion. While Mfn 1 and 2 mediate the merging of the two OMMs, the IMM fusion is supported by Opa1 [103]. The loss of mitochondrial ΔΨm induces OPA1 cleavage by protease OMA1, a process that further dampens mitochondrial fusion [104].

The process of mitochondrial fission not only acts to eliminate dysfunctional mitochondria but is also an adaptation that occurs in response to the changes in energy demand [105] in low proliferating cells, and decreased ATP production by OXPHOS [106]. Mitochondria fusion occurs under starvation conditions or higher OXPHOS activity. This increases cristae formation and provides more surface area for OXPHOS and FAO. Memory T cells, commonly in a quiescent state, have fused mitochondria phenotype, associated with the increased FAO rates. In activated T cells, the mitochondria are fragmented [107] (Fig. 9). The cellular functions are also affected by the mitochondrial distribution within cells and this depends on their interaction with the cytoskeleton and molecular motors. The movement in the cell depends on micro-anchoring proteins in the OMM that interact with molecular motors (kinesin or dynein) in the microtubules [108]. The size of mitochondria may impact mitochondrial transport across the cell. In that sense, small mitochondria can be transported easier than larger ones, easily reaching the immune synapses.

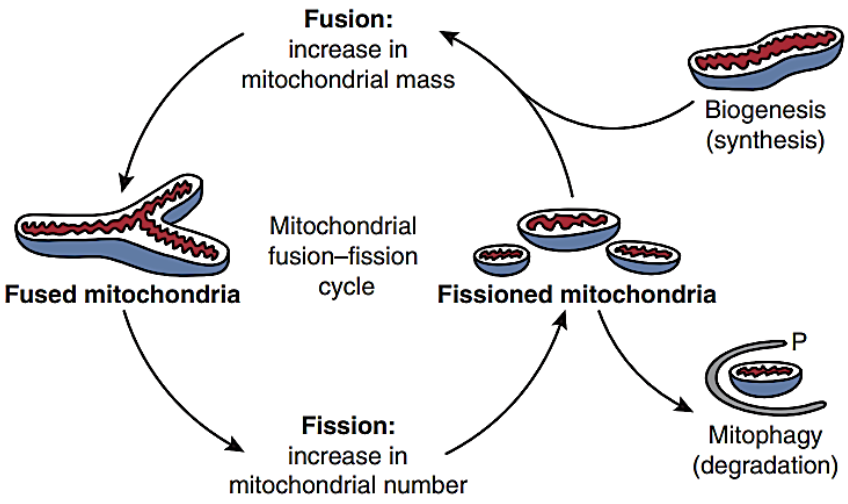

Figure 9. Mitochondrial fusion-fission cycle. (Adapted from Seo *et al.,* 2010 [109])

1.8.2. Regulation of mitochondria ATP transport

The mitochondrial VDAC, also known as the mitochondrial porin, is the most abundant protein in the outer mitochondrial membrane and is responsible for regulating the ion and metabolite flux between mitochondria and cytosol [110]–[112]. Several molecules are capable of modulating VDAC conductance, for example, adenine nucleotides, tubulin, and hexokinase (HK) [113]–[115]. ATP/ADP ratios and NAD(P)H levels modulate outer mitochondrial membrane permeability and respiration rates [113]. The inhibition of VDAC by free tubulin limits mitochondrial respiration and could be a reason for the Warburg effect. Once, activated cells require tubulin to support rapid division. The increase in free tubulin by microtubule destabilizing compounds as rotenone and nocodazole are also able to decrease the mitochondrial membrane potential [116]. Free tubulin can decrease VDAC conductance and ultimately lead to outer mitochondrial membrane permeabilization and cell death [117]. The role of HK in mediating the VDAC closure is controversial, once the closure would inhibit nucleotide exchange and burden the ATP supply by which HK depends on for its enzymatic activity [118]. The VDAC shutdown due to HK detachment leads to mitochondrial swelling and, consequently, to cell death via an undefined pathway [119].

1.8.3. The sphingolipid influence in mitochondrial metabolism

Several studies reported the importance of sphingolipid metabolism in sustaining mitochondria functionality. Mitochondrial neutral sphingomyelinase activity and ceramides contribute to the damage of mitochondrial integrity and impaired OXPHOS in the heart reperfusion damage model [120]. In skeletal muscle myotubes, neutral sphingomyelinase inhibits ATP production, mitochondrial gene expression, and enhance fatty acid-induced lipotoxicity [121]. Furthermore, astrocytes ceramides regulate mitochondrial ATP release [122]. ASM inhibition is implied in impaired

Akt/mTOR pathway activation in α-CD3/CD28 stimulated human naive, memory, and Th17 differentiated $CD4_+$ T-cells [123].

2. Aim of the thesis

Previous work has established the role of neutral sphingomyelinase 2 in the regulation of signaling and activation of T cells. The importance of sphingolipid metabolism in sustaining mitochondria functionality has been documented for cells of non-hematopoietic origin but still not totally comprehended. Little is known about the role of sphingomyelinases in the regulation of T-cell metabolic activity.

This thesis aims to define the role of NSM2 in the general understanding of molecular mechanisms involved in sphingomyelinase dependent control of T-cell energy metabolism.

3. Materials

3.1. Cell Lines

Table 1 - Cell lines

Cell line	Cell type	Species	Origin
CRISPR/Cas9 NSM KD Jurkat T cells (ΔNSM)	Lymphoblast T cells	human	University Bern, Prof. Dr. Annette Draeger
HEK 293T	Human embryonic kidney cells transformed by SV40 T-antigen	human	Virology Würzburg
Jurkat (CTRL)	Lymphoblast T cells	human	Virology Wurzburg

3.2. Primary cells

Primary cells were isolated from leukocyte reduction chambers supplied by the University Hospital of Wurzburg, Institute for Transfusion Medicine and Hemotherapy (ethically approved, vote S. Schneider-Schaulies).

3.3. General buffers, solutions, and media

Table 2 - General buffers, solutions, and media

Buffers/solutions/Media	Manufacturer/content
Acrylamide/bisacrylamaid	AppliChem
APS	Carl Roth
ATP	Thermo Fischer
ATP Determination Kit	Invitrogen
ATP Lysis Buffer	PSB (w/o Ca2+/Mg2+) 1% Triton-X
ATV	136,89 M NaCl 5,36 M KCl 3,22 M D(+)-glucose

	6,90 M NaHCO3 0,05 % trypsine 0,54 M EDTA ad aqua dest., pH 7,4
BCA	Sigma-Aldrich
BSA	Serva
Chemiluminescent Western Blot Detection	ThermoScientific
Complete, EDTA-free, Protease Inhibitor Cocktail	Roche
D-Glucose	Sigma-Aldrich
DMEM	Gibco
DMSO	AppliChem
Dynabeads Human T-Activator CD3/CD28	Invitrogen
EDTA	Sigma-Aldrich
EGTA	Sigma-Aldrich
FACS buffer	PBS (w/o Ca^{2+}/Mg^{2+}) 0,5 % (w/v) BSA 0,02 % (w/v) NaN_3
FCS	Biochrome AG
Gel Red	Sigma-Aldrich
HEPES	Sigma-Aldrich
Histopaque-1077	Sigma-Aldrich
HMU-PC	Moscerdam Substrates
HMU-PC solution	1,35 mM HMU-PC 0,25 M Na-acetate 30 µM Na-taurochlorate ad aqua dest., pH 7,4
HPLC-grade water	AppliChem
Ingenio® Electroporation solution	MirusBio
Lysis buffer	1% (w/w) Nonidet P-40 (NP-40) 120mM NaCl 10mM NaF, pH=7.2 50mM Hepes, pH=7.4, 40mM b-glycerophosphat 1mM EDTA 1 tablet protease inhibitors cocktail

	per 10ml lysis buffer
MACS Buffer	10mM EGTA 3% FCS PBS (-/-)
MagniSort™ Human CD4 T cell Enrichment Kit	Thermofischer
MEM	Gibco
Mitochondria Isolation Media	300mM sucrose 10mM HEPES 200µM EDTA 1mg/mL BSA, pH 7.4
Mitochondria Isolation Media w/o BSA	300mM sucrose 10mM HEPES 200µM EDTA pH 7.4
Mounting media	Southern Biotech
NaCl	AppliChem
NSM Assay lysis buffer	20 mM HEPES pH 7,4 10 mM b-glycerolphosphate protease inhibitor cocktail ad aqua dest.
NSM Assay resuspension buffer	20 mM HEPES pH 7,4 15 mM MgCl2 10 mM b-glycerolphosphate protease inhibitor cocktail ad aqua dest.
NSM Assay stop buffer	0,2 M glycine 0,2 M NaOH 0,25 % Triton-X ad aqua dest., pH 11
Paraformaldehyde (PFA)	AppliChem
PBS	137 mM NaCl 2,7 mM KCl 10 mM Na2HPO4 x H2O 1,8 mM KH2 PO4 1 mM CaCl2 x 2 H2O

	0,5 mM MgCl2 x 6 H2O ad aqua dest.
PBS (w/o Ca^{2+}, Mg^{2+}); PBS (-/-)	137 mM NaCl 2,7 mM KCl 10 mM Na2HPO4 x H2O 1,8 mM KH2 PO4 ad aqua dest.
Penicillin/Streptomycin (100 i.e./mL)	Sigma-Aldrich
Plasmid Maxi Kit	QIAGEN
Plasmid Mini Kit	QIAGEN
Poly-L-Lysine	Sigma-Aldrich
Propidium Iodide	Immunotools
Pyruvate	Sigma-Aldrich
RPMI-1640	Gibco
Saponin	Sigma-Aldrich
SDS	AppliChem
Seahorse XF Basis Medium DEMEM	Agilent
Seahorse XF Calibrant Solution	Agilent
Sucrose	Sigma-Aldrich
TEMED	Carl Roth
Tris	Carl Roth
Triton-X	Sigma-Aldrich
Trypan-blue	0,25 % (w/v) in PBS (w/o Ca^{2+} /Mg^{2+})
TWEEN-20	VWR
Versene	PBS (w/o Ca^{2+}, Mg^{2+}) EDTA 0.02%
WB blocking buffer	5 % w/v skim-milk in PBS
WB loading buffer	200 mM Tris pH 6.8 4 % w/v SDS 20 % w/v glycerol 0.02 % w/v bromophenolblue 200 mM DTT
WB washing buffer	PBS/0.05 % Tween-20

3.4. Chemicals, Inhibitors, and siRNAs

Table 3 - Chemicals, Inhibitors, and siRNAs

Chemicals/Inhibitors/siRNAs	Manufacturer
2-Deoxyglucose	Sigma-Aldrich
Antimycin A	Sigma-Aldrich
CTRL non-targeting siRNA	Sigma-Aldrich
D-Glucose	Sigma-Aldrich
ES048	A gift from Christoph Arenz
FCCP	Sigma-Aldrich
GW4869	Sigma-Aldrich
Nocodazole	Sigma-Aldrich
Oligomycin	Sigma-Aldrich
Rotenone	Sigma-Aldrich
siRNA targeting human SMPD3 (NSM2) (5′-UGCUACUGGCUGGUGGACC-3’ 5′-GGCUCCACCAGCCAGUAGCA-3′)	Sigma-Aldrich

3.5. Antibodies and dyes

***Table 4* - Antibodies and dyes**

Antigen/Target/Dyes	Catalog no.	Manufacturer	Dilution/concentration
6-NBDG	13961	Cayman Chemicals	50µM
α-CD28 (Clone: CD28.2)	555725	Beckton-Dickinson Biosciences Pharmingen	1:1000
α-CD3 (Clone: UCHT-1)	555329	Beckton-Dickinson Biosciences Pharmingen	1:1000
α-CD4-FITC	21459043	Immunotools	1:100 (FACS)
α-CD69-FITC	21459693	Immunotools	1:100 (FACS)
α-CD25-PE	21270254	Immunotools	1:100 (FACS)
α-mouse IgG	115-035-146	Dianova	25µg/mL
GLUT1	ab115730	Abcam	1:50 (FACS)
MitoTracker Green FM	9074S	Cell Signalling	200nM

MitoTracker Red CMXRos	9082S	Cell Signalling	200nM
Secondary antibody Alexa488 chicken anti-rabbit	A-21441	Life Technologies	1:100 (FACS, IF)
Phospho-mTOR (Ser2448) (D9C2)	5536S	Cell Signalling	1:50 (IF) 1:2000 (WB)
Phospho-S6 Ribosomal Protein (Ser235/236)	4858S	Cell Signalling	1:50 (FACS) 1:2000 (WB)

3.6. Disposable Material

***Table 5* – Disposable material**

Disposable Material	Manufacturer
6, 12, 24 well cell culture plates	Greiner Bio-One
75 25 cm2 cell culture flasks	Greiner Bio-One
96 well flat bottom plate, black	Nunc
96 well flat bottom plate, white	Corning®
Cover glass for IF	Marienfeld-Superior
Cuvettes – semi-macro	Hartenstein
Electroporation cuvettes	VWR
FACS-tubes	Falcon
Lab-Tek® II Slide, 8 Chamber	Emsdiasum
Leucocyte reduction chambers	University Hospital Würzburg
Pasteur pipettes	Hartenstein
Pipette tips	Brand
Plastic pipettes (5, 10, 25 mL)	Sarstedt
Plastic tubes (50, 15 mL)	Greiner Bio-One
Reaction tubes (0.5, 1.5, 2.0 mL)	Eppendorf
Seahorse XF96 V3 PS Cell Culture Microplates	Agilent
Seahorse XFe96 sensor cartridges	Agilent
Sterile Filter (Attachment for Disposable Syringes): Diameter 50 mm, Pore Size 0.2 µm	Sartorius Stedium Biotech

3.7. Equipment

***Table 6* – Equipment**

Apparatust	Manufacturer
Accu-jet pro	Brand
Amaxa® Nucleofector®	Lonza
BioPhotometer Model #6131	Eppendorf
Centrifuge Mikro 200	Hettich
Centrifuge Rotanta 460 R	Hettich
Confocal microscope LSM 780	Zeiss
EasySep™ Magnet	StemCell Technologies
FACScan Calibur	Becton Dickinson
Fluorescent microscope DMi8	Leica
Heating block	Liebisch
Incubator 37 °C, 5 % CO2	Heraeus
Laminar workflow	Gelman
Luminometer Centro XS3 LB960	Berthold
Microliter pipettes	Brand, Eppendorf
Neubauer cell counting chamber	Hartenstein
Odyssey FC	Li-Cor
PH meter	Mettler Toledo
Safire2 – Fluorescence plate reader	Tecan
Seahorse XFe96 Analyzer	Agilent
Shaker platform WS5	Edmund Bühler
Vortex Mixer	Neo Lab
Water bath	Kotterman

3.8. Software

Table 7 – Software

Software	Company
CellQuest Pro	Becton Dickinson
FlowJo_v10	FlowJo
GraphPad Prism 6	GraphPad Software Inc.
Image Studio Lite	Li-Cor
ImageJ	NIH
MikroWin	Berthold
Office Excel Home Office PowerPoint Home Office Word Home	Microsoft
Tecan-i-controlTM 1.7	Tecan
Wave	Agilent
Zen	Zeiss

4. Methods

4.1. Cell Culture

4.1.1. Cell lines

Cells were culture in plastic flasks proper for cell culture with filter lids in a humified incubator at a temperature of 37ºC and a 5% CO2 atmosphere. CTRL and ΔNSM Jurkat T cells were cultured in RPMI 1640 media, supplemented with Penicillin/Streptomycin (100i.e/mL) and 100% heat-inactivated fetal calf serum (FCS). The serum was heat-inactivated at 50ºC for 1h. Jurkat cells were split every 2 to 3 days at a ratio of 1:3 to keep a density between $1x10^5$ and $1x10^6$ viable cells per mL.

4.1.2. Thawing and cryopreservation of cells

For long-term storage, 1x107 cells were centrifuged (5 min, 280 x g, RT), and the pellet was resuspended in 1 mL freezing medium containing FCS + 10% DMSO and transferred to -20ºC for 2h and subsequently to -80ºC for overnight. Finally, the cells were transferred to -140°C. For thawing, standard cell culture media is heated to 37°C, and frozen cells are quickly thawed and diluted in 10 mL of the medium. The medium is changed after 24 h to minimize cellular stress.

4.1.3. Isolation of Primary Human T Cells

Peripheral blood mononuclear cells (PBMCs) were obtained from blood samples with permission of the ethics committee of the medical faculty from the department of transfusion medicine of the Universitätsklinikum Würzburg as leucocyte reduction chambers. The blood in the chamber was first transferred into a 50mL canonical tube and diluted with Versene in a 1:5 dilution, final volume 50mL, and mixed gently thoroughly a plastic pipette. The final volume of 50mL was divided into two and added

smoothly in tubes containing 9 mL of Histopaque to form 2 layers. The density gradient was performed at 160g for 30 min at room temperature. During centrifugation, cells can be separated accord to their density. Graphical representation of the tube before and after centrifugation is illustrated in the figure below (Fig. 10).

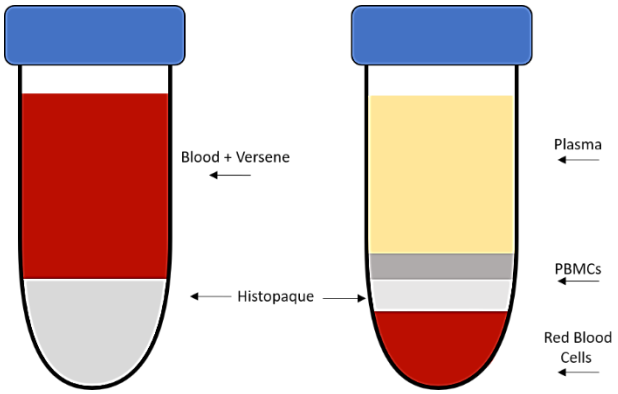

Figure 10. Illustration of Layer distribution before (left) and after (right) density gradient centrifugation.

After centrifugation, the layer contained the PBMCs were yield and washed three times with sterile and pre-warmed PBS (-/-) and resuspended in RPMI 1640 5% FCS and incubated for 2h at 37º C. This step allows the monocytic and leucocytic fractions to be separated, during this time the monocytic cells will adhere to the plastic, while the T cells and B cells will remain in suspension. Peripheral blood lymphocytes (PBLs), the non-adherent fraction, are used as a source for primary human T cells. MagniSort™ Human CD4 T cell Enrichment Kit was used to recover only the positive CD4 cells from the PBLs pool using magnetic separation by negative selection. PBLs were counted, centrifuged, and resuspended in a density of $1x10^7$ cells per 100µL in MACS buffer. Firstly, 20µL of Enrichment Antibody Cocktail was added per 100µL of cells, mixed and incubated at RT for 10 minutes. The Enrichment Antibody Cocktail contains Anti-Human CD8 Biotin, Anti-Human CD11b Biotin, Anti-Human CD14 Biotin,

Anti-Human CD16 Biotin, Anti-Human CD19 Biotin, Anti-Human CD20 Biotin, Anti-Human CD36 Biotin, Anti-Human CD56 Biotin, Anti-Human CD123 Biotin, Anti-Human CD235a Biotin, and Anti-Human γδ TCR Biotin. After incubation, cells were washed one time with MACS buffer and centrifuged. After the centrifugation, cells were resuspended in MACS buffer in $1x10^7$ cells per 100µL density. MagniSort® Negative Selection Beads B were added, mixed, and incubated for 5 minutes at RT. Later, cells were collected and transferred to a canonical 5mL tube and placed in an EasySep™ Magnet. After 5 minutes, the cells in the tube were collected by pouring into a different tube. The magnet step was repeated 1x. Cells were counted, centrifuged, and cultured in a density of $4x10^6$ cells per mL. The purity of about 95% is achieved. Workflow can be observed in figure 11.

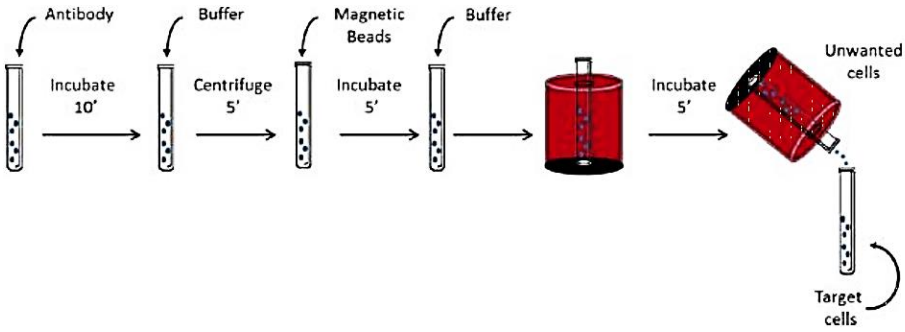

Figure 11. Illustration of workflow from CD4+ isolation procedure. Source: *MagniSort™ Human CD4 T cell Enrichment Kit protocol*

4.1.4. Co-stimulation with soluble antibodies

Co-stimulation were performed by adding α-CD3 (clone UCHT-1) together with CD28-specific antibody (clone CD28.2) (1 µg/ml) (both:Beckton-Dickinson Biosciences Pharmingen) on ice for 20 min, subsequently transferred to plates pre-coated with 25 µg/ml α-mouse IgG (Dianova) (2 h at 37 ºC). Cells were stimulated for different time points.

4.1.5. Labeling with C16 ceramide

A total of 5×10^7 CTRL or ΔNSM cells were extensively washed and resuspended in 186 RPMI/2% FBS containing 25µM C16-ceramide (Avanti Polar Lipids), incubated overnight at 37°C and washed three times with PBS before performing flow cytometry or mitochondria isolation.

4.2. Inhibitor treatment and CD4+ cells transfection

Pharmacological inhibition of NSM was obtained by using treatment with ES048. Cells were incubated prior experiment for 2 hours at 37ºC with ES048 1,5µM. The concentration and pre-incubation time have been optimized in the laboratory by previous students[124]. NSM inhibition was measured with an enzymatic reaction.

The genetic ablation of NSM was performed using a siRNA system. Primary CD4+ cells were transfected with siRNA targeting the NSM gene. The following siRNAs were used:

nSMase2 sense: *5'-UGCUACUGGCUGGUGGACC-3'*

nSMase2 anti-sense: *5'-GGCUCCACCAGCCAGUAGCA-3'*

Each transfection was performed using $1x10^7$ cells, cells were centrifuged and resuspended in 100µL of transfection medium, and 100pM siRNA, CTRL, or against NSM was added, gently mixed, and transferred into a fresh electroporation cuvette. For electroporation, cuvettes were placed into Amaxa Nucleofector II, and the pre-installed program U-14 (T cells, human, high viability) was used. After electroporation, cells were placed into 3mL pre-warmed RPMI 10% FCS in a 6-well plate. The procedure is repeated on day one, and on day three, the maximum gene knockdown is achieved on day 5. NSM inhibition was measured with an enzymatic reaction.

4.2.1. NSM activity assay

The NSM enzyme activity is measured by the conversion of HMU-PC pH 7,4 into a reaction product which emits detectable fluorescent light. Cells were collected in a density of $1x10^6$, centrifuged, pelleted, and resuspended in a 40µL lysis buffer. The tube was placed into -80ºC freezer for 5 minutes and back into RT. A 3 times freeze/ thaw cycle was performed. This procedure assures that the whole cell is lysate, and the enzyme floats into the supernatant. Cell debris was removed by centrifugation for 5 minutes at 4ºC at 1200 x g. The following reaction mix is prepared for triplicates per sample, plus a background measurement:

NSM Assay Reaction Mix:	
Resuspension buffer	10 µL
HMU-PC (pH 7,4)	10 µL
ATP (10 mM)	2,2 µL
Cell Lysate	10µL

Background Reaction Mix:	
Resuspension buffer	10 µL
HMU-PC (pH 7,4)	10 µL
ATP (10 mM)	2,2 µL
Lysis Buffer	10µL

The samples were placed at 37ºC overnight, and the reaction is stopped by the addition of a 200µL stop buffer. Samples were transferred into a black flat-bottom 96-well plate, and the fluorescence (excitation = 360 nm, emission = 460 nm) was measured. The background is subtracted from the sample values (Fig. 10).

4.3. Bacterial transformation and plasmid isolation methods

4.3.1. Transformation of bacteria

Ecoli XL10-Gold ultracompetent cells were used for plasmid transformation. 50 ng of plasmid DNA were added to 50µL of bacteria, mixed, vortexed gently, incubated 30 min on ice and then for 1 min at 42°C in a water bath followed by cooling on ice for 5 min. 1mL of antibiotic-free Lennox L Broth (LB) medium was added to the bacteria, which were incubated for 1h on a shaker at 220 rpm at 37°C. 50µL of this bacterial culture was then spread on an LB agar plate surface, containing 100µg/mL of Ampicillin, which were incubated at 37°C for 24h. Colonies formed were selected and further inoculated in LB medium for Miniprep and Maxiprep plasmid isolation.

4.3.2. Miniprep and Maxiprep plasmid isolation

A single bacterial colony from the LB agar plate or 10 µL of colony suspension was inoculated in 5 mL of LB medium containing antibiotics and incubated in a bacterial shaker at 220 rpm overnight at 37°C. The plasmid Miniprep isolation was performed using the QIAGEN Plasmid Mini Kit according to the manufacture's instruction. The isolated plasmids were then diluted in 50 µL of TE buffer, and the O.D. was measured using the photometer device and used for restriction enzyme digestion to verify their identity. For maxipreparation, 2 mL of the amplified bacterial colony was added to 200 mL of LB medium containing antibiotics and incubated in a bacterial shaker at 220 rpm overnight at 37°C. Bacteria were then recovered by centrifugation at 6000×g for 15 min at 4°C, and plasmid DNA was isolated using QIAGEN Plasmid Maxi Kit according to manufactures instruction. The plasmid DNA was resuspended in TE buffer at the final concentration of 1 µg/µL and stored at -20°C.

4.4. Generation of Mitochondria GPF Jurkat cell lines

4.4.1. Transient transfection

PEI was used for the transfection of plasmids in HEK 293T. These were seeded in a 6-well-plate at the density of 1 x 10^6 cells per well and incubated at 37°C for 24 h and were up to 80% confluency. The medium was replaced by MEM 10% FCS without antibiotics 5h before transfection. Two mixtures were prepared in separate tubes. Mix 1: PEI + 150 mM NaCl (vortex for 1 min) and Mix2: Plasmid DNA + 150 mM NaCl (for 1 µg of total DNA add 4µl of PEI). Mix 1 and Mix 2 were combined, mixed by gentle pipetting, and incubated at room temperature for 20-30 mins to enable the formation of DNA-PEI complexes, which were then applied as droplets onto the cells kept at 37°C. The medium was replaced the next day of transfection with an antibiotic-free medium, and cells were incubated further for 24-48h.

4.4.2. Generation of lentiviral particles

For lentiviral delivery of the mitochondrial-targeted pre-sequence of the CoxV (kindly provided by V. Kozjak-Pavlovic), a packaging system using psPAX2 and pVSV-G packaging plasmids together with pLVTHM vector was used. Transfection of HEK 293T cells for this purpose was carried out as described above with mixture 1 (PEI mix) containing 50 µl PEI + 600 µl 150 mM NaCl (vortexed for 1 min) and mixture 2 containing 3µg mitochondrial lentiviral construct + 4µg psPAX2 + 4µg pVSV-G + 600 µL sterile 150 mM NaCl (mixed and vortexed). The supernatant containing viral particles was harvested after 2 to 3 days post-transfection. Cell debris was removed by centrifugation at 2000-3000 RPM at 4°C in 50 mL centrifuge tubes and subsequent sterile filtration (0.2 µM filter pore size) followed by freezing aliquots at -80°C.

4.4.3. Lentiviral transduction

CTRL and ΔNSM Jurkat cells were seeded in a six-well plate at the density of $1x10^5$ cells per well, and the supernatant containing lentiviral particles was added. To increase the efficiency of transduction and obtain maximum expression of target genes, plates were centrifuged at 400×g for 30 min at 37°C and then incubated at 37°C for 48h. Subsequently, cells were kept in culture for five days, and the efficiency of the transduction was measured by flow cytometry. After three passages, cells were sorted by FACS, and 98% of GFP cells were recovery and keep in culture until being utilized.

4.5. ATP measurements

4.5.1. Sample preparation

Human CD4+ T cells were pre-treated or not with 1 µM oligomycin, 25 mM 2-DG, or both for 20 min and with Nocodazole 10µM for 1h. At the end of the incubation period, cells were collected, pelleted, and washed once with ice-cold PBS. Cells were permeabilized with 1% triton, centrifuged at 8000 RPM for 2 min at 4ºC, and the supernatant was collected and used for the ATP assay. The supernatant was kept on ice, or frozen in -80º C until the quantification.

CTRL and ΔNSM Jurkat cells were left untreated or pre-treated with Nocodazole 10µM for 1h, and mitochondrial were isolated as described below. A concentration of 1ng protein was used in the ATP assay.

4.5.2. Mitochondrial isolation

Cells were harvested, pelleted, and resuspended in cold mitochondrial isolation media (MIM, 300mM sucrose, 10mM HEPES, 200µM EDTA, and 1mg/mL BSA, pH 7.4) at a ratio of $5x10^7$ per 500µL of MIM. Cells were homogenized with a plastic homogenizer for ten strokes. After homogenization, samples were centrifuged at 1600 RPM at 4º C for 7 minutes to separate the mitochondria from the remaining cellular material. The supernatant was collected and centrifuged at 13000 RPM at 4º C for 10 minutes to obtain the mitochondrial pellet. The mitochondrial pellet was washed with cold-BSA free MIM. Isolated mitochondria were utilized in different experiments.

4.5.3. ATP Quantification

Total or mitochondrial ATP was measured by using the ATP determination kit (Molecular Probes). The ATP kit is based in a bioluminescence assay for the quantitative determination of ATP with recombinant firefly luciferase and its substrate D-luciferin. The assay is based on luciferase's absolute requirement for ATP in producing light (emission maximum ~560 nm at pH 7.8) from the reaction:

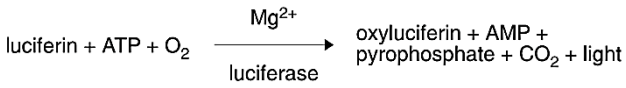

Figure 12. Luciferin/Luciferase reaction. Source: ATP Determination Kit (A22066) protocol

On the day of the experiment, samples were thaw on ice and kept cold until measurement. Following the manufacture's protocol, a 10mL Standard Reaction Solution (SRS) was prepared, it contains:

Reagent	Volume	Concentration
dH_2O	8.9 mL	
Reaction Buffer	500µL	20X
DTT	100µL	100µM
D-luciferin	500µL	10 mM
Firefly luciferase stock solution.	2.5 µL	5 mg/mL
Final volume	**10mL**	

The workflow of the experiment consists in adding a volume of 90µL of SRS into a white flat bottom 96 well plate, and background measurement. Subsequently, 10µL of the sample was added, and a new reading was performed. The Centro XS3 LB960 luminometer microplate reader was utilized. Using the Mikrowin software, the parameter for the measurement was: 20s of shaking + 1s reading.

4.5.4. ATP data

The results were expressed in arbitrary units, and the files were exported into an excel file. To assure the real concentration in each sample, an ATP curve (10mM -> 0,0001mM) was performed. Using the standard ATP curve, measurements with background deducted were interpolated, and real ATP concentration was analyzed. All samples were normalized by protein amount.

4.6. Flow Cytometry

The flow cytometry, the technique consists of a laminar flow in which cells are singularized and pass through a laser that allows detection of the size (FSC, forward scatter), granularity (SSC, sideward scatter) and fluorescent labeling. Different fluorescent labels and their intensities are measured and allow the characterization of different subpopulations in a mixture of cells. For this purpose, cells are either labeled by antibodies linked to fluorescent dyes or dyes are incorporated into cells.

4.6.1. 6-NBDG uptake

6-deoxy-6-[(7-nitro-2,1,3-benzoxadiazol-4-yl)amino]-D-glucose (6-NBDG) is a non-hydrolysable fluorescent glucose analog. And displays an excitation/emission maxima of 465/535 nm. Humans CD4+ T cells were kept in RPMI 1% FCS without glucose for 2h before the experiment. 6-NBDG was diluted in DMSO in a stock concentration of 50mM. For the uptake experiment, 6-NBDG was diluted in RPMI 0,5% FBS without glucose into a concentration of 50µM. Cells were incubated for 60 min at 37°C, then washed with FACS buffer twice prior measurement.

4.6.2. Mitochondrial profiling

For mitochondrial profiling, two different dyes were used: MitoTracker Green FM, which stains mitochondria, independently of mitochondrial membrane potential. And displays an excitation/emission of 490/516 nM. And MitoTracker Red CMXRos that stains mitochondria in live cells and its accumulation is dependent upon membrane potential. And shows an excitation/emission of 579/599 nM. Human CD4+ T cells were collected and incubated with 200 nM MitoTracker Green or Red for 30min at 37ºC then washed once with FACS buffer prior measurement.

4.6.3. Extra and Intracellular stainings

To determine the levels of the Glucose Transporter, GLUT1 and mTOR activity cells were fixed with 4% paraformaldehyde at room temperature for 20min. Then washed with FACS buffer, stained for phospho-S6 ribosomal protein (Ser235/236) or Anti-Glucose Transporter GLUT1 antibody for 1h at 4ºC, antibodies were diluted in PBS with 0,3% saponin for intracellular staining, washed and incubated with secondary antibody Alexa488 for 30 min at 4ºC. Cells were washed twice with FACS buffer.

4.6.4. Surface Activation Markers

For quantification of the activation markers with FITC conjugated anti-CD69 and PE-conjugated anti-CD25 antibodies. CD4+ were co-stimulated for the indicated time points, then washed with PBS and incubated for 30 min on ice in the dark with 10µL of anti-CD25 and anti-CD69 antibodies in 100µL FACS buffer. Cells were washed twice with FACS buffer.

4.6.5. Viability assay

For viability assay, we utilized Propidium iodide (PI). PI is a small fluorescent molecule that binds to DNA but cannot passively traverse into cells that possess an intact plasma membrane. Cells were stimulated on a plate with α-CD3/CD28, and on day five cells were collected washed once, and PI incubated with PI for 15 minutes, then cells were washed once and measured on FACS.

4.6.6. Sample analysis

In this study, flow cytometry was performed using the BD FACSCalibur. A minimum of 15000 events was collected, and data analysis was performed by CellQuestPro or FlowJo 10.4.2 software.

4.7. Metabolic Profiling

4.7.1. Seahorse XF Analyzers

Seahorse XF Analyzers measure oxygen consumption rate (OCR) and extracellular acidification rate (ECAR) of live cells, interrogating critical cellular functions such as mitochondrial respiration and glycolysis. Real-time measurements of OCR and ECAR are made by isolating a tiny volume (about 2 µL) of the medium above a monolayer of cells within a microplate. Cellular oxygen consumption (respiration) and proton excretion (glycolysis) cause rapid, easily measurable changes to the concentrations of dissolved oxygen and free protons in this "transient microchamber," which are measured every few seconds by solid-state sensor probes residing 200 microns above the cell monolayer. The instrument measures the concentrations for 2-5 minutes then calculates the OCR and ECAR, respectively.

4.7.2. Cell Preparation

The Amaxa electroporation technique used to transfect primary T cells with NSM2 specific RNA was not compatible with Seahorse technology, which was extremely sensitive to the presence of apoptotic or dead cells in transfected T cell culture. During the electroporation procedure, cells receive electric pulses that disrupt the integrity of the plasma membrane, allowing the siRNA to enter the cells [125].

The procedure is highly efficient in delivering nucleic acids in the cell. NSM activity was reduced by about 50% in both electroporated, and ES048 treated cells. However, it can lead to increased cell death due to the necrosis or apoptosis caused by electro sensitization [126]–[129]. Therefore, we used pharmacological inhibition of NSM by ES048 for the seahorse experiments throughout the thesis.

Cells were kept without stimulation or co-stimulated for 24h prior experiment. On the day of the experiment, cells were washed three times with Seahorse XF Base Medium,

pH 7.4. Depending on which experiment, the Seahorse XF Base Medium has different compositions. The complete medium contains 250mM Glucose, 1mM Pyruvate, and 2mM L-Glutamine. Cells were then seeded at a density of 1 x 10^6 cells/well (8 wells per condition) and kept in a 37 ºC incubator without $C0_2$ for 1h for calibration. Afterward, the plate was placed into the XF96 analyzer.

4.7.3. Metabolic Response Upon Stimulation

To assess the metabolic response upon stimulation, cells were kept in a complete medium, and four basal measurements were performed, followed by one injection with α-CD3/CD28 10µg/ml and more ten post-injection measurements. ECAR and OCR were measured.

4.7.4. Mitochondria Stress Test

The mitochondria stress test consists of 3 distinct injections after four cycles each. The cells kept in full nutrient medium receive the first injection of 1µM oligomycin, a chemical responsible for blocking the mitochondrial ATP production, and stop the mitochondrial respiration. The second injection is 1.5µM FCCP, a chemical responsible disrupt the potential of the membrane of the mitochondria and assessing the maximal cellular respiration, the third injection is a combination of 100µM Rotenone and 1µM Antimycin A, both responsible for blocking the complexes I and III, respectively, in the electron transport chain. The orders of the injection allow calculations of different parameters and more precise results about the mitochondria functionality, as seen below:

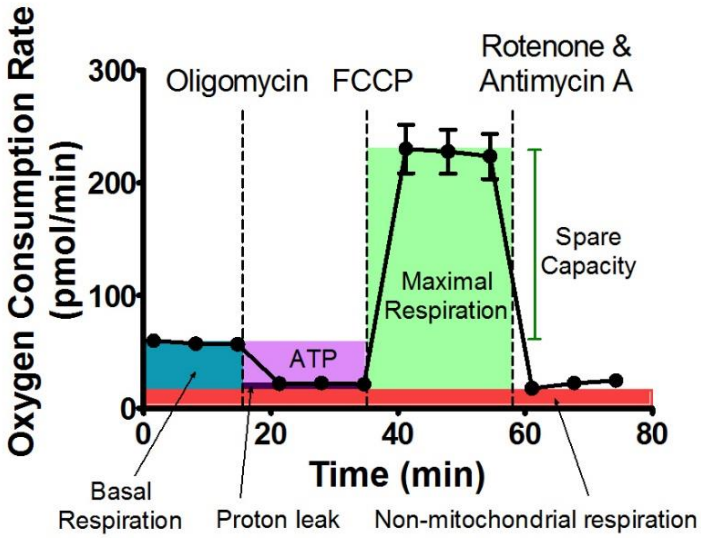

Figure 13. Mitochondria stress test. Source: Agilent

Basal respiration: Oxygen consumption used to meet cellular ATP demand resulting from mitochondrial proton leak. Shows the energetic needs of the cell under baseline conditions.

ATP Production: The decrease in oxygen consumption rate upon injection of the ATP synthase inhibitor oligomycin represents the portion of basal respiration that was being used to drive ATP production. Shows ATP produced by the mitochondria that contribute to meeting the energetic needs of the cell.

H+ (Proton) leak: Remaining basal respiration not coupled to ATP production. Proton leak can be a sign of mitochondrial damage or can be used as a mechanism to regulate mitochondrial ATP production.

Maximal respiration: The maximal oxygen consumption rate attained by adding the uncoupler FCCP. FCCP mimics a physiological “energy demand” by stimulating the respiratory chain to operate at maximum capacity, which causes rapid oxidation of substrates (sugars, fats, and amino acids) to meet this metabolic challenge. Shows the maximum rate of respiration that the cell can achieve.

Spare respiratory capacity: This measurement indicates the capability of the cell to respond to an energetic demand as well as how closely the cell is to be respiring to its theoretical maximum. The cell's ability to respond to demand can be an indicator of cell fitness or flexibility.

Nonmitochondrial respiration: Oxygen consumption that persists due to a subset of cellular enzymes that continue to consume oxygen after the addition of rotenone and antimycin A. This is important to get an accurate measure of mitochondrial respiration.

4.7.5. Glycolytic Stress Test

The glycolytic stress test consists of 3 distinct injections after four cycles each. The cells kept without glucose receive the first injection of 10mM glucose to assess the basal glucose utilization; the second injection is 1µM oligomycin, a chemical responsible for blocking the mitochondrial ATP production, forcing the cells to utilize glycolysis, the third injection is 25mM 2-DG. This glucose analog blocks glycolysis. The orders of the injection allow calculations of different parameters and more precise results about the glycolytic demand, as seen below:

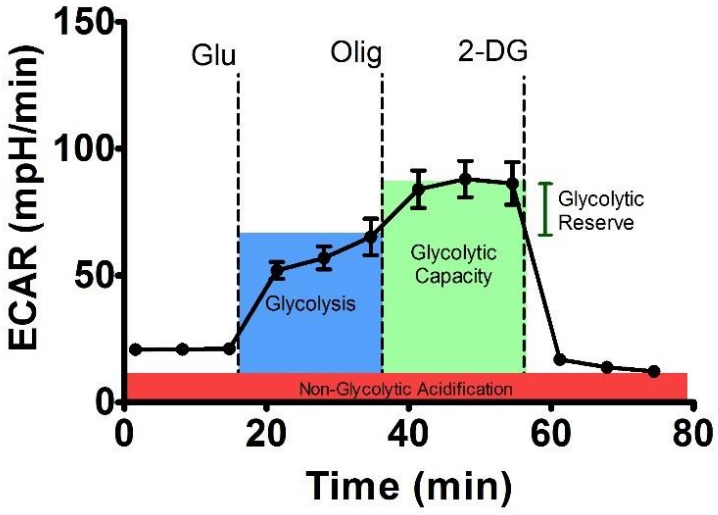

Figure 14. Glycolytic stress test. Source: Agilent

Glycolysis: The process of converting glucose to pyruvate. The XF Glycolysis Stress Test presents the measure of glycolysis as the ECAR rate reached by a given cell after the addition of saturating amounts of glucose.

Glycolytic capacity: This measurement is the maximum ECAR rate achieved by a cell following the addition of oligomycin, effectively shutting down oxidative phosphorylation and driving the cell to use glycolysis to its maximum capacity.

Glycolytic reserve: This measure indicates the capability of a cell to respond to an energetic demand as well as how close the glycolytic function is to the cell's theoretical maximum.

Non-glycolytic acidification: This measure other sources of extracellular acidification that are not attributed to glycolysis.

4.8. Confocal Microscopy

Imaging was performed by the confocal laser scanning microscope LSM 780, Zeiss, which is equipped with an incubation system and objectives with the following specifications: oil 63x/1.4, oil 40x/1.4, air 40x/0.95, 20x/0.8, 10x/0.45 plan apochromat. Fluorescence dyes were excited by laser lines 488 nm and 568nm.

4.8.1. Immunostaining and fixed-cell microscopy

Transfected CD4+ T cells were seeded in Lab-Tek® II Chamber Slide System with α-CD3/CD28 coated beads for different time point. Cells were washed once with PBS and fixed with 4% PBS for 30 min RT. After washing, cells were permeabilized using triton 0,1% X-100 in PBS 5% BSA for 15 min. Cells were incubated with primary antibody Phospho-mTOR (Ser2448) in PBS 5% BSA overnight at 4º C, washed three times, and cells were stained with α-rabbit Alexa488-conjugated secondary antibody and DAPI for nucleus visualization for 1 h at RT. After washing, the samples were mounted into slides.

CTRL and ΔNSM mitochondria GFP cells were seeded in Lab-Tek® II Chamber Slide System and fixed with 4% PFA for 15 minutes and washed three times with PBS. After washing, the samples were mounted into slides.

4.8.2. Image Analysis

The confocal images were pre-processed using DAQ software ZEN2012 black. The acquired images of cells were taken from different fields of view randomly selected across the entire coverslip area, and their mitochondrial morphology was analyzed using the semiautomated morphometric tool MiNA [130] within Fiji. A minimum of 50 cells was analyzed.

4.9. Protein quantification

The protein concentration in lysates was measured using BCA, and the rest of the samples were stored at -20°C. For protein quantification, 5 µL of samples or protein standard was applied to 995 µL of a solution of CuSO4 diluted 1:50 with BCA solution (1 mL BCA with 20 µL of CuSO4) in 1.5 mL tubes, vortexed, and incubated at 60°C for 15 min. Samples were transferred into cuvettes for the protein absorbance measurements using the Biophotometer.

4.10. Western Blot

The western blot method allows the detection of proteins of interest by separating them according to their electrophoretic mobility via Sodium dodecyl sulfate-polyacrylamide gel electrophoresis (SDS-PAGE) in the electrical field. Two gels were used to separate the proteins; the first gel is known as stacking gel with a neutral pH in which loaded proteins are concentrated and a separating gel with pH 8.7. Gels used in this study were 8 or 10 % polyacrylamide, and 30 of protein from the cell lysates were used.

The lysates were mixed were 3X Laemmeli buffer, incubated at 95°C in a heating block for 5 min and loaded onto the gel. The electrophoresis was performed at a constant eight mA overnight. Following electrophoresis, proteins we transferred to a nitrocellulose membrane. Whatman papers, membrane, and gel were soaked in the anode or cathode buffers and placed onto the transfer apparatus. After the transfer at 125 mA for 1 h, the nitrocellulose membrane was washed 1 x with PBS/0.1% Tween, blocked 30 min at RT in 5% non-fat dry milk or BSA in PBS/0.1% Tween (depending on the primary antibody) and washed once with PBS/0.1%Tween. The membrane was incubated overnight on a shaker at 4°C with the primary antibody diluted in 5% non-fat dry milk or BSA in PBS/0,1 % Tween and washed three times 15 min at RT. The secondary antibody diluted in 5% milk/PBS/0.1%Tween was added, incubated for 1h at RT, and washed three times with PBS/0.1%Tween followed by the acquisition of the membrane image in a Li-cor Odyssey Fc Imaging system. The following antibodies were used in this study: pMTOR, pS6, VDAC, aldolase, and HK II.

4.11. Statistical Analysis

Data were analyzed with GraphPad Prism software (GraphPad San Diego, USA). Data shown were acquired in at least three independent experiments involving individual donors. For statistical analyses of data sets, unpaired Student's t-test ($* p < 0.05$, ns: non- significant) was used throughout the manuscript. Bars show standard deviations

.

5. Results

5.1. NSM activity is increased after co-stimulation

To understand the dynamics of NSM2 activity in T cells, we measured the NSM2 activity in unstimulated cells pre-incubated for 2h with 1,5µM ES048 (SMPD3 specific inhibitor) [124] or 1µM GW4869 (SMPD2 and SMPD3 specific inhibitor) before and after stimulation for 1h or 24h (Fig 15 A). The results demonstrate that both inhibitors have substantial NSM activity inhibition, with ES048 having the best results. We choose to work with this inhibitor for the entire thesis. Surprisingly, the NSM activity is still increased after 24 hours of co-stimulation, and both of the inhibitors keep the NSM activity low. To confirm if the genetic approach CrispR-CAS9 and siRNA (Fig. 15B) have the desired impact on NSM2 expression, we measured the NSM2 activity in those cells. The results demonstrated that both techniques could inhibit NSM activity.

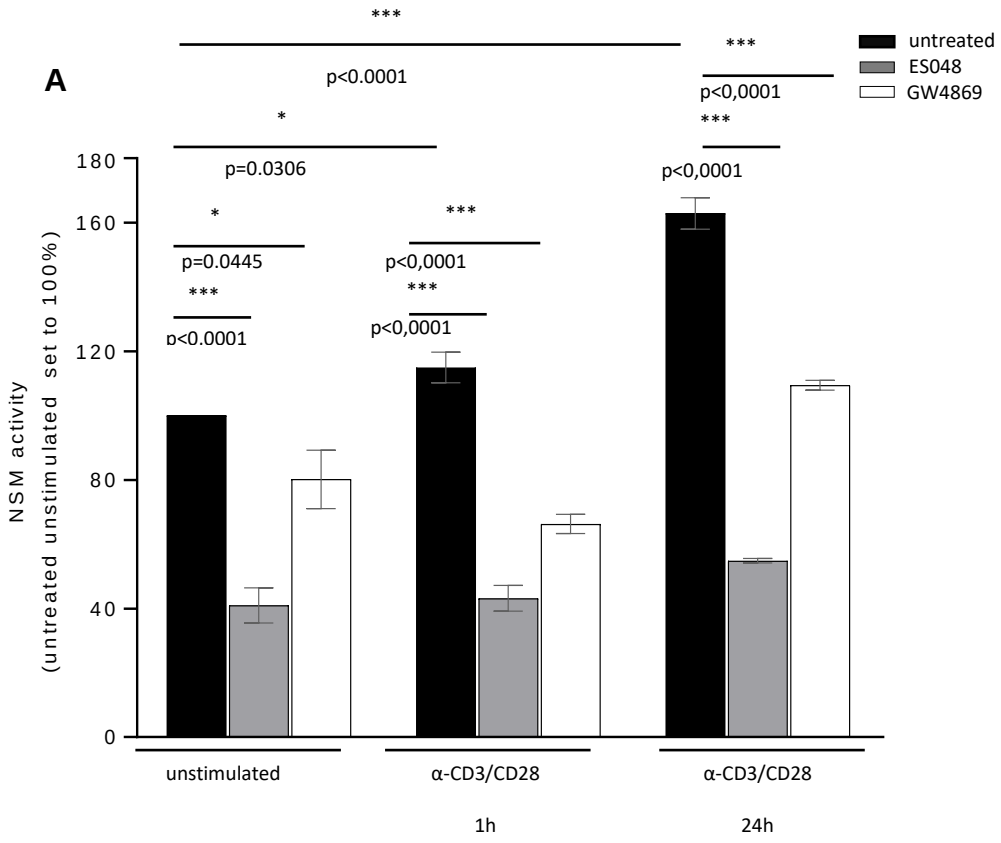

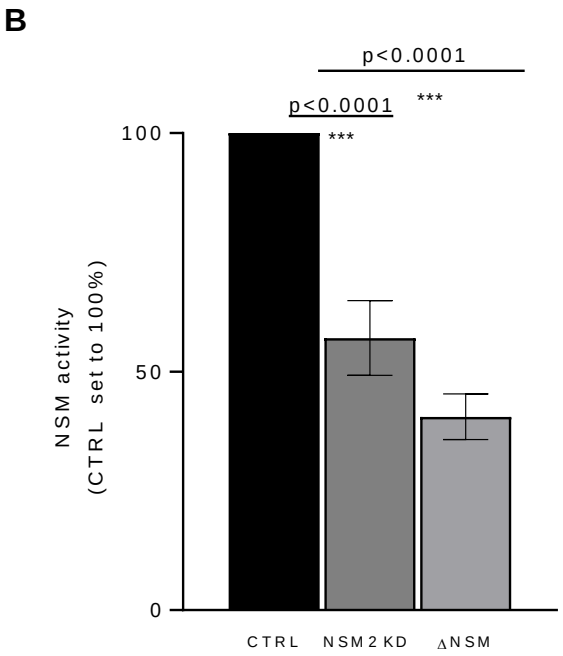

Figure 15. NSM assay. NSM activity was calculated from the HMU-PC fluorescence, after background subtraction. Measurements were normalized. Untreated and unstimulated cells set to 100%. p-value is shown on the top of significant (marked with a *) or not a significant difference (ns).

5.2. NSM2 activity is required to maintain the quiescence of T cells

5.2.1. NSM2 activity interferes in the ATP production

Previous work from our group demonstrated that NSM deficiency renders T cells hyper-responsive to T cell receptor (TCR)/CD28 stimulation [32]. Primary NSM2 KD T cells transfected with NSM2 specific siRNA show enhanced spreading response on stimulatory surfaces and rapid calcium mobilization in the first minutes upon α-CD3/α-CD28 co-stimulation. Sustained calcium flux and ATP production are essential processes in the regulation of T cell signaling and energy metabolism accordingly [131]. To investigate if the initially increased response of NSM2 deficient cells is energetically supported by ATP production, we first quantified the ATP levels in unstimulated primary CTRL and NSM2 KD cells transfected with CTRL and NSM2 specific siRNAs. For the generation of NSM2 KD cells, we used human $CD4^+$ T cells

isolated from peripheral blood that is a mixed population of naïve and memory T cells in the quiescent state, which is defined as cells being in G0 stage with low proliferative and metabolic activity. Unstimulated NSM2 deficient T cells showed significantly higher total ATP levels compared to CTRL cells sufficient for NSM2 (Fig. 16).

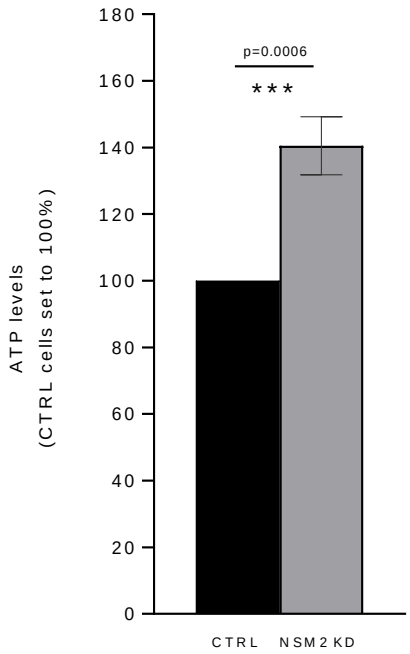

Figure 16. NSM is essential to dampen ATP production in unstimulated T cells. Unstimulated CTRL and NSM2 KD $CD4^+$ T cells were lysed, and total ATP levels were measured. Values obtained from three different donors are normalized against CTRL cells set to 100%. Mean values with standard deviations are shown. The p-value is shown on the top of significance (marked with asterisks).

Ceramide plays a vital role in keeping the mitochondria functionality, being very decisive to control the cellular apoptosis through mitochondria [132]. Recent studies demonstrated the critical role of NSM2 generated ceramides in tubulin dynamics and association with VDAC in mitochondria-associated membranes (MAMs), thereby regulating mitochondrial ADP/ATP transport in astrocytes [33], [122]. To evaluate the T cell-specific role of tubulin in cellular ATP production and accumulation in the

mitochondria, $CD4^+$ human primary T cells were left untreated or pretreated with nocodazole, a drug which disrupts microtubule assembly/disassembly dynamics, for 1h and ATP levels were measured in the lysates of CTRL and NSM2 specific siRNA transfected cells (A) or mitochondria isolated from untreated CTRL and NSM2 inhibitor ES048 treated cells (B) (Fig. 17). The results demonstrated that nocodazole treatment did not affect the total ATP levels (Fig. 17A). Interestingly, preincubation with nocodazole increased ATP levels in the isolated mitochondria from both: untreated CTRL and ES048 treated cells (Fig. 17B). Taken together, these results demonstrate that NSM2 and tubulin are essential to regulate the accumulation of ATP in mitochondria.

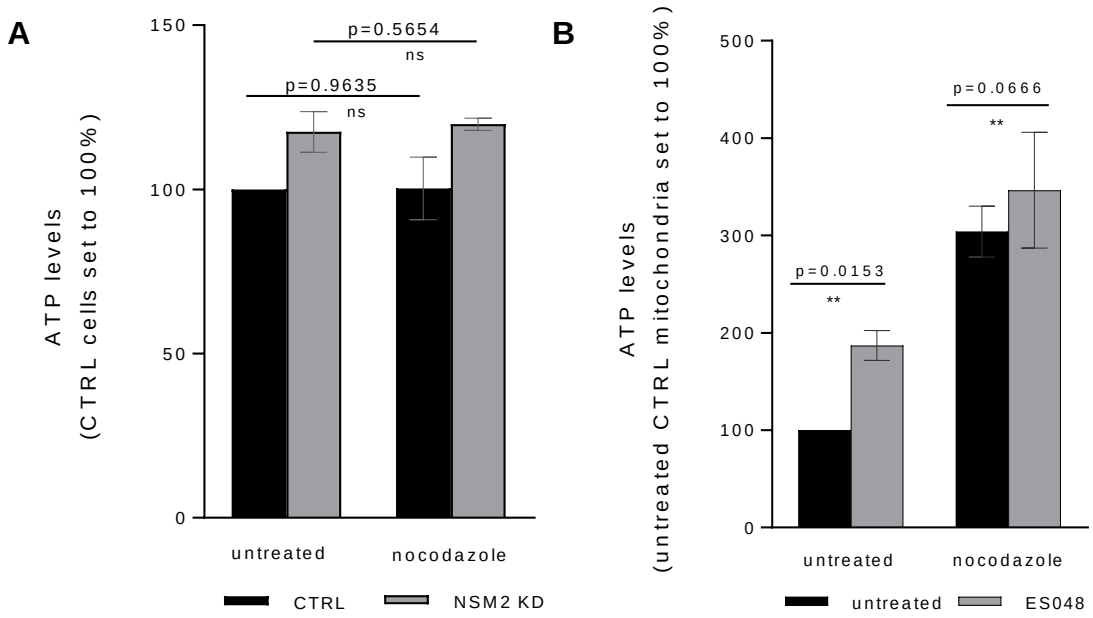

Figure 17. Tubulin and NSM2 dependent regulation of ATP production. Unstimulated $CD4^+$ were left untreated or pre-treated with nocodazole 10µM for 1h, and total (A) or mitochondrial ATP (B) levels were measured. CTRL or untreated cells in black bars. NSM2 KD or ES048 grey bars. Mean values with standard deviations are shown. p-values are shown on the top of significant (marked with asterisks) or not significant differences (ns).

We wanted to investigate the source of the total ATP increase in NSM2 deficient T cells. Therefore, unstimulated CTRL or NSM2 siRNA transfected $CD4^+$ T cells were pre-treated with 1μM oligomycin, to block the mitochondrial ATP production, 25mM 2-Deoxy-D-glucose (2-DG), to prevent the glycolytic ATP production, or with oligomycin and 2-DG together for 20 min. Cells were harvested, and total ATP levels were measured (Fig. 18). The results demonstrate that CTRL cells rely more on the oxidative phosphorylation (OXPHOS) in mitochondria, with the significant inhibition coming from the oligomycin treatment. This is expected from quiescent cells that have reduced glycolytic activity, and rely more on mitochondria to produce ATP [133]. On the contrary, the NSM2 KD cells exhibit a significant ATP production inhibition after both treatments: oligomycin and 2-DG. This indicates that NSM2 KD cells increase glucose utilization during T cell quiescent state while simultaneously keeping the ATP production by OXPHOS.

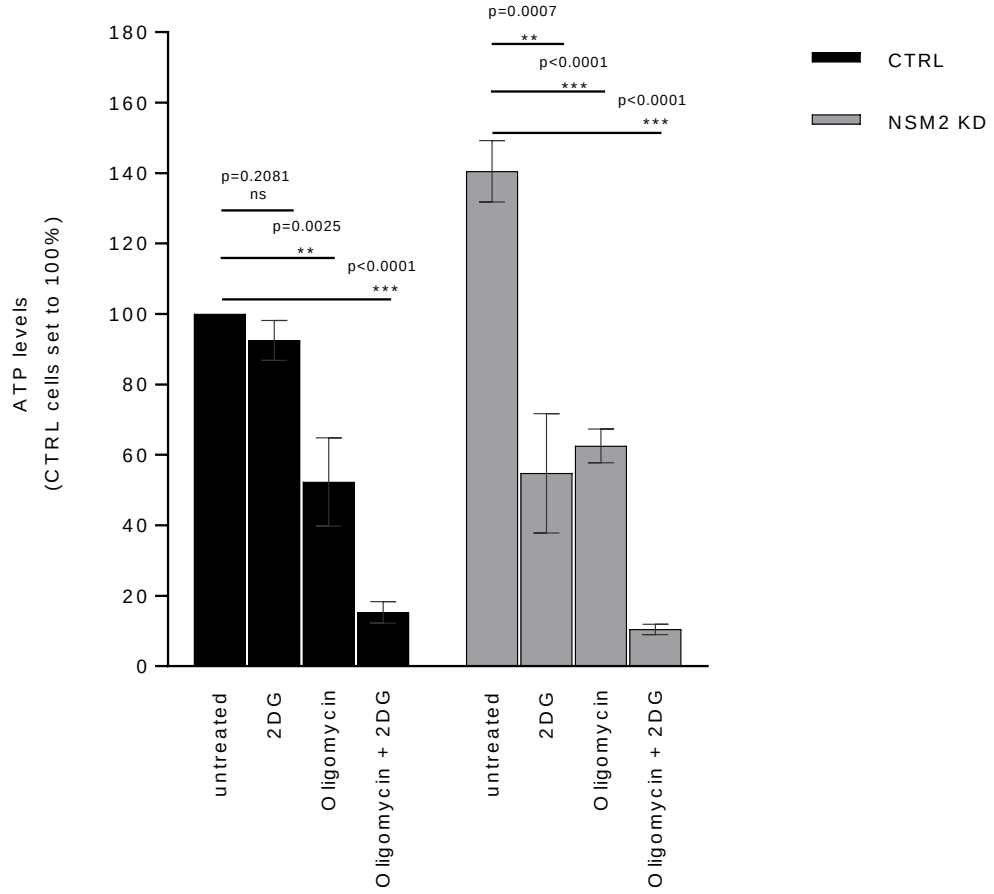

Figure 18. ATP production by OXPHOS and glycolysis in resting NSM2 deficient T cells. Unstimulated $CD4^+$ T cells were pre-treated with 1µM oligomycin or 25mM 2-DG or both together for 20 minutes. Total ATP levels were measured. Mean values with standard deviations are shown. p-values are shown on the top of significant (marked with asterisks) or not significant differences (ns).

5.2.2. Enhanced glucose uptake in NSM2 deficient T cells

Enhanced ATP levels in resting NSM2 deficient cells indicated a heightened glycolytic activity of those cells. Glucose uptake assay was performed to investigate the role of NSM2 in the homeostatic regulation of the glycolytic pathway in unstimulated, non-proliferating T cells. $CD4^+$ T cells were preincubated in the cell culture medium without glucose for 2h, followed by further incubation in medium supplemented with 100µM 6-NBDG, a non-metabolized glucose analog, for 1h and the uptake was measured by flow cytometry. The results showed an elevated 6-NBDG

uptake in NSM2 deficient cells (Fig. 19). Both: pharmacological inhibition with ES048 (Fig. 19A) or genetic ablation (Fig. 19B) of NSM2 resulted in significantly enhanced uptake of glucose analog.

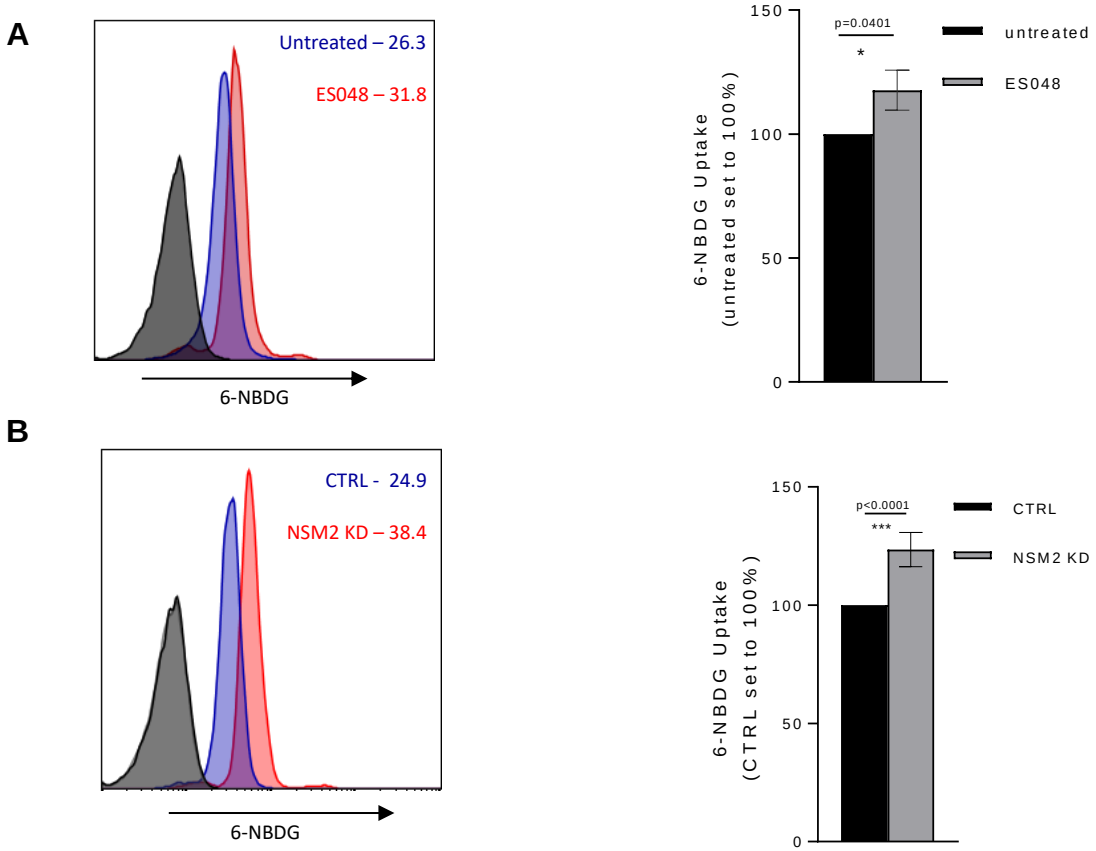

Figure 19. Enhanced glucose uptake in NSM2 deficient T cells. Unstimulated CD4⁺ T cells with pharmacologically inhibited (A) or genetically ablated (B) NSM2 were kept in media without glucose for 2h then incubated with 100μM 6-NBDG for 1h and analyzed by FACS. Representative histograms (left graphs) and a summary of three independent experiments (right graphs) are shown. Data are normalized. Mean values with standard deviations are shown. p-values are shown on the top of significant (marked with asterisks) or not significant differences (ns).

Further on, we analyzed the surface expression of glucose transporter 1 (GLUT1) by flow cytometry. GLUT1 is the most expressed glucose transporter in T cell and, facilitates the transport of glucose across the plasma membranes to fuel the glycolysis [133]. In line with the elevated glucose uptake, the results demonstrated that ES048 treatment (Fig. 20A) and NSM2 genetic ablation (Fig. 20B), both induced enhanced expression of GLUT1 on the cell surface.

Surprisingly, when the total levels of GLUT1 were quantified, we observed an increase of the protein levels in the NSM KD cells (Fig. 21A), but not in pharmacologically inhibited, ES048 treated T cells (Fig. 21B), which possibly are not able to increase GLUT1 protein expression within 2 hours of ES048 pretreatment. The results indicate an essential role of basal NSM2 activity in the regulation of GLUT1 surface expression in T cells.

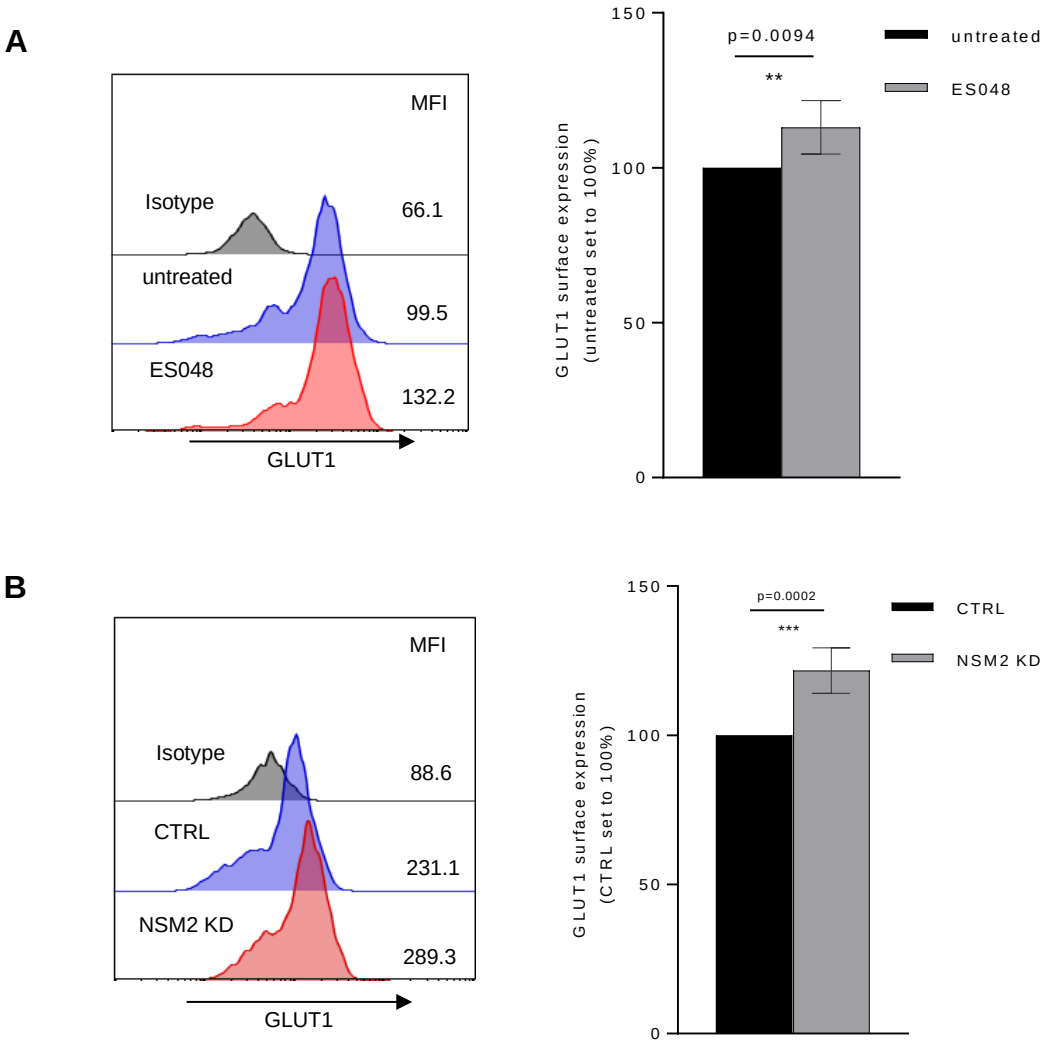

Figure 20. GLUT1 surface expression is increased in NSM2 deficient T cells. Unstimulated CD4⁺ T cells were pharmacologically inhibited (A), or genetically ablated (B) were kept in media without glucose for 2h. GLUT1 surface expression was measured by flow cytometry. Representative histograms (left graphs) and a summary of three independent experiments (right graphs) are shown. Mean values with standard deviations are shown. p-values are shown on the top of significant (marked with an asterisk) or not significant differences (ns).

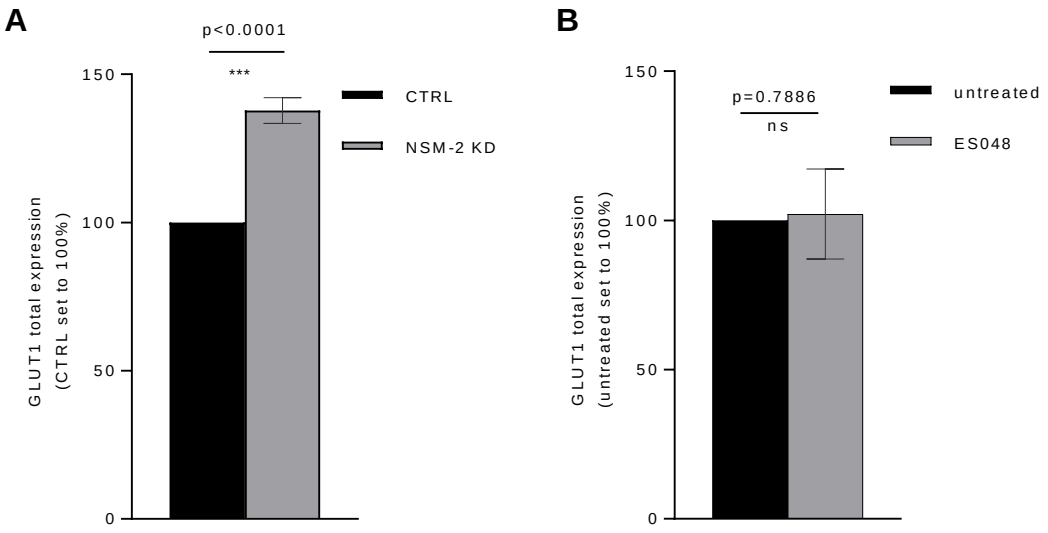

Figure 21. GLUT1 total expression in NSM2 deficient T cells. Unstimulated $CD4^+$ T cells were genetically ablated (A) or pharmacologically inhibited (B) and kept in media without glucose for 2h. GLUT1 total expression was measured by flow cytometry of permeabilized cells. Mean values with standard deviations are shown. p-values are shown on the top of significant (marked with an asterisk) or not significant differences (ns)

As previously shown, NSM2 deficient cells do not support tubulin polymerization and dynamics. Now we show increased ATP accumulation in mitochondria upon nocodazole treatment or NSM2 inhibition, indicating that both: tubulin and NSM2 are essential regulators of mitochondrial ATP transport in T-cells, and NSM2 is affecting mitochondrial ATP accumulation through deregulation of tubulin dynamics.

5.2.3. Hyperactive homeostatic metabolism in NSM2 deficient T cells

NSM2 inhibition promotes enhanced glucose uptake and ATP production via the glycolytic pathway. We performed a metabolic flux analysis, using a seahorse 96XF technology to find out if previously shown data reflects enhanced basal metabolic activity of NSM2 deficient T cells. The seahorse is a powerful tool for measuring glycolysis through medium acidification after lactate production. The OXPHOS is measured as the oxygen consumption rate.

All metabolic flux experiments were performed in T cells treated with the NSM2 inhibitor ES048 since the process of repeated electroporation of specific RNA was increasing cell death in transfected cultures, rendering them unsuitable for seahorse technology depending on high-quality cell culture [134]. Cells were pre-treated for 2 h with ES048, and the glycolytic stress test was performed subsequently. The glycolytic stress consists of 3 following injections: 10mM glucose, 1µM oligomycin, and 25mM 2-DG at different time points after initiation of measurement of the Extracellular Acidification Rate (ECAR). Supporting the previous findings, the NSM inhibition shows the enhanced glycolytic function in unstimulated T cells. The glycolytic stress test in T cells allowed us to calculate non-glycolytic acidification and glycolysis, both of them being significantly elevated in ES048 treated $CD4^+$ T cells, supporting the role of NSM in suppressing the homeostatic glycolytic activity in resting T-cells (Fig. 22).

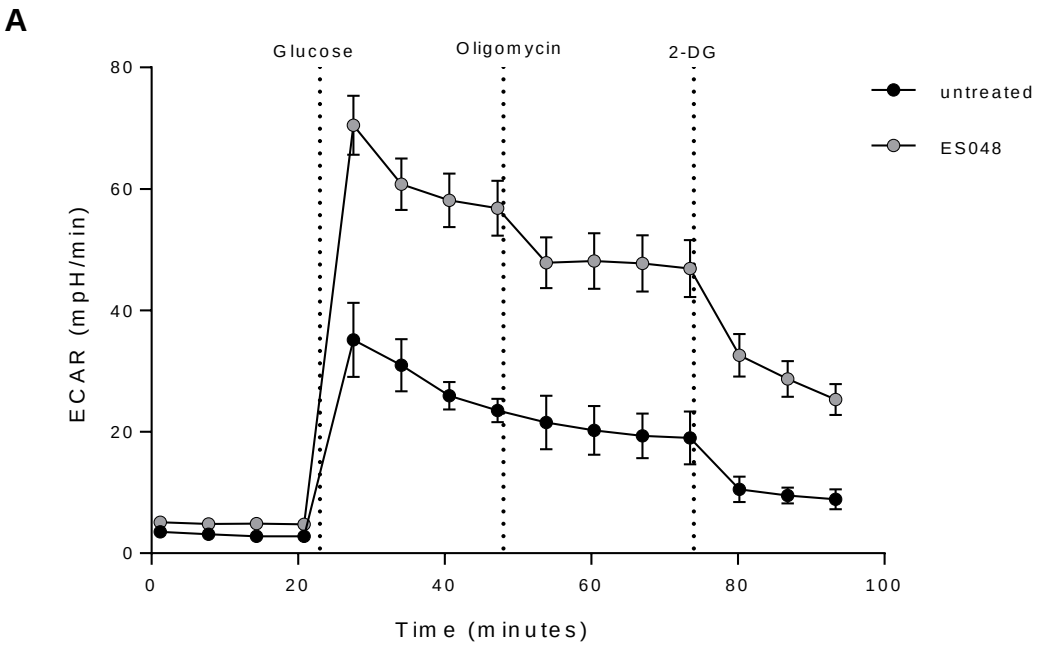

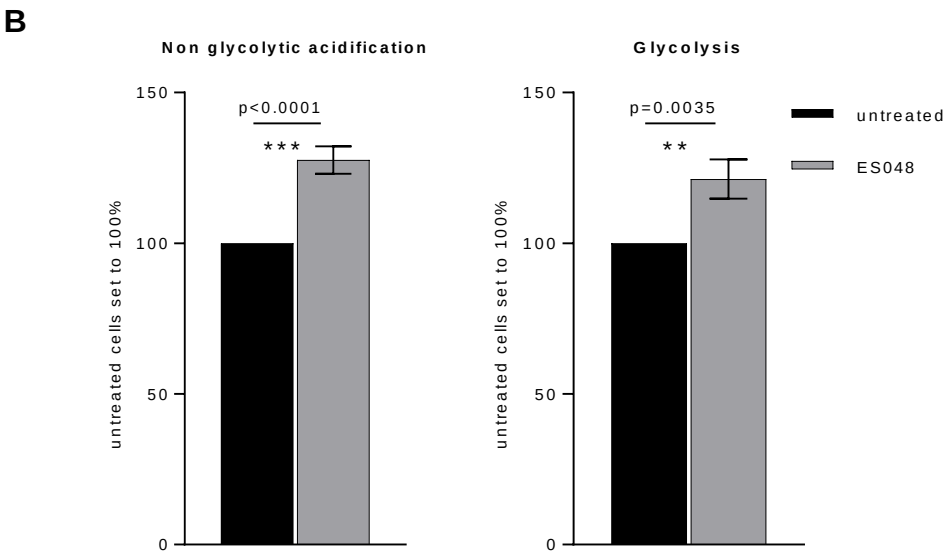

Figure 22. Glycolytic stress test. Unstimulated CD4⁺ T cells were pre-treated with ES048 for 2h, and kinetics of extracellular acidification rate was measured using a seahorse 96XF analyzer. A representative graph of a glycolytic stress test is shown with glucose, oligomycin, and 2-DG injections at subsequent time points. In B, parameters calculated from three independent experiments are shown: non-glycolytic acidification and glycolysis. Mean values with standard deviations are shown. p-values are shown on the top of significant (marked with an asterisk).

As shown above, ATP was accumulating in mitochondria of NSM2 deficient T cells. To determine if the NSM inhibition affects the mitochondrial activity to produce ATP, a mitochondrial stress test was performed. The test consists of 3 subsequently injections (1µM oligomycin, 1,5µM FCCP and 100µM Rotenone (R)/1µM Antimycin(A)) at distinct time points. Kinetics of oxygen consumption rates (OCR) of untreated CTRL and ES048 treated CD4⁺ T cells were measured. T cells showed slightly but significantly elevated OCR after pharmacological NSM2 inhibition. All the measurable parameters (basal respiration, ATP production, maximal respiration, spare respiratory capacity, proton leak, and non-mitochondrial respiration) were elevated, indicating that NSM2 regulates mitochondria metabolic activity in unstimulated T cells (Fig. 23). Taken together, NSM activity is essential to maintain metabolic homeostasis of quiescent T cells.

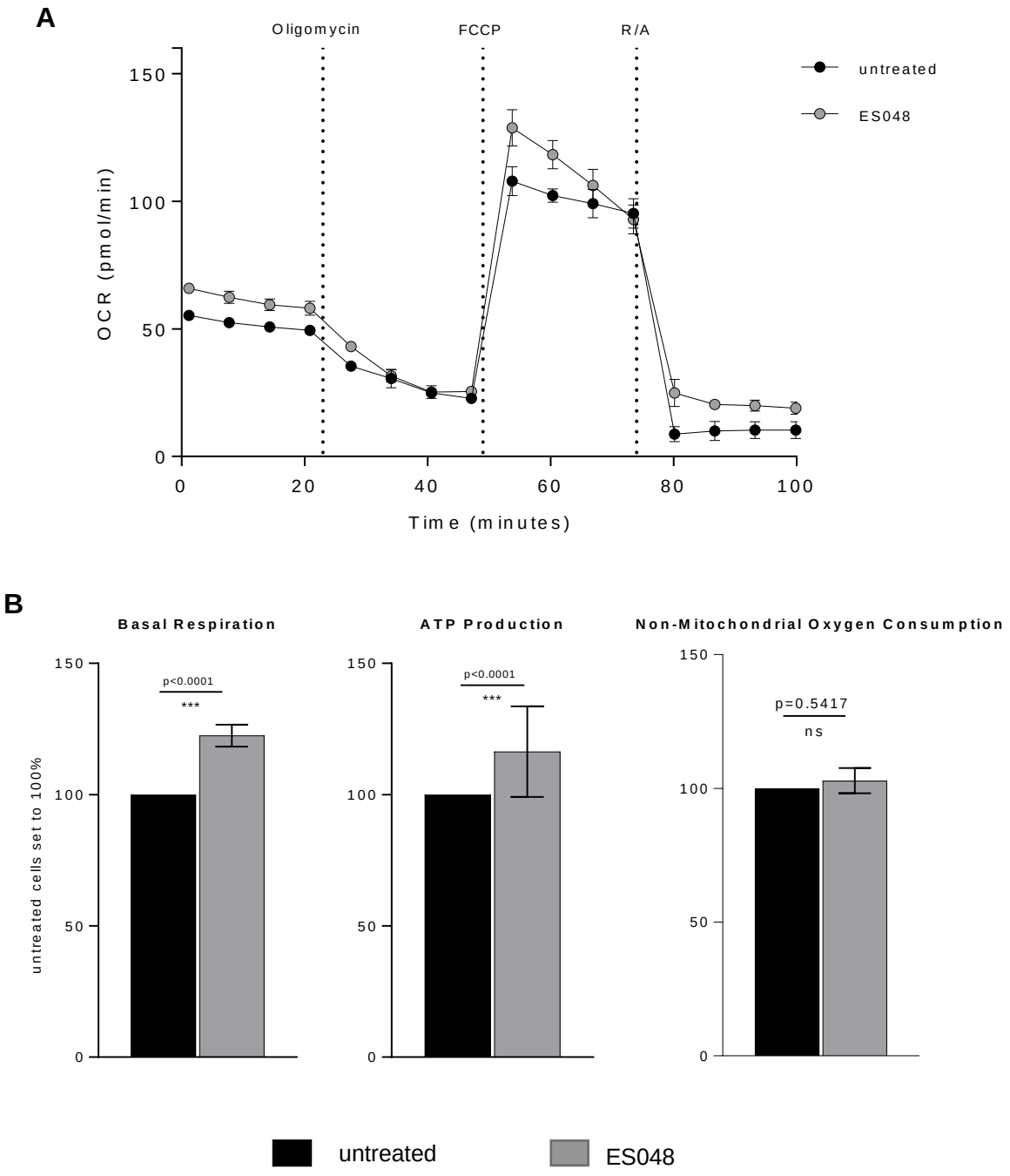
A
Oligomycin
FCCP
R/A
untreated
ES048
OCR (pmol/min)
150
100
50
0
0
20
40
60
80
100
Time (minutes)
B
Basal Respiration
ATP Production
Non-Mitochondrial Oxygen Consumption
untreated cells set to 100%
p<0.0001
***
p<0.0001
***
p=0.5417
ns
150
100
50
0
untreated
ES048

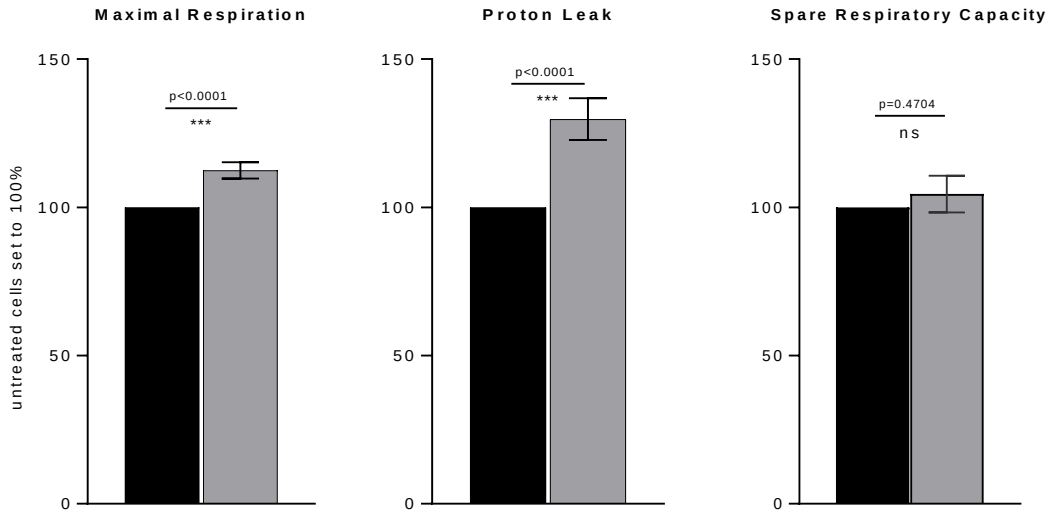

Figure 23. Enhanced metabolic activity of mitochondria in NSM2 deficient cells. Mitochondria stress test was performed in unstimulated $CD4^+$ T cells pre-treated with ES048 for 2h. Oxygen consumption rates were measured using a seahorse 96XF analyzer. Representative graph of a mitochondrial stress test is shown in A. Calculated parameters of mitochondria functionality from three independent experiments: basal respiration, ATP production, maximal respiration, spare respiratory capacity, proton leak, and non-mitochondrial respiration, are shown in B. Mean values with standard deviations are shown. p-values are shown on the top of significant (marked with an asterisk) or not significant differences (ns).

5.3. NSM2 regulates early metabolic responses to antigenic stimulation in T cells

As previously described, the disruption in the NSM activity leads to an enhanced basal metabolic phenotype. The TCR ligation with co-stimulatory molecule CD28 triggers an increase in metabolic activity, induces ATP production to support and initiate cell expansion [135]. The glycolytic switch that occurs following activation plays a vital role in the proliferation and acquisition of effector function [136], [137]. Tonneti et al. [138] described that NSM could be activated after antibody ligation of TCR, indicating the potential role of the enzyme in the regulation of the immune system. The knowledge of the NSM role in TCR dependent signaling is expanding [13], [139], but the relation of sphingolipid and energy metabolism in T cells is still in need to define.

To better apprehend the role of NSM2 in the regulation of the metabolic responses immediately after antigenic stimulation, α-CD3/CD28 antibodies were added to the T cells pretreated or not with ES048 in seahorse metabolic flux analyzer by direct injection followed by measurement of ECAR (Fig. 24A) and OCR (Fig. 24B) levels for several hours. Initially, basal metabolism was measured for 12 minutes before the injection of the stimulatory antibodies. Correlating with the enhanced ATP levels and increased glucose uptake in unstimulated NSM2 deficient cells, the basal levels of ECAR and OCR were higher in ES048 treated compared to untreated T cells. After the injection of α-CD3/CD28 antibodies, T cells enhanced glycolysis about two-fold within minutes after TCR/CD28 stimulation as measured by ECAR, reaching a peak within 15 min and kept the enhanced glycolysis for the duration of the assay. Quantification of the glycolytic flux showed the enhanced ECAR levels in ES048 treated T cells before and immediately after α-CD3/CD28 antibody stimulation (Fig. 24A right graph). OCR levels reflecting mitochondria activity showed a similar tendency, being enhanced in T cells treated with NSM2 inhibitor immediately before and early after TCR/CD28 stimulation (Fig. 24). Quantification of OCR revealed that NSM2 inhibition promoted an increase of basal and stimulated respiration (Fig. 24B).

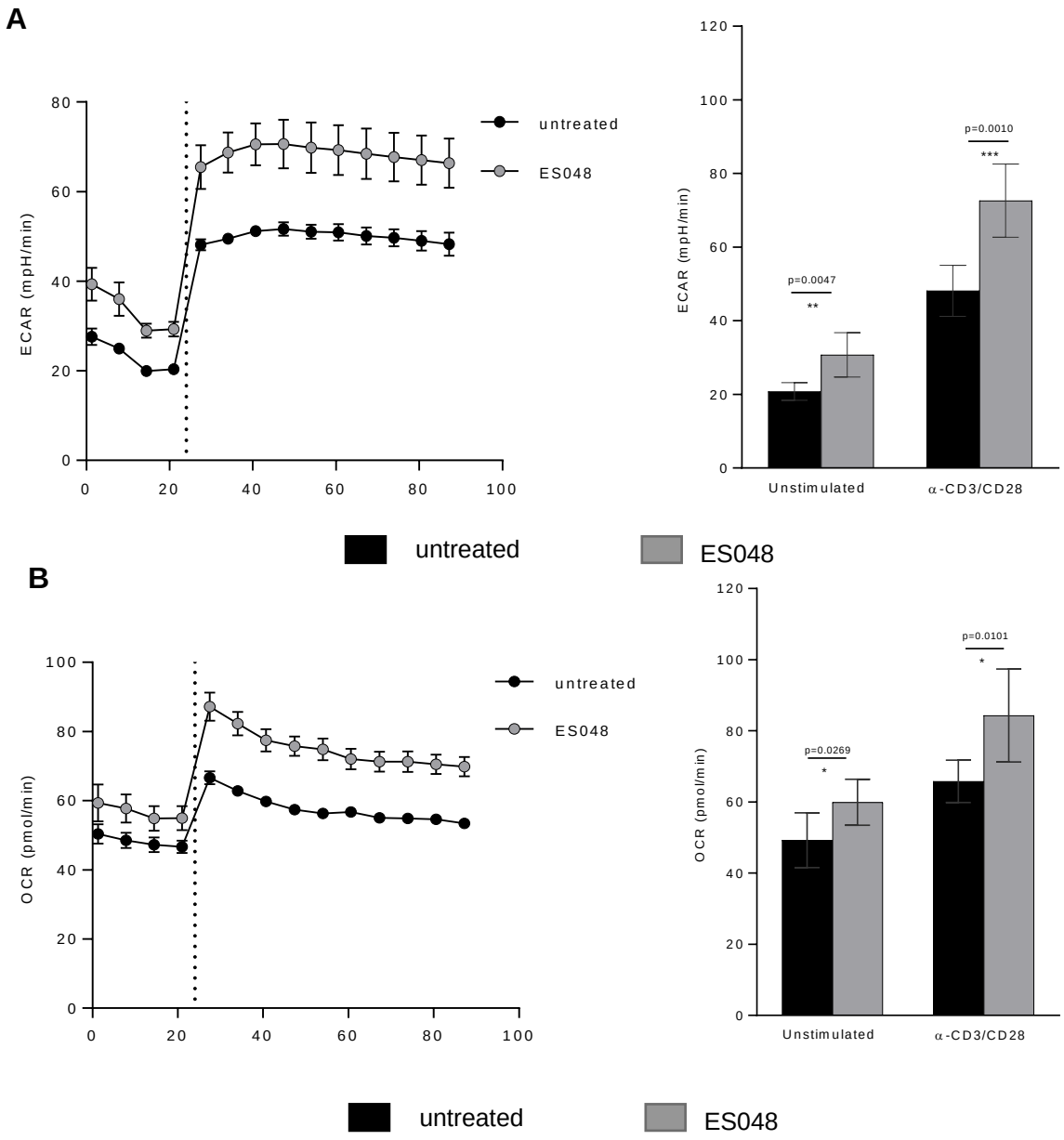

Figure 24. Upregulated ECAR and OCR levels in ES048 treated T cells. ECAR and OCR quantification – Unstimulated CD4⁺ T cells were pre-treated ES048 for 2h, and metabolic flux was analyzed using a seahorse 96XF metabolic flux analyzer. (A) ECAR and (B) OCR were analyzed before and after α-CD3/CD28 injection. The curves of seahorse measurements are shown on the left. Quantification and statistical analysis are shown on the right. Mean values with standard deviations are shown. p-values are shown on the top of significant (marked with asterisks) differences.

The state of energetic metabolism can be pictured as the cell energy phenotype reflecting the relationship of glycolytic and mitochondria respiration activities (Fig. 25). Summarizing the data shown above, the downregulation of NSM2 activity in

unstimulated T cells leads to the highly energetic phenotype which is contained within the first hours after TCR/CD28 co-stimulation.

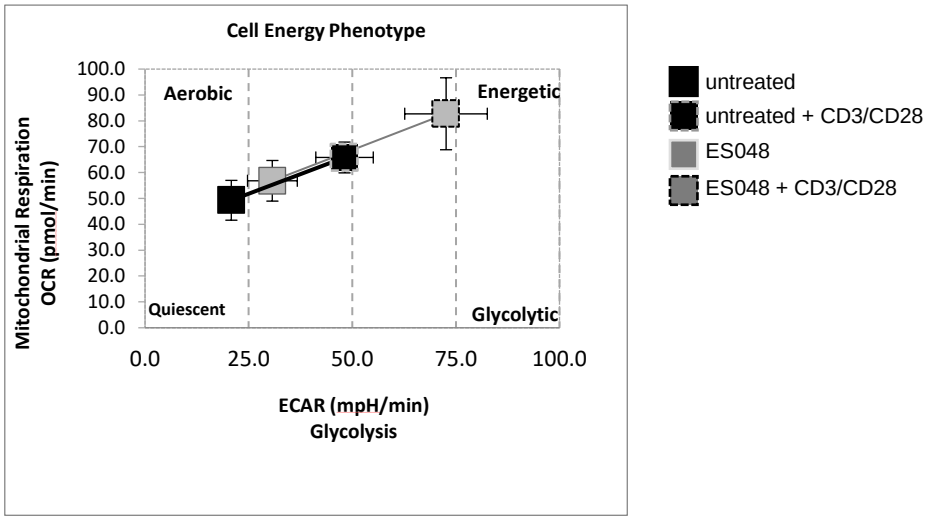

Figure 25. The highly energetic phenotype of ES048 treated T cells. The cell energy phenotype was analyzed using Seahorse Calculator and data shown in Fig.24. Mean values with standard deviations are shown.

As shown above, unstimulated NSM2 deficient T cells produce more intracellular ATP and have enhanced metabolic activity. To investigate if the increased burst of the OCR and ECAR after TCR/CD28 stimulation correlates with an increase in ATP production, the kinetics of ATP levels was measured in CTRL, and NSM KD $CD4^+$ T cells stimulated with α-CD3/CD28 antibodies for 1 hour. We observed a gradual increase of ATP production in both: CTRL and NSM KD cells, within the first 20 minutes after stimulation, whereas ATP levels in NSM2 deficient cells were significantly higher in comparison with the NSM2 sufficient cells (Fig.26A). The boost in ATP production is correspondent with increased GLUT1 surface expression after stimulation with α-CD3/CD28 antibodies (Fig. 26B). Summarizing, the unstimulated NSM KD cells are highly metabolically active in comparison to CTRL cells and respond more vigorously to TCR/CD28 stimulation producing higher levels of ATP early after engagement with stimulatory antibodies.

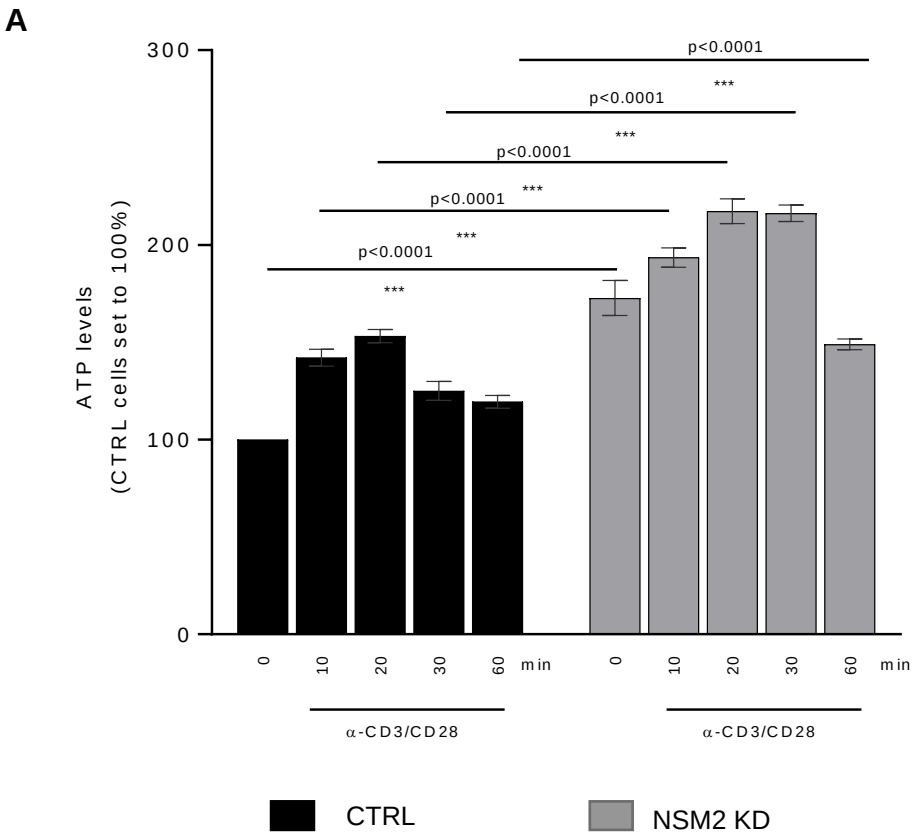
A
300
200
100
0
ATP levels
(CTRL cells set to 100%)
p<0.0001
***
p<0.0001
***
p<0.0001
***
p<0.0001
***
p<0.0001
***
0
10
20
30
60
min
0
10
20
30
60
min
α-CD3/CD28
α-CD3/CD28
CTRL
NSM2 KD

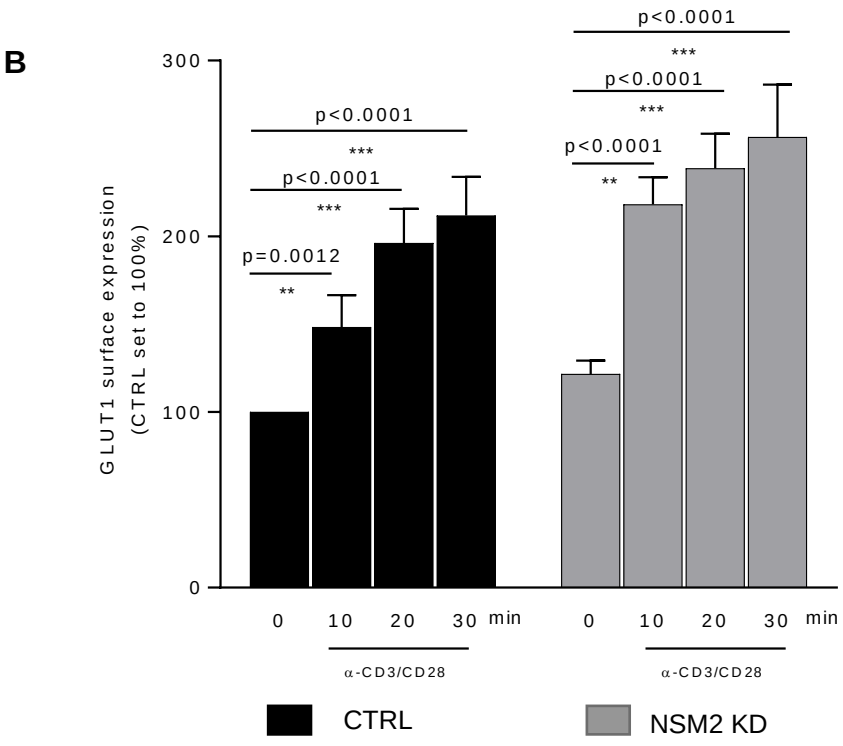
B
300
200
100
0
GLUT1 surface expression
(CTRL set to 100%)
p<0.0001
***
p<0.0001
***
p=0.0012
**
p<0.0001
***
p<0.0001
**
p<0.0001
***
0
10
20
30
min
0
10
20
30
min
α-CD3/CD28
α-CD3/CD28
CTRL
NSM2 KD

Figure 26. ATP production and GLUT1 surface expression in response to α-CD3/CD28 stimulation. CTRL and NSM KD CD4⁺ T cells were stimulated with α-CD3/CD28antibodies, each 1µg/mL for different time points. ATP levels in cell lysates were measured (A) or surface GLUT1 expression (B). Mean values with standard deviations are shown. The p-values are shown on the top of significant (marked with asterisks).

5.4. NSM2 is required to sustain the metabolic activity of stimulated T cells

As shown above, NSM2 is vital to keep the energetic homeostasis of resting T cells. The NSM2 deficiency leads to enhanced metabolic activity and ATP production in unstimulated or shortly stimulated T cells within the first hour of TCR/CD28 ligation. To analyze the effects of NSM2 ablation in the long-term stimulation, untreated or ES048 pretreated CD4⁺ T cells were co-stimulated for 24h on a plate with α-CD3/CD28 1µg/mL for 24h and used for the analysis of energetic metabolism in stimulated T cells. Mitochondria are essential to support T cell proliferation and effector functions [140]. Therefore, first, we analyzed mitochondria functionality and performed a mitochondrial stress test using a seahorse metabolic flux analyzer. Overall levels of OCR were increased in activated CD4⁺ T cells. Nevertheless, the ES048 treated cells showed significantly impaired levels of basal respiration, ATP production, maximal respiration, and non-mitochondrial respiration (Fig. 27).

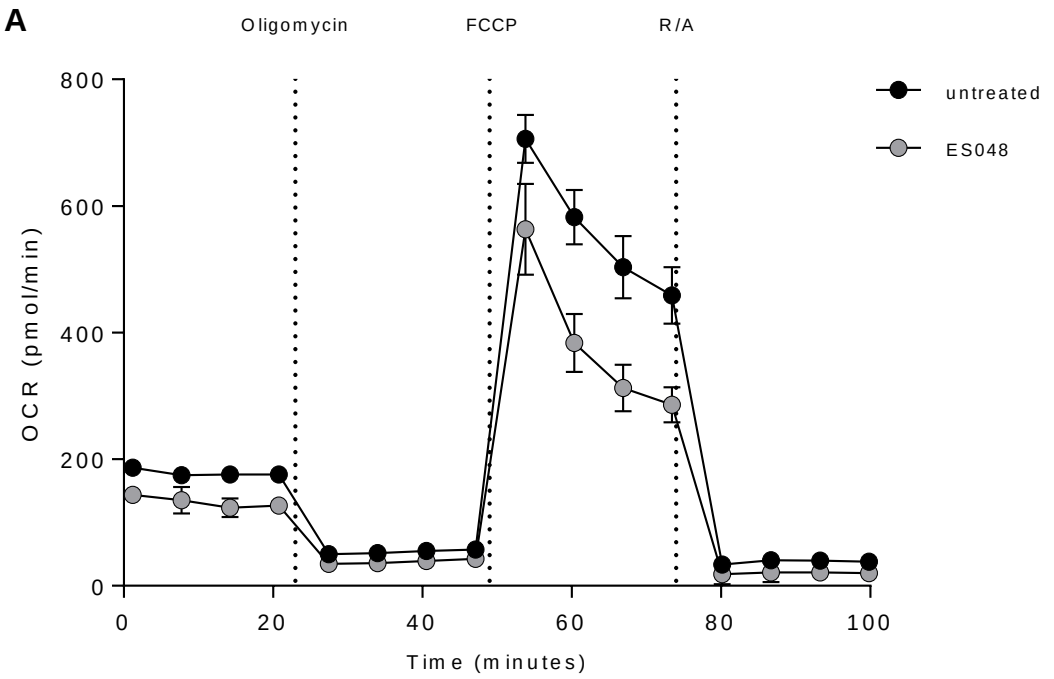
A
Oligomycin
FCCP
R/A
untreated
ES048
OCR (pmol/min)
800
600
400
200
0
0
20
40
60
80
100
Time (minutes)

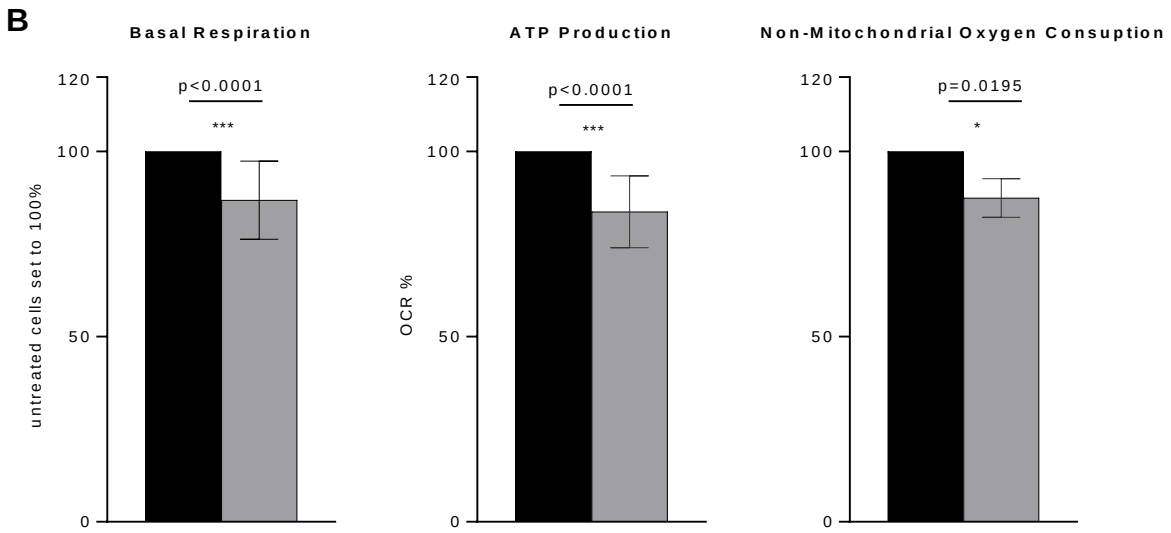
B
Basal Respiration
ATP Production
Non-Mitochondrial Oxygen Consuption
untreated cells set to 100%
OCR %
p<0.0001
***
p<0.0001
***
p=0.0195
*
120
100
50
0

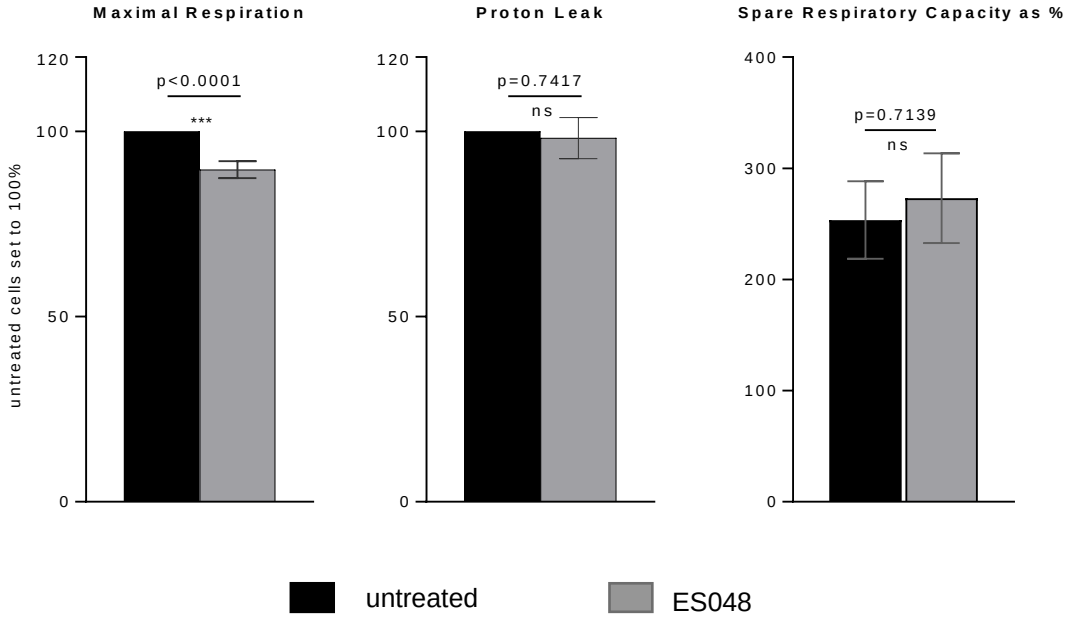

Figure 27. Mitochondrial stress test in activated primary T cells. $CD4^+$ T cells were pre-treated with ES048 for 2h and co-stimulated on a plate with α-CD3/CD28 for 24h and Oxygen Consumption Rate (OCR) was measured using a seahorse 96XF metabolic flux analyzer. Representative graph of one mitochondrial stress test (A) and quantification of basal respiration, ATP production, maximal respiration, spare respiratory capacity, proton leak, and non-mitochondrial respiration (B) are shown. Mean values with standard deviations are shown. p-values are shown on the top of significant (marked with asterisks) or not significant differences (ns).

To better understand how the NSM2 affects the metabolism of activated T cells, we also used Jurkat cells: an immortalized human T cell line [141]. We investigated the mitochondria functionality of Jurkat cells, in which NSM2 was genetically depleted by CrispR/Cas9 [33], from now called ΔNSM. The usage of this cell line gave us the advantage to analyze the effect of NSM2 long term genetic ablation on stimulated T cell metabolism in comparison to the pharmacological inhibition of NSM2 by ES048. Mitochondria stress test performed in ΔNSM cells confirmed the data obtained in primary ES048 treated $CD4^+$ T cells. CTRL cells showed the heightened basal respiration in comparison with the ΔNSM. After FCCP injection, the maximal respiration was significantly reduced in ΔNSM cells, suggesting that the mitochondria functionality is impaired in the absence of NSM. All the calculated mitochondria

parameters, except for the non-mitochondrial oxygen consumption, demonstrated around 50% decrease in comparison with the CTRL cells (Fig. 28).

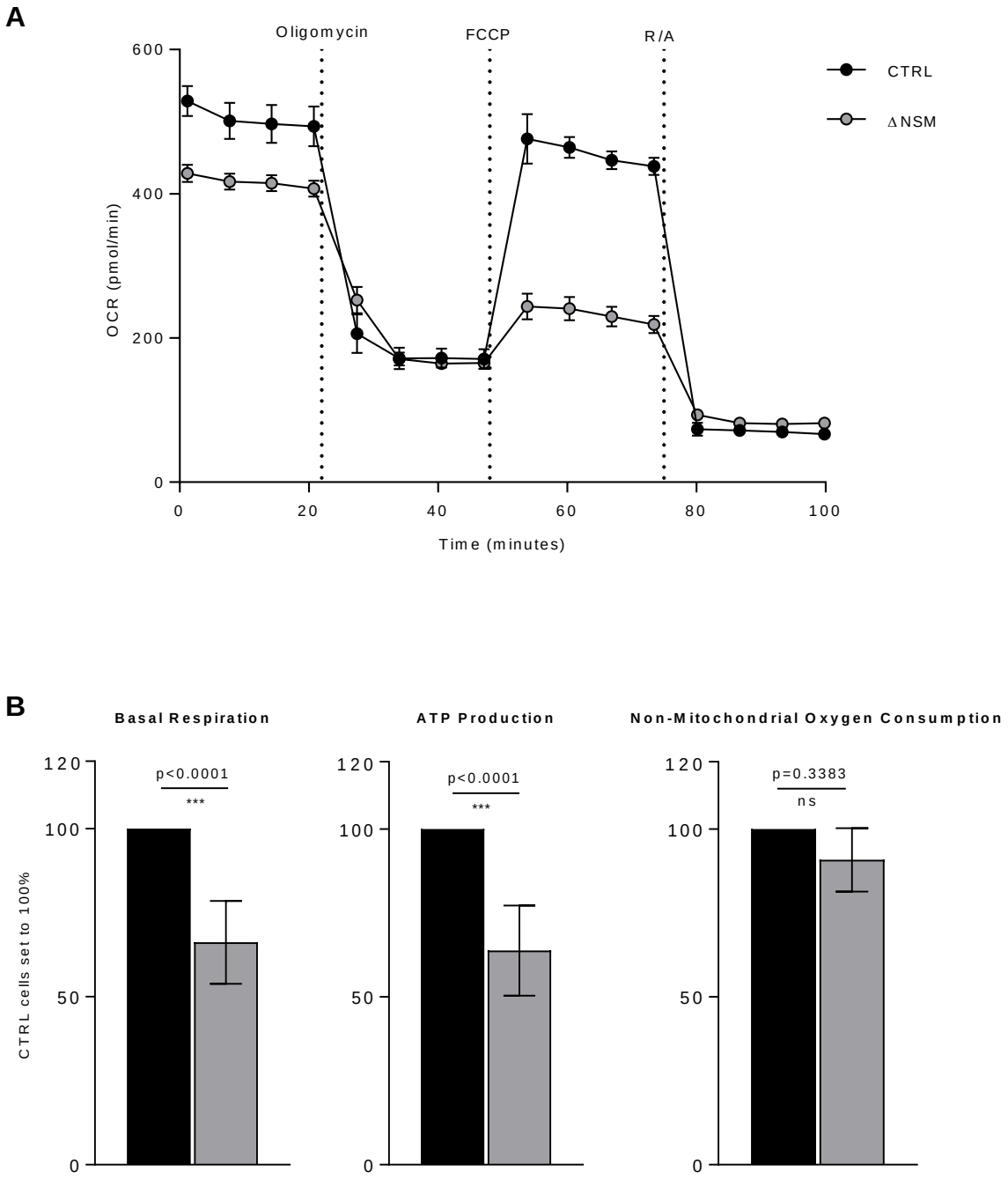

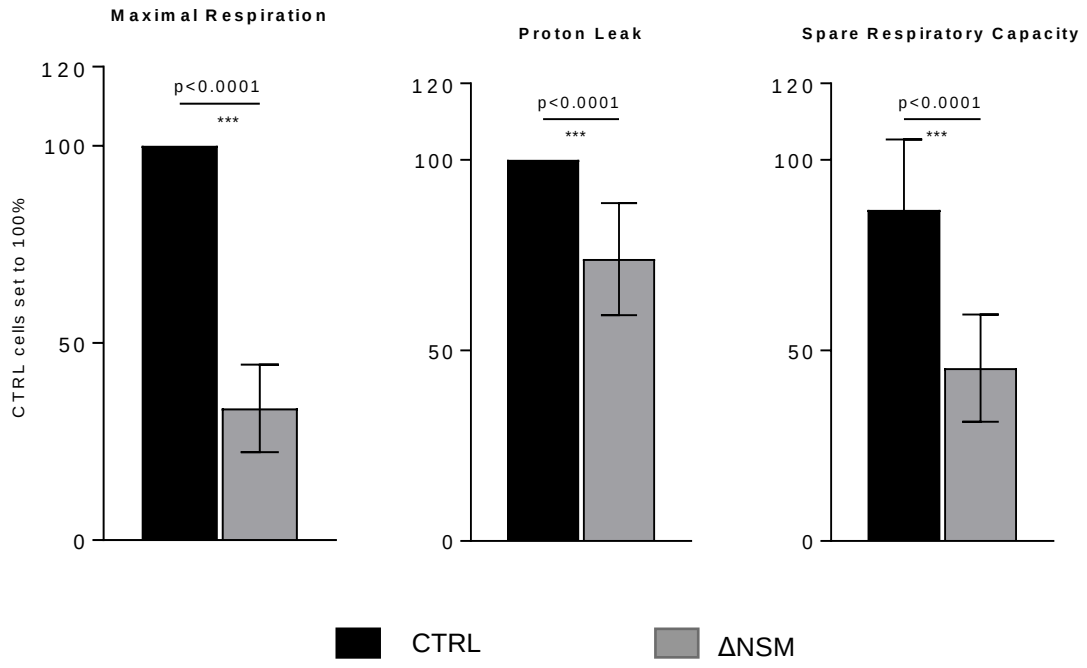

Figure 28. Impaired mitochondria functionality in NSM2 deficient Jurkat cells. Oxygen consumption rate (OCR) was measured in CTRL and ΔNSM Jurkat cells using a seahorse 96XF metabolic flux analyzer. Representative graph of a mitochondrial stress test (A) and quantification of basal respiration, ATP production, maximal respiration, spare respiratory capacity, proton leak, and non-mitochondrial respiration (B) are shown. Mean values with standard deviations are shown in the graphs. p-values are shown on the top of significant (marked with asterisks) or not significant differences (ns).

A glycolytic stress test was performed to evaluate the effects of NSM inhibition on the glycolytic pathway in activated T cells. Unexpectedly, the stress test did not show significant differences between glycolytic activities of untreated and ES048 pretreated cells (Fig. 29). Only non-glycolytic acidification was significantly decreased in ES048 treated cells, which could be related to the NSM2 regulated production of respiratory CO_2 generated by the TCA cycle.

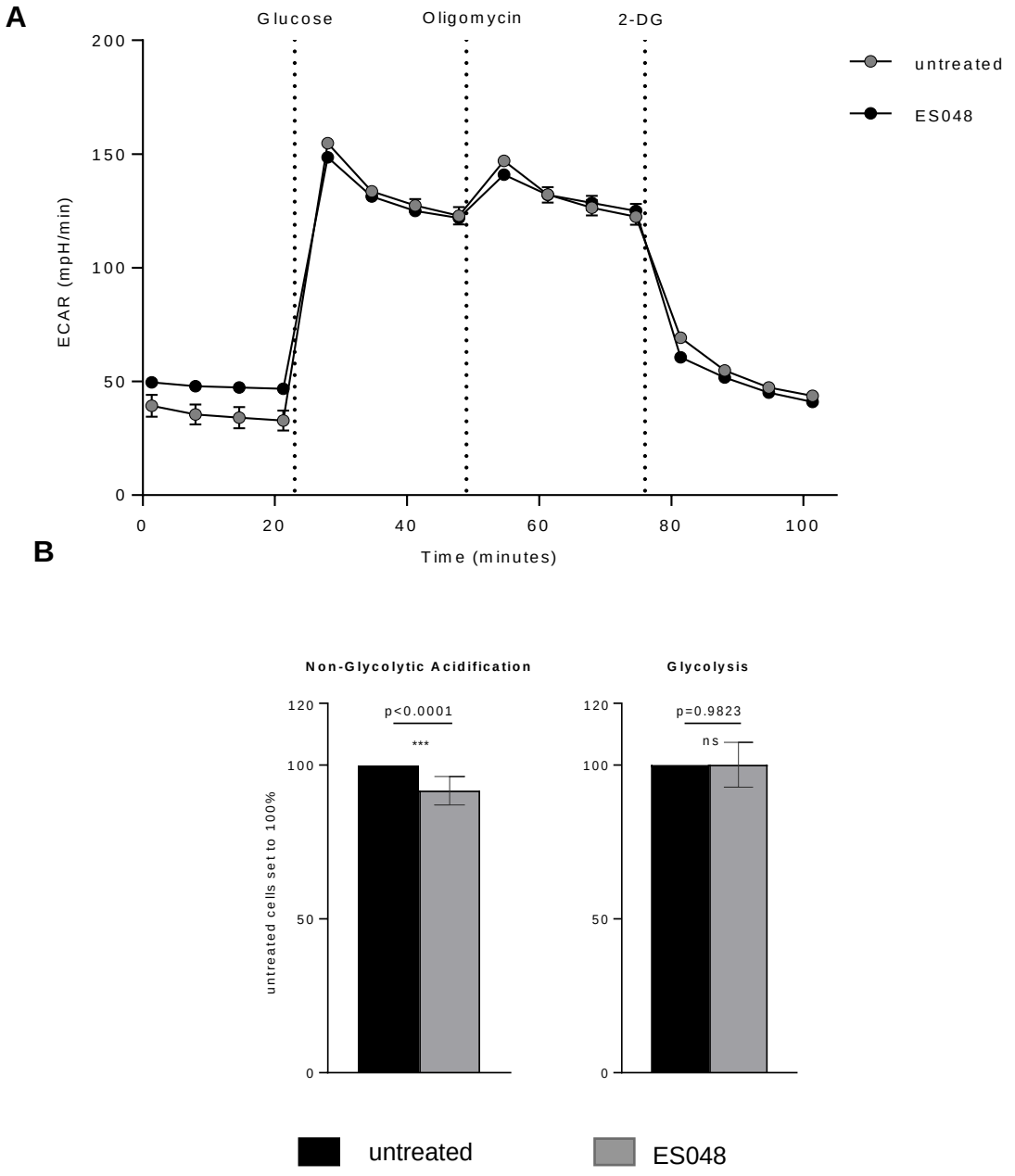

Figure 29. Glycolytic stress test in TCR/CD28 stimulated T cells. CD4⁺ T cells were pre-treated with ES048 for 2h and co-stimulated on a plate with α-CD3/CD28 for 24h. Extracellular acidification rate (ECAR) was measured using a seahorse 96XF metabolic flux analyzer. Representative graph of a glycolytic stress test (A) and quantification of non-glycolytic acidification, glycolysis (B) are shown. Mean values with standard deviations are presented. p-values are shown on the top of significant (marked with asterisks) or not significant differences (ns).

The glycolytic stress test performed in ΔNSM Jurkat cells confirmed NSM2 independent regulation of glycolytic activity of activated T cells (Fig. 30).

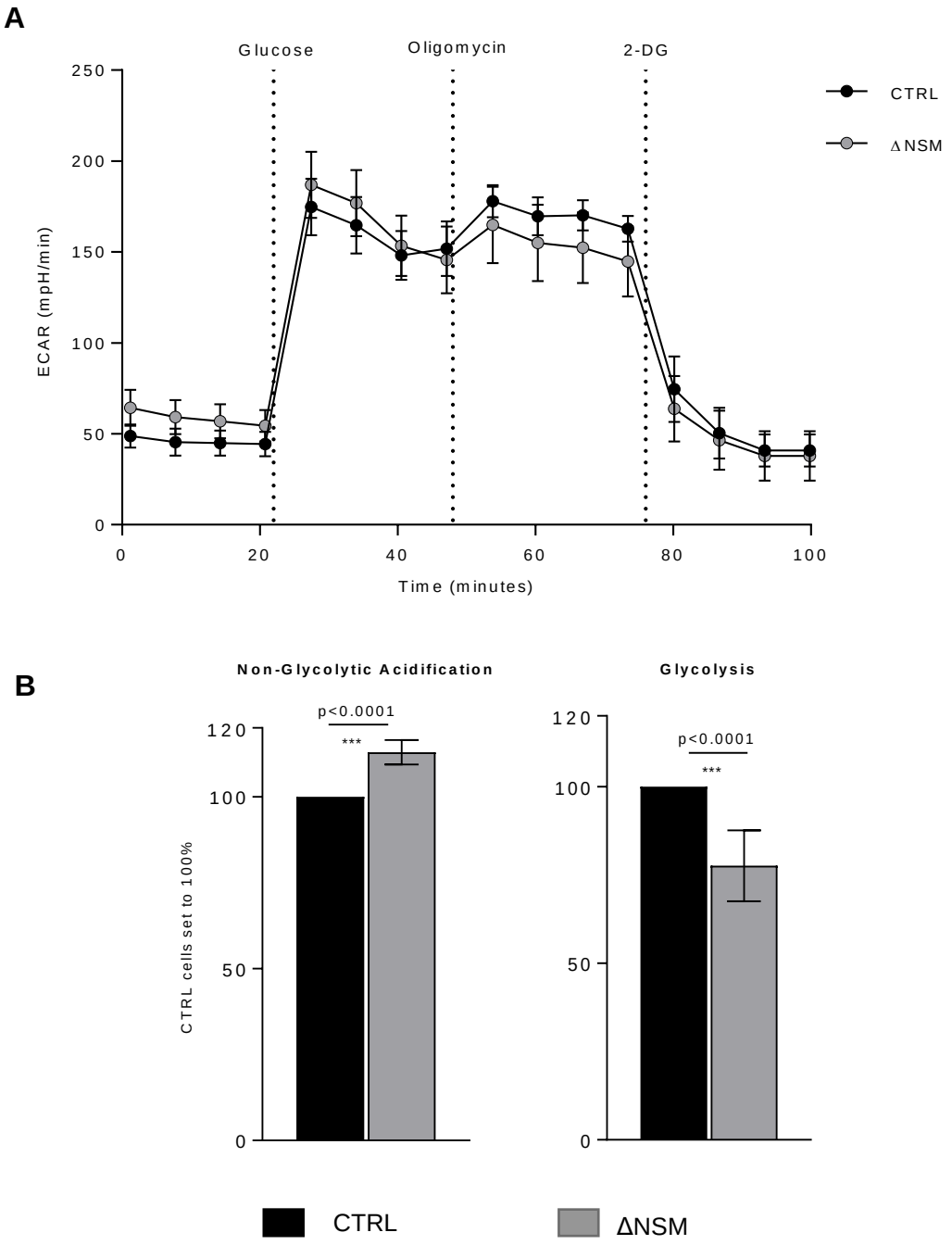

Figure 30. Glycolytic stress test in NSM2 deficient Jurkat cells. $CD4^+$ T cells were pre-treated with ES048 for 2h and co-stimulated on a plate with α-CD3/CD28 for 24h. Extracellular acidification rate (ECAR) was measured using a seahorse 96XF metabolic flux analyzer. Representative graph of a glycolytic stress test (A) and quantification of non-glycolytic acidification, glycolysis (B) are shown. Mean values with standard deviations are presented. p-values are shown on the top of significant (marked with asterisks) or not significant differences (ns).

To analyze the glycolytic activity in NSM2 deficient cells, we measured GLUT1 protein levels (Fig. 31) and the glucose uptake (Fig. 32) in $CD4^+$ T cells treated with ES048 (Fig. 31A/32A) transfected with NSM2 specific siRNA (Fig. 31B/32B) or ΔNSM Jurkat cells (Fig. 31C).

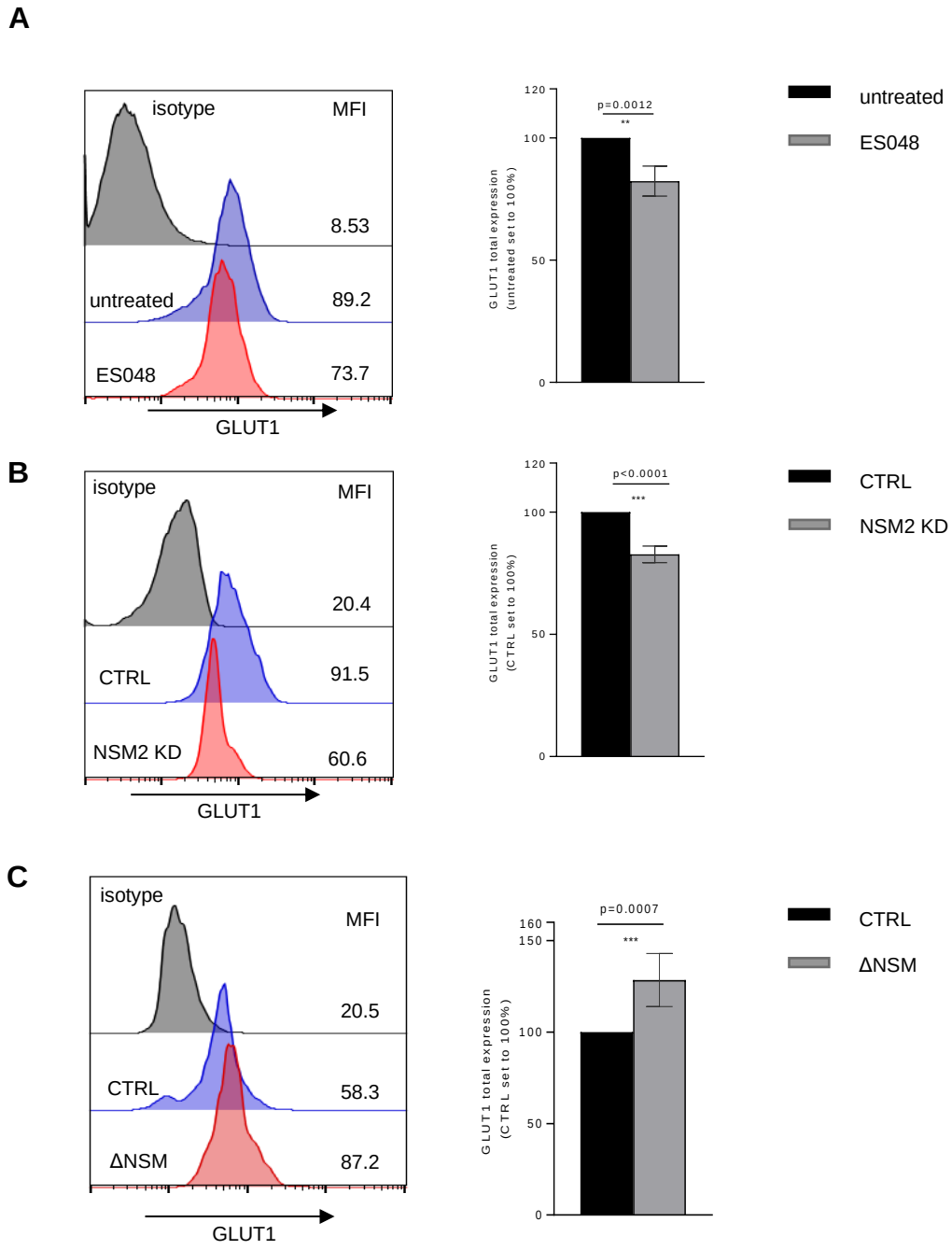

Figure 31. GLUT1 total expression– CD4+ were co-stimulated on a plate with α-CD3/CD28 for 24h. CD4+ pharmacologically inhibited (A), genetically ablated (B), or Crispr/cas9 Jukarts (C) were kept in media without glucose for 2h. GLUT1 total expression by flow cytometry. On the left, representative histograms. Mean values with standard deviations are shown. p-values are shown on the top of significant (marked with asterisks) or not significant differences (ns)

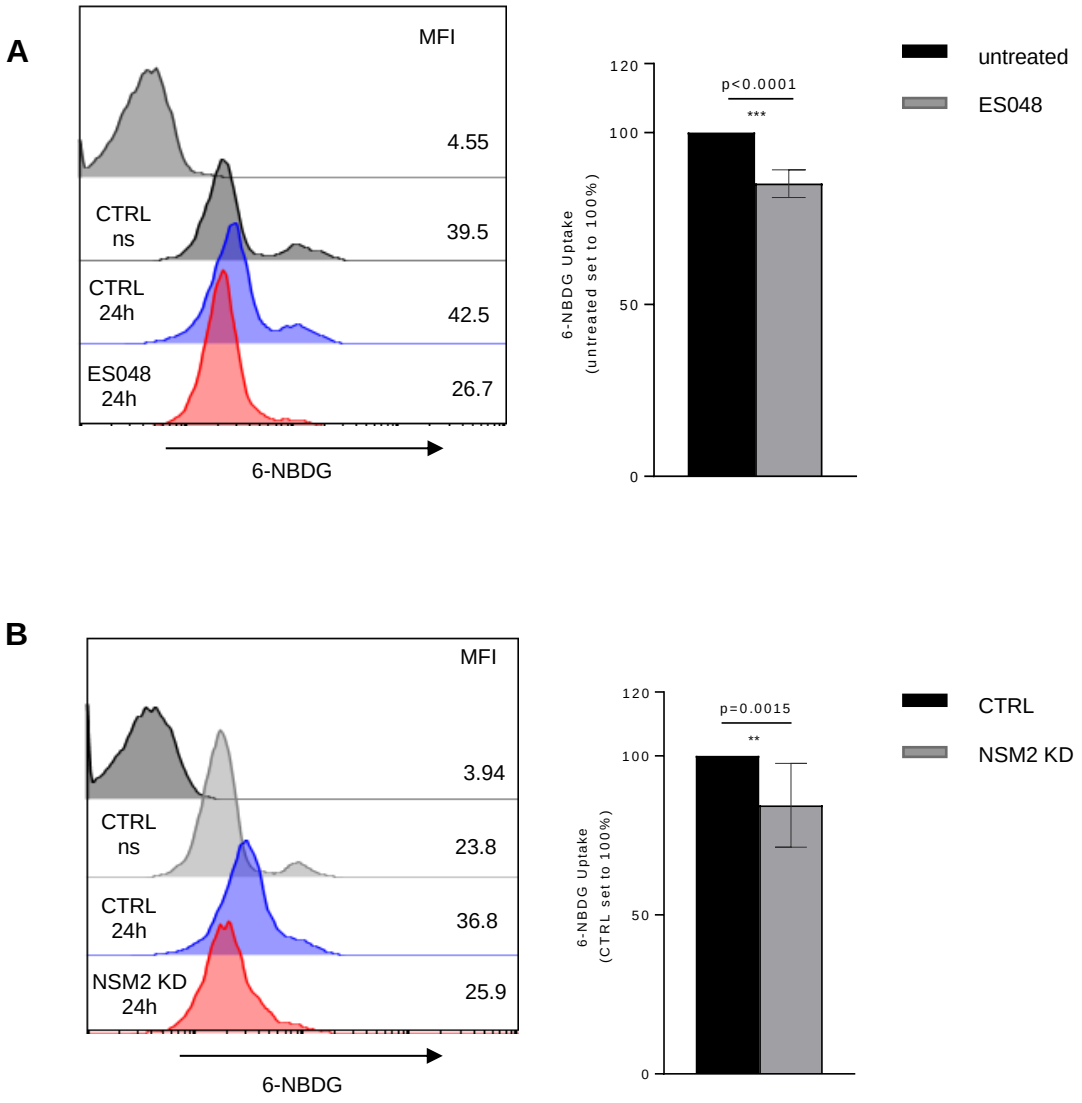

Figure 32. 6-NBDG uptake – CD4+ were co-stimulated on a plate with α-CD3/CD28 for 24h. CD4+ pharmacologically inhibited (A) or genetically ablated (B) was kept in media without glucose for 2h, and 100μM 6-NBDG was added for 1h and measured by flow cytometry. On the left, representative histograms. Mean values with standard deviations are shown. p-values are shown on the top of significant (marked with asterisks) or not significant differences (ns).

We analyzed expression levels of glycolytic enzymes: hexokinase II, aldolase a and GAPDH, in CTRL and NSM2 KD cells after 24 and 48 hrs of co-stimulation. Both CTRL and NSM2 KD T cells upregulated the expression of those proteins upon stimulation (Fig. 33) with NSM KD cells showing even enhanced protein levels after

stimulation. The results demonstrated that NSM2 absence could negatively affect the GLUT1 expression induced by TCR/CD28 activation (Fig. 31 A, B). For a consequence, a decrease in 6-NBDG uptake was also observed in those cells (Fig. 32 A, B).

Nevertheless, after stimulation, cells can upregulate different types of glucose and amino acids transporters, in line with the unimpaired glycolytic stress test in the NSM deficient cells, there is no difference in the glycolytic stress test (Fig. 29) [142]. We did not observe the downregulation of GLUT1 proteins in ΔNSM Jurkat cells (Fig 31C). Cancer cells are more dependent on glycolysis [143]; therefore, they can sustain the elevated GLUT1 protein levels, even if they lack NSM2.

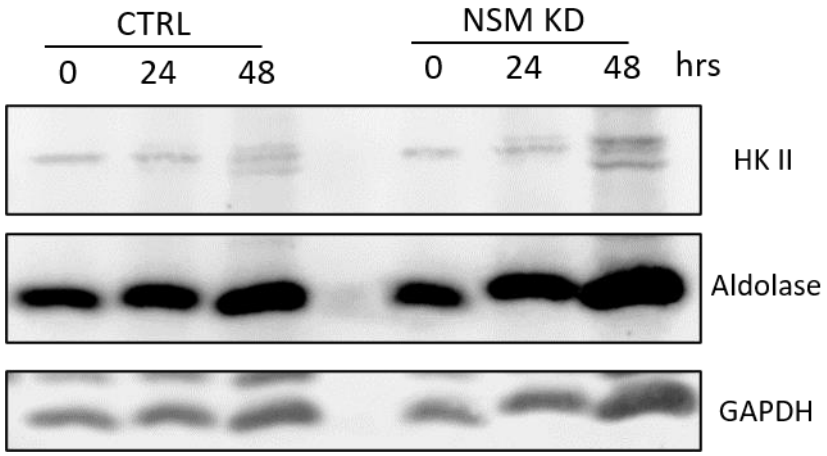

Figure 33. Glycolytic protein expression is unaltered in NSM2 KD cells. $CD4^+$ T cells were left unstimulated or co-stimulated on a plate with α-CD3/CD28 for 24h, or 48h, and expression of key glycolytic enzymes was analyzed by western blot.

Activated T cells increase ATP production to meet the enhanced energetic requirements [144]. We measured the ATP production in overnight stimulated CTRL, or NSM2 specific siRNA transfected $CD4^+$ T cells. Correlating with the stress tests (Fig. 22 and 23), CTRL cells have 45% more ATP then NSM KD cells. We also analyzed which metabolic pathways are used to produce ATP in activated NSM2 deficient T cells

(Fig. 34). 2DG treatment was highly effective in CTRL cells, inhibiting the ATP production by about 70%.

In contrast, the oligomycin treatment reduced ATP production by approximately 25%, indicating that the glycolytic pathway is a significant source of ATP in TCR/CD28 co-stimulated T cells. In contrast, stimulated NSM KD $CD4^+$ T cells show significantly reduced ATP levels which are not affected considerably by oligomycin and 2DG treatments. Altogether, results indicate that NSM2 is necessary for the metabolic switch to glycolysis as the primary source for energy in TCR stimulated T cells.

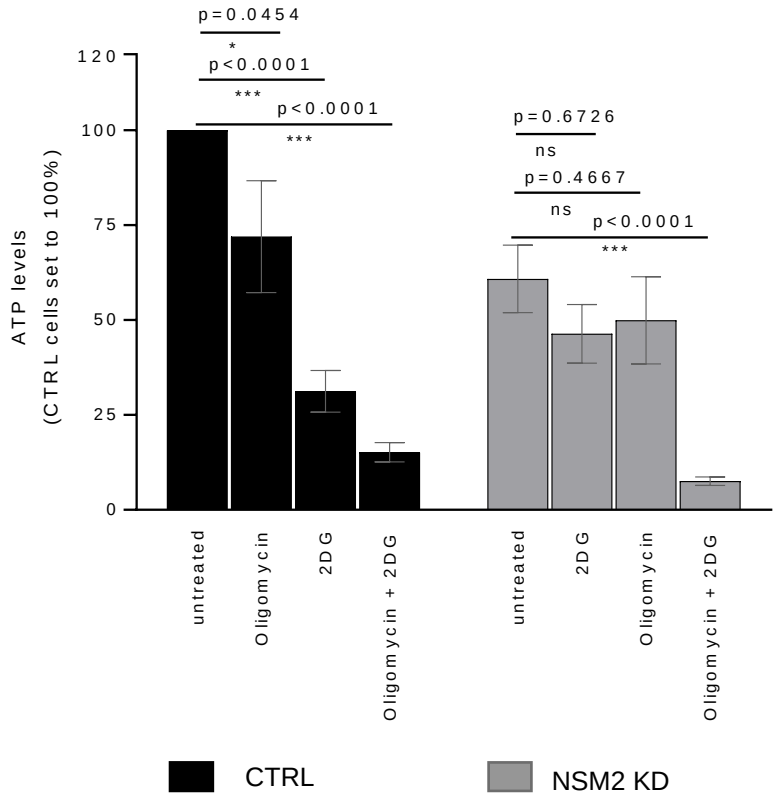

Figure 34. ATP production in stimulated T-cells is NSM2 dependent. $CD4^+$ T cells were co-stimulated on a plate with α-CD3/CD28 for 24h, left untreated or pre-treated with oligomycin, 2-DG, or both for 20 minutes and total ATP levels were measured in cell lysates. Mean values with standard deviations are shown. p-values are shown on the top of significant (marked with asterisks) or not significant differences (ns).

Even so stimulated NSM2 sufficient and deficient T cells showed similar glycolytic stress responses, only NSM2 expressing T cells use glycolysis as the main source for ATP production to support activation. Next, we investigate if NSM2 can regulate the VDAC protein expression, and therefore affect the mitochondrial functionality (Fig. 35). We observed that CTRL and NSM2 cells do not show differences in VDAC levels in any of the time points analyzed by western blot.

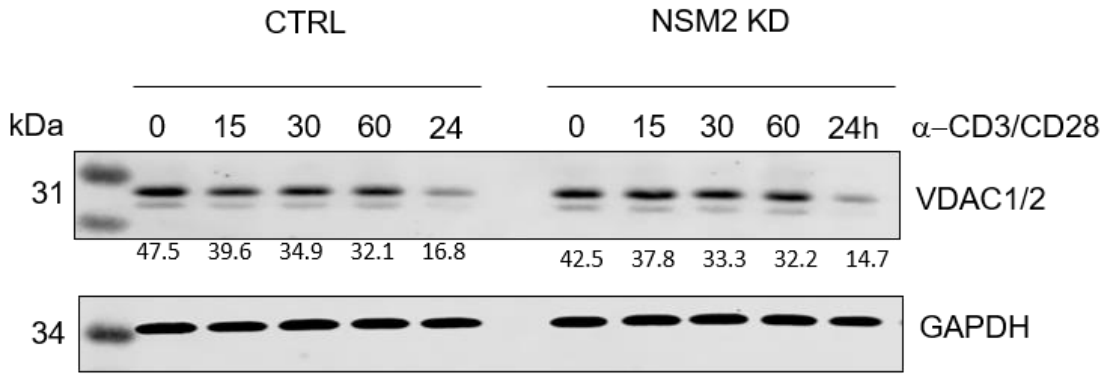

Figure 35. NSM2 independent VDAC protein expression T cells. CTRL and NSM KD $CD4^+$ T cells were stimulated with α-CD3/CD28 antibodies for different time points, and VDAC was detected by Western blot.

Taken together, the results establish dependency of NSM2 in the regulation of mitochondrial activity, without directly affecting the aerobic glycolysis.

5.5. NSM2 is necessary to sustain mTOR pathway activity in activated T cells

To uncover what determines the downregulation of mitochondrial activity, we aimed to analyze the mammalian target of rapamycin (mTOR). According to its role as a master regulator of cell growth, nutrient sensor, and mitochondria oxidative metabolism, mTORC1 activity is modulated by different extracellular signals and intracellular mechanisms [145], [146]. To understand how mTOR signaling is affected by NSM ablation, we analyzed the phosphorylation of MTOR upon stimulation using confocal microscopy and phosphorylation of its downstream target ribosomal protein S6 by flow cytometry and Western blot. We observed fast and strong phosphorylation of MTOR in the synapses between NSM2 KD T cells and stimulatory α-CD3/CD28 coated beads, as shown by the confocal microscopy images and quantification of the mean fluorescence after 20 min of stimulation (Fig. 36A). Phosphorylation of S6 analyzed by flow cytometry followed the pattern of pMTOR by significantly increased mean fluorescence of pS6 in NSM2 deficient cells 20 and 30 min after stimulation (Fig. 36B) is repeated with fast and robust phosphorylation happening in the NSM2 KD cells, in the first minutes. These results corroborate with previously published results showing hyperactive early signaling in NSM2 KD T cells [32].

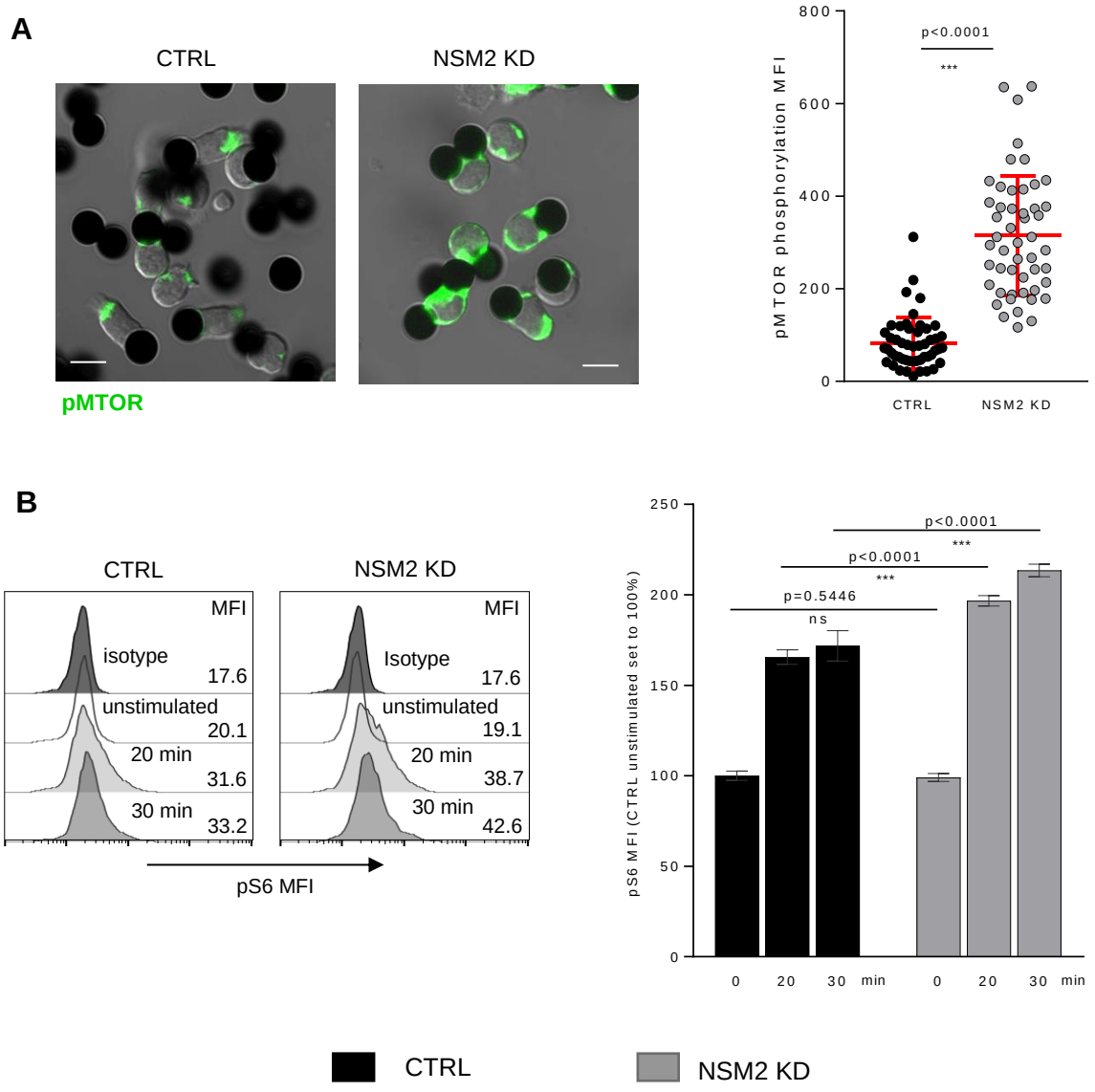

Figure 36. NSM2 dampens the early activation of the mTOR pathway in T cells. pMTOR and pS6 quantification– CTRL and NSM2 KD cells were stimulated with α-CD3/CD28 coated beads (A) or soluble α-CD3/CD28 antibodies (B) for different time points, and pMTOR (A) and pS6 (B) was measured by confocal microscopy or flow cytometry accordingly. Mean values with standard deviations are shown. p-values are shown on the top of significant (marked with asterisks) or not significant differences (ns).

To analyze the mTOR pathway in activated T cells NSM2 KD and CTRL cells were stimulated with α-CD3/CD28 for 24 hours, and signal intensities of phosphorylated mTOR and S6 proteins were analyzed by confocal microscopy and flow cytometry (Fig. 37).

Surprisingly, the strong and robust phosphorylation of mTOR and S6 observed in NSM2 deficient cells shortly after stimulation was not sustained and was significantly reduced after 24h of α-CD3/CD28 co-stimulation. Data analysis showed about a 30% reduction in mean fluorescence intensities of pMTOR and pS6 in stimulated NSM2 KD $CD4^+$ T cells.

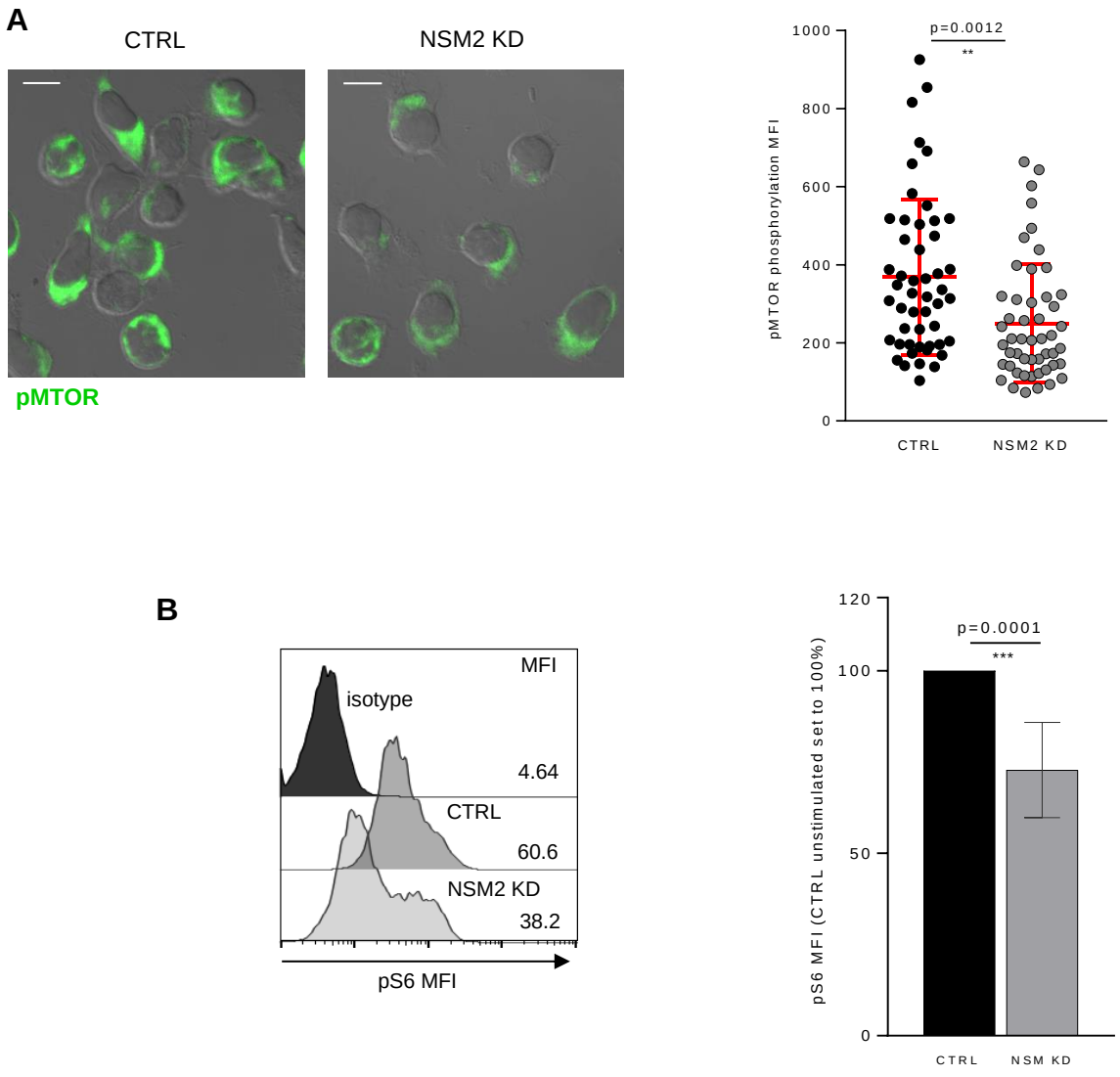

Figure 37. NSM2 is necessary for sustained MTOR pathway activity in stimulated T cells. CTRL and NSM2 KD cells were stimulated with α-CD3/CD28 soluble antibodies for 24h and mTOR (A), and pS6 (B) was measured by confocal microscopy or flow cytometry. Mean values with standard deviations are shown. p-values are shown on the top of significant (marked with asterisks).

Western blot analysis of S6 phosphorylation kinetics within 24 hours of a-CD3/CD28 co-stimulation confirmed the data obtained by flow cytometry analysis. S6 was phosphorylated after 30 min of stimulation in NSM2 deficient T cells, but the signal was not preserved after 24 hours (Fig. 38). Taken together, the results revealed the critical role of NSM2 to sustain the TCR/CD28 signal mediated MTOR pathway activity. [147].

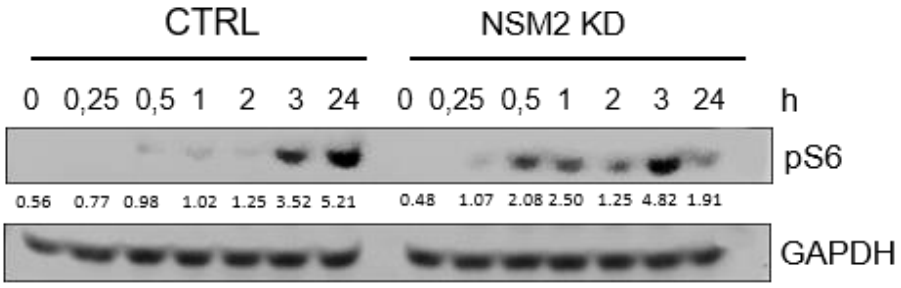

Figure 38. NSM2 is necessary for sustained S6 phosphorylation in stimulated T cells. CTRL and NSM KD cells were stimulated with α-CD3/CD28 on a plate for different time points, and pS6 was measured by western blot.

5.6. NSM2 regulates mitochondria biogenesis and membrane potential in Jurkat cells

As shown above, mitochondrial respiration and ATP production were significantly impaired in stimulated NSM deficient T cells. Mitochondria functionality is strongly related to their morphology changes, which are required for metabolic reprogramming of T cells upon TCR ligation. To analyze mitochondria morphology in NSM2 deficient T cells, we developed a Jurkat cell line stably expressing mitochondria-targeted GFP protein (mito-GFP). CTRL (Fig. 39A) and ΔNSM (Fig.39B) was visualized in confocal microscopy and z-stack analyzed in shown below:

A

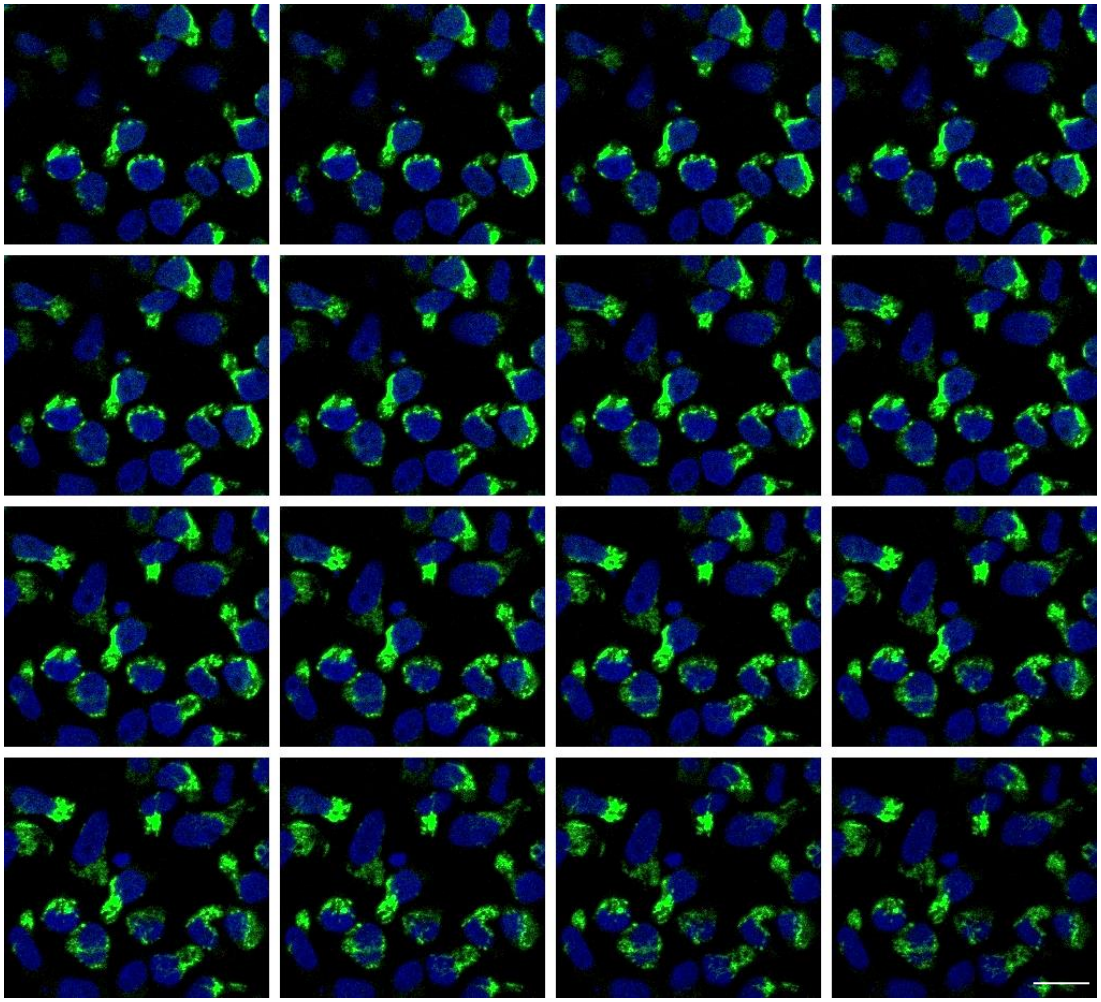

Mito-GFP
DAPI

B

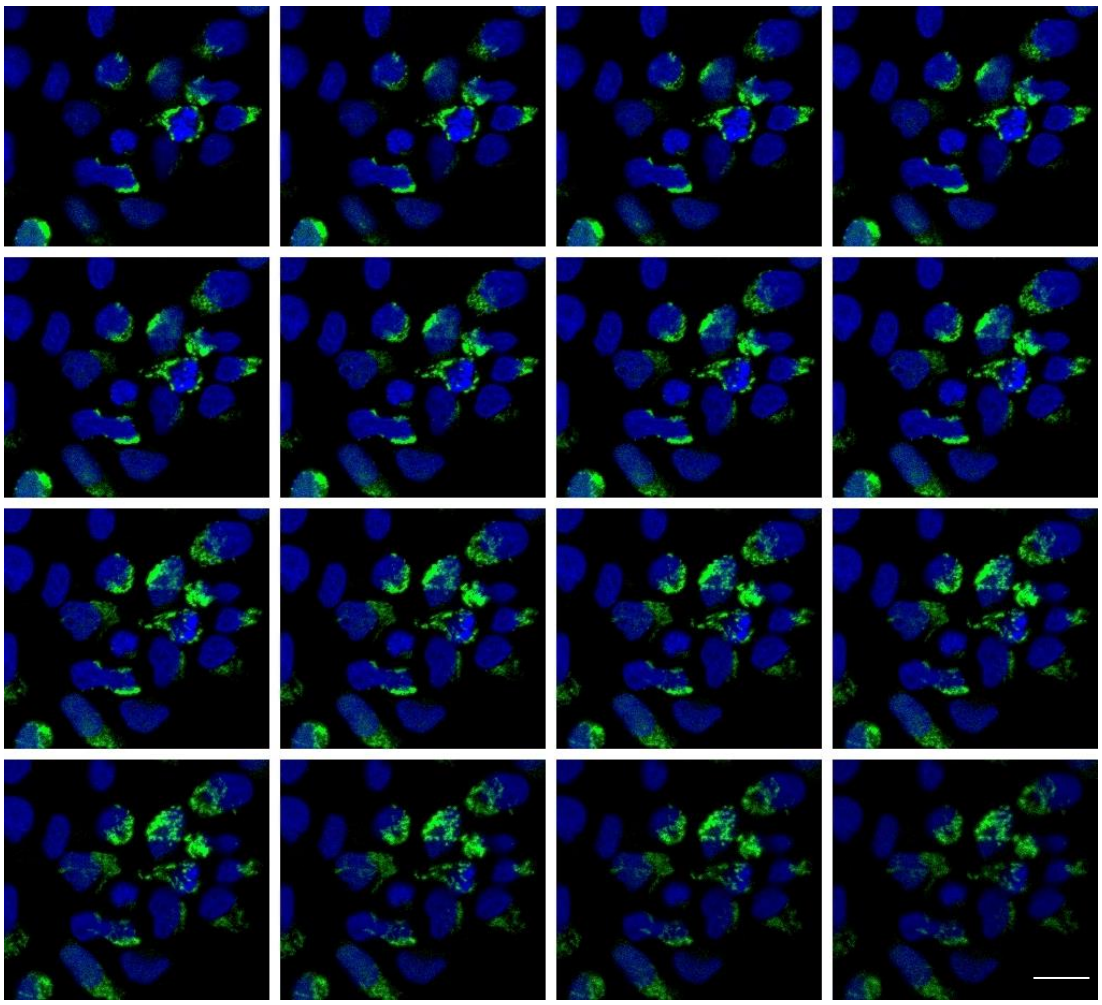

Figure 39. Representation of a z-stack confocal image of Jurkat cell line stably expressing mito-GFP – CTRL (A) and ΔNSM (B) Nuclei were stained with DAPI shown in blue.

We quantified the mitochondria size by confocal microscopy using the MinaTool, a plugin within the Fiji program, that can quantify the fluorescence signal related to the mitochondria and translate it into mitochondrial network morphology [130]. Using this tool, we were able to compare the degree of mitochondria size and fragmentation in CTRL and ΔNSM Jurkat cells stably transfected with mito-GFP. We determined the area/volume of the GFP signal, interpreted as the mitochondrial footprint.

The mitochondrial footprint revealed significantly reduced mitochondria mass in ΔNSM cells (Fig. 40). Unfortunately, the mitochondria of Jurkat cells were densely packed, and the plugin was not suitable for the quantification of the structural details within the organelles.

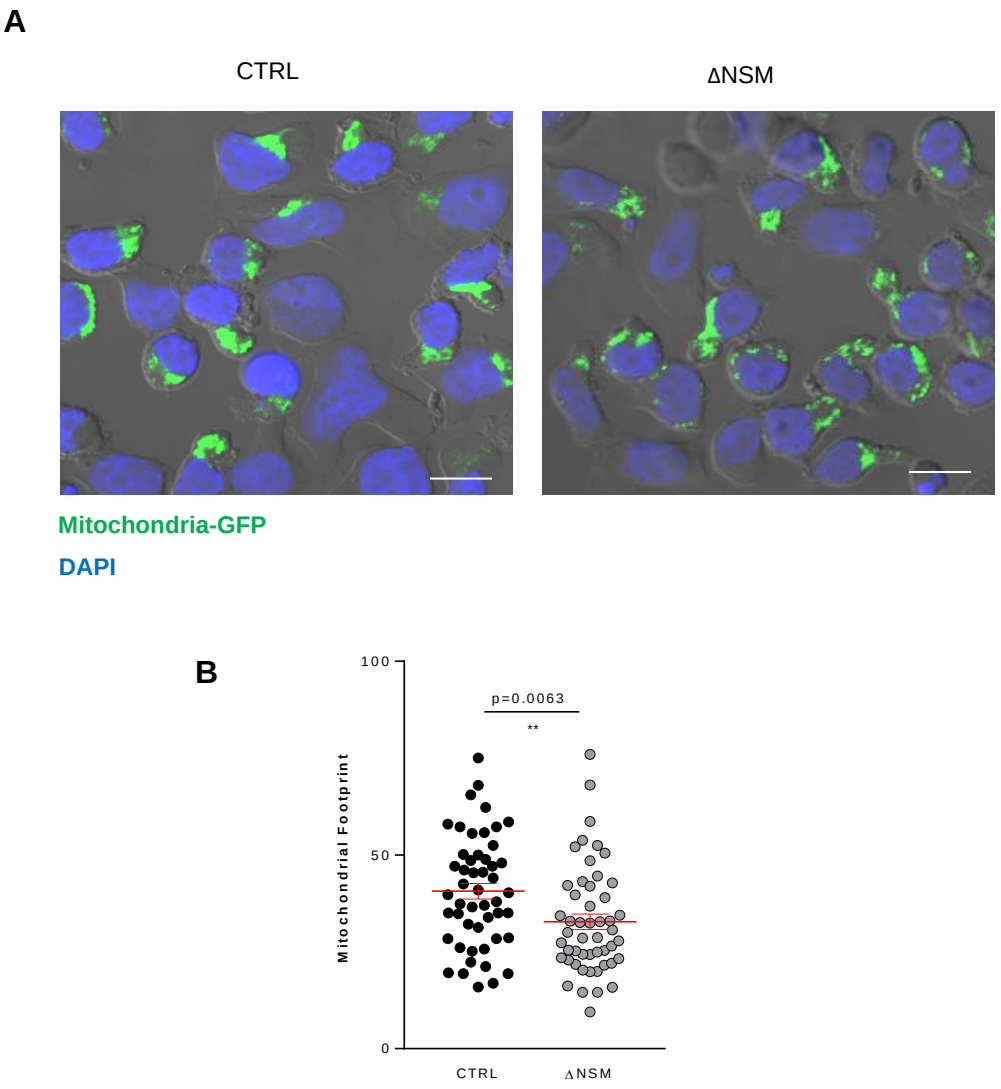

Figure 40. Reduced mitochondria volume in NSM2 deficient Jurkat cells. CTRL and ΔNSM Jurkat cells stably expressing mito-GFP were analyzed by confocal microscopy. Representative images (A) and analysis of mitochondrial footprints by MiNA Tool (B) are shown. Green color– mitochondria, blue – DAPI. Mean values with standard deviations are shown. The p-value is shown on the top of the significant (marked with asterisks) difference.

To validate the mitochondria morphological analysis data obtained by confocal microscopy and to analyze mitochondria respiration, we used MitoTracker Green and Red to perform flow cytometry analysis of the mitochondria mass and mitochondria membrane potential, respectively. Mitochondria mass and membrane potential were significantly reduced in the ΔNSM cells as compared to the CTRL cells (Fig. 41A). Results obtained by flow cytometry analysis correlated with the impaired mitochondria volume and reduced respiration measured by confocal microscopy and Seahorse metabolic flux analyzer respectively in ΔNSM cells. NSM2 activity is associated with ceramide generation at the plasma membrane of T cells. To investigate the impact of ceramides on mitochondria functionality, we fed CTRL and ΔNSM2 Jurkat cells with ceramide C16 overnight and analyzed mitochondria size, membrane potential, and ATP levels (Fig. 41B). We did not observe improvement in the parameters examined. Results suggest that the NSM2 dependent functionality of mitochondria in stimulated T cells is not solely reliant on ceramides.

A

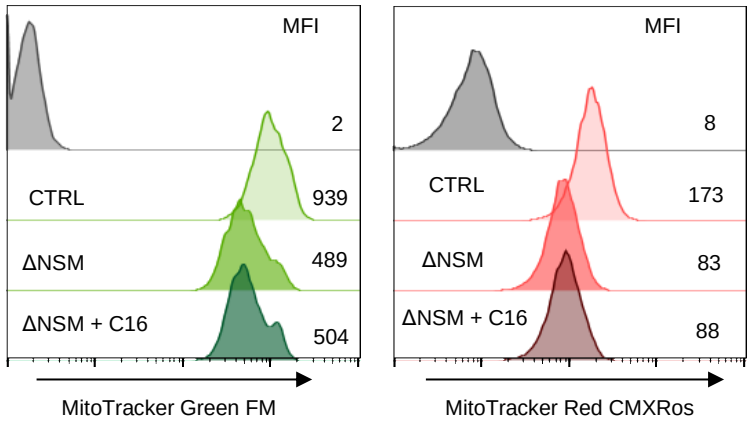

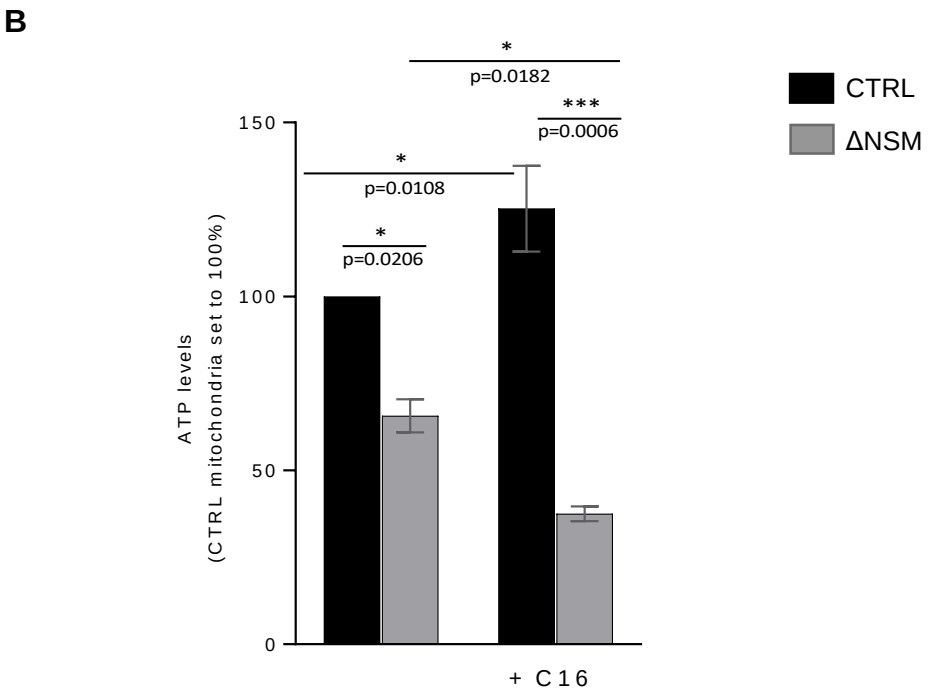

Figure 41. The upregulation of mitochondria mass and functionality is NSM2 but not ceramide dependent. CTRL and ΔNSM Jurkat cells were cultured in medium supplemented or not with ceramide C16 overnight. Subsequently, mitochondria mass and membrane potential were analyzed by flow cytometry using MitoTracker green and red, respectively. Alternatively, mitochondria were isolated, and ATP levels were measured. Mean fluorescence (MFI) values are shown within the flow cytometry histograms

We also used NSM2 deficient primary $CD4^+$ T cells generated by genetic NSM2 depletion or treated with pharmacological NSM2 inhibitor ES048 for the labeling with MitoTracker Red or Green. The cells were left unstimulated or α-CD3/CD28 stimulated for 24 hours before mitochondria mass and membrane potential were measured by flow cytometry (Fig. 42 and 43). The non-significant tendency of reduced mitochondria membrane potential was observed only for stimulated (Fig. 43) but not for unstimulated (Fig. 42) NSM2 deficient T cells.

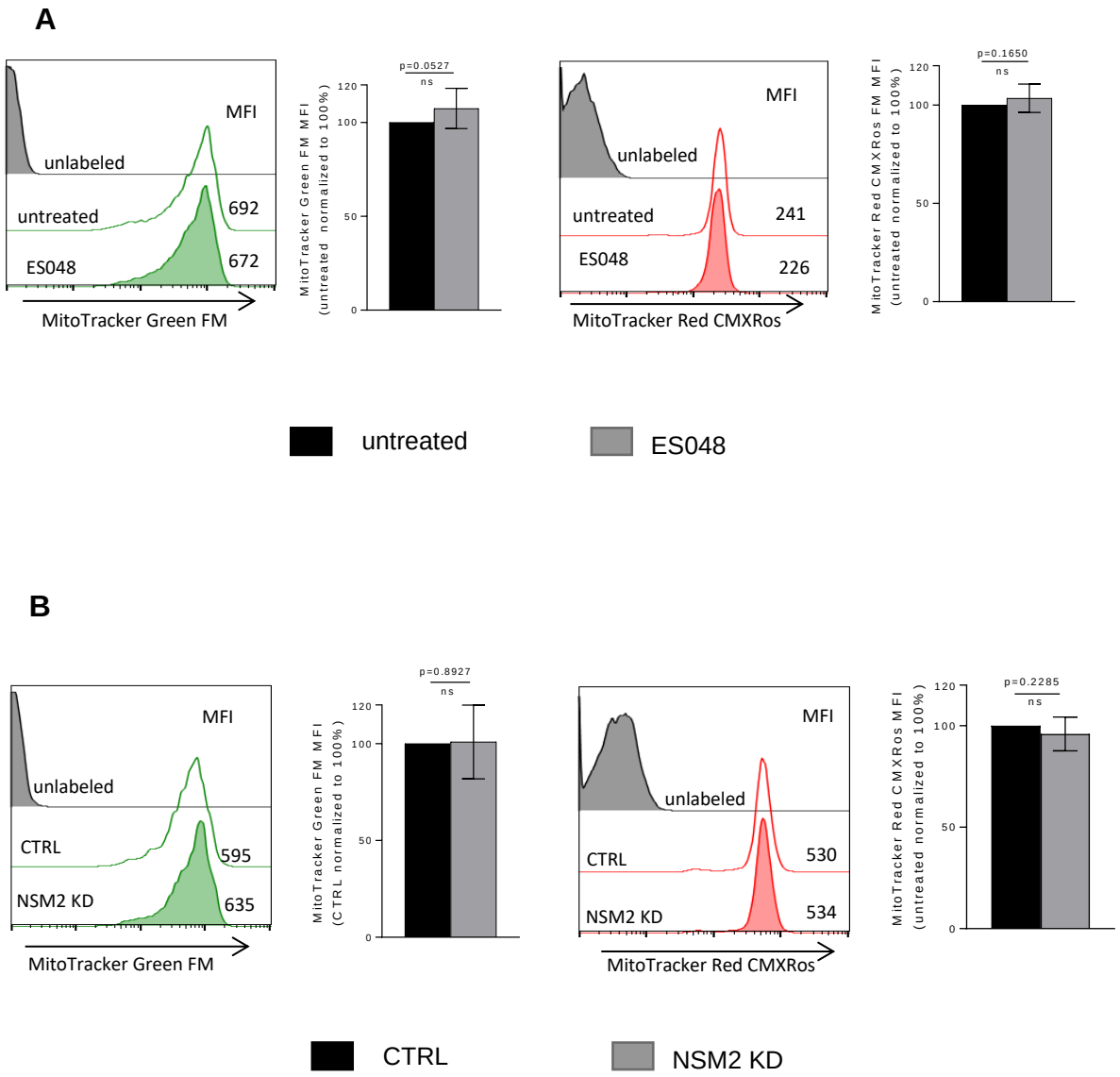

Figure 42. Mitochondria mass and membrane potential in unstimulated primary T cells deficient for NSM2 activity. Untreated or ES048 treated (A) or CTRL, NSM KD (B) $CD4^+$ T cells were left unstimulated, labeled with MitoTracker Red or Green, and analyzed by flow cytometry. Mean fluorescence intensity (MFI) values are shown within the histograms.

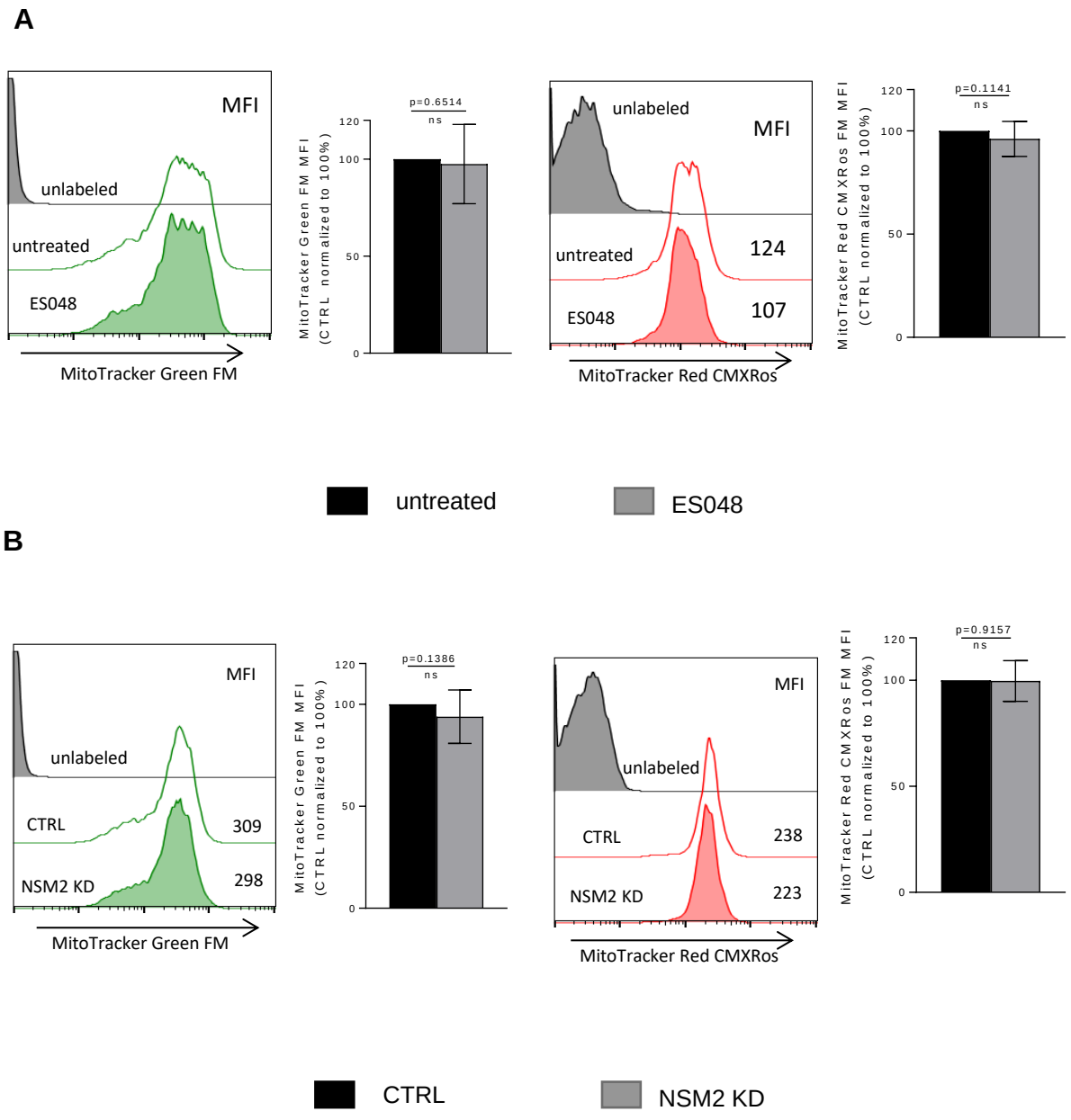

Figure 43. Mitochondria mass and membrane potential in stimulated primary T cells deficient for NSM2 activity. Untreated or ES048 treated (A) or CTRL, NSM KD (B) $CD4^+$ T cells were stimulated for 24h with α-CD3/CD28 antibodies and subsequently analyzed by flow cytometry. Mean fluorescence intensity (MFI) values are shown within the histograms.

5.7. NSM2 activity supports T cell expansion

Being aware of the NSM2 as the important effector of cell metabolism and mitochondrial activity in stimulated T cells, we wanted to determine the role of NSM2 in the T cell exit of quiescence and proliferation. First, we analyzed if CTRL and NSM KD cells would differentially upregulate activation markers CD69 (human transmembrane C-type lectin) and CD25 (alpha subunit of IL2 receptor). CTRL and NSM KD cells were stimulated on a plate with α-CD3/CD28 for 24h, 48h, and 72h. No significant differences were observed between CTRL and NSM KD cells (Fig. 44A). Nevertheless, the difference is only visible after five days of co-stimulation (Fig 44B), indicating that NSM2 is important to sustain proper activation in the following points.

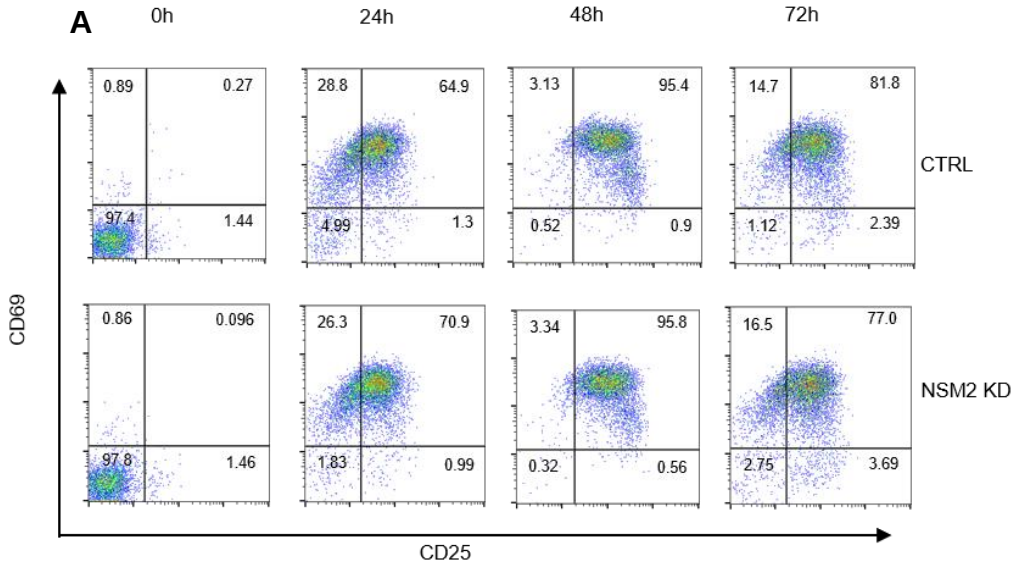

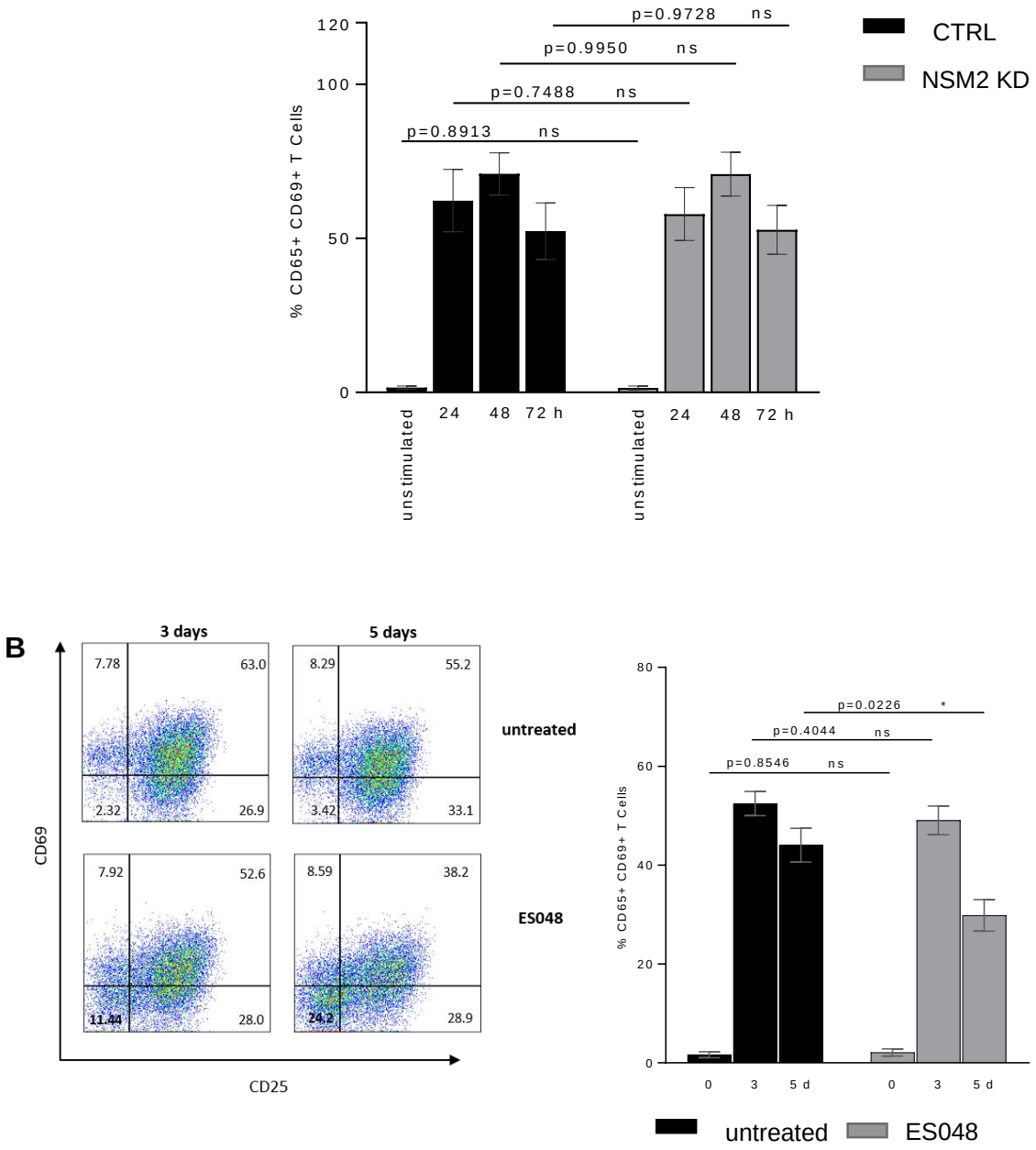

Figure 44. NSM2 independent CD69 and CD25 expression in activated T cells. Purified CTRL and NSM KD CD4⁺ T cells were stimulated with α-CD3/CD28 for 24h, 48h, and 72h (A). Purified CD4⁺ T cells were left untreated or pre-treated with ES048 for 2h and stimulated with α-CD3/CD28 for 3 and 5 days. The surface expression of CD25/CD69 was measured by flow cytometry. Representative plots (upper panels/left panels) and a summary of three independent experiments (bottom graph/right graph) are shown. Mean values with standard deviations are shown. The p-values are shown on the top of not significant differences (ns).

Further, we analyzed if efficient activation and exit of quiescence would resolve in the proliferation of NSM deficient T cells as they are notably recognized by the ability to

expand after being activated [148]. Cells were left untreated or pre-treated with ES048 for 2h and stimulated on a plate for five days, on the day before the measurement, cells were loaded with ^{3}H-Thymidine to measure the proliferation (Fig 45A). ES048 CD4^{+} T cells showed a three-fold reduction in proliferation, indicating the important role of NSM2 in long term expansion of T cells. To rule out that the low proliferation is due to the increase in mortality rates. We performed a viability assay with propidium iodide (PI) in cells co-stimulated for five days (Fig. 45B). The results demonstrated NSM2 affects T cell expansion without affecting cell survival.

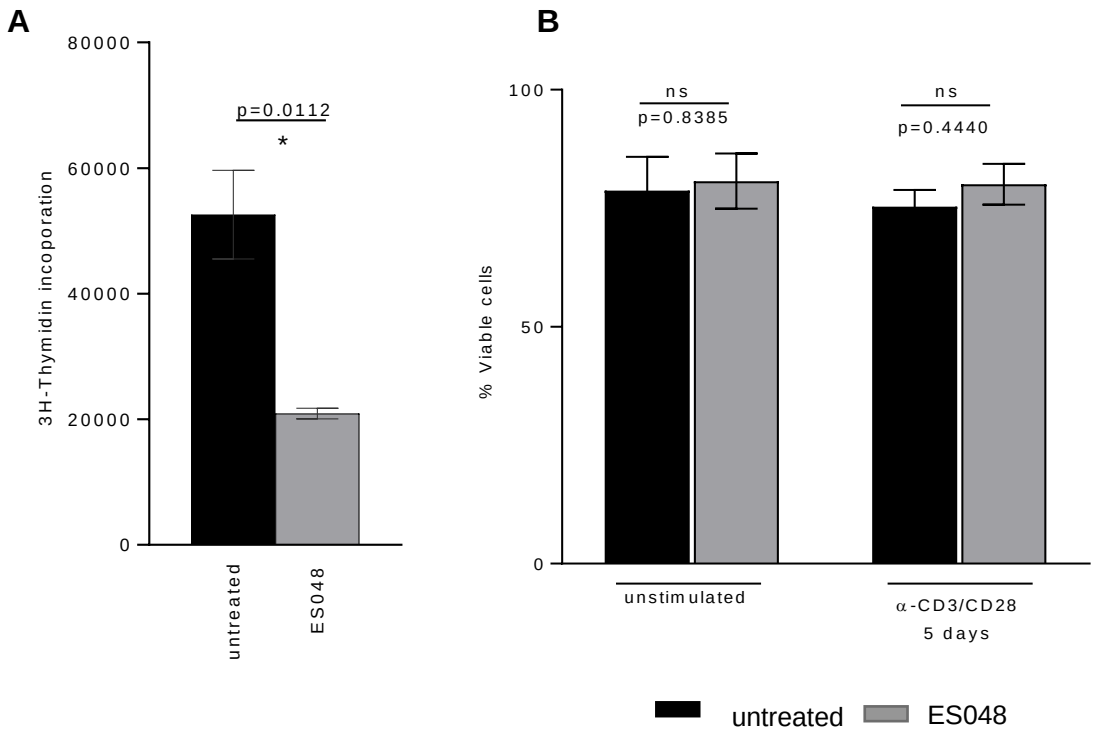

Figure 45. NSM2 supports T cell expansion without affecting survival. Purified CD4^{+} T cells were left untreated or pre-treated with ES048 for 2h. and subsequently stimulated on a plate for five days. Or one day before the measurement, cells were loaded with ^{3}H-Thymidine (A). Cells were loaded after five days of stimulation with PI, and cell viability was measured by FACS (B). Mean values with standard deviations are shown. p-value is shown on the top of the significant (marked with asterisks) difference.

6. Discussion

6.1. NSM2 regulates metabolic activity of quiescent T-cells

T cells are an important part of immunity and need precise metabolic coordination to mount a proper adaptive immune response. Precisely regulated energy metabolism in T cells in a resting state affects the immune responses to chronic viral infections, the efficiency of anti-tumor responses, and the functionality of aging cells [149]–[151] Quiescent T cells have reduced mitochondrial activity and glucose uptake, producing ATP mainly from the mitochondrial oxidative phosphorylation [133]. The regulation of T cell metabolism upon exit from quiescence and activation is relatively well studied, whereas the regulatory role of sphingolipid metabolism there is still purely addressed. Our results demonstrate that the pharmacological inhibition or genetic ablation of NSM2 deregulates the energy metabolism of T cells in the quiescent state characterized by increased accumulation of intracellular ATP and enhanced basal glycolytic activity.

Several reports reveal sphingolipids ceramides as essential regulators of mitochondria membrane functionality. Ceramides can form the channels in mitochondria membranes or bind voltage-dependent anion-selective channel protein VDAC2 to initiate mitochondria-mediated cell apoptosis [152], [153]. VDAC1 is established as the primary channel promoting the exchange of ATP, ADP between mitochondria and cytoplasm [154]. Maldonado *et al.* [155] showed that free tubulin could modulate the mitochondrial membrane potential in cancer cells. A recent study described ceramides interacting with cytoplasmic tubulin in mitochondria-associated membranes and regulating VDAC1 dependent ATP transport to the cytoplasm [156]. NSM2 plays a vital role in sphingolipid metabolism: its absence leads to a 50% decrease in the total amount of cellular ceramide [18]. Remarkably, NSM2 deficiency in T cells leads to the

specific reduction of plasma membrane-localized ceramides [157], leaving organelle associated ceramide pool unchanged. NSM2 also supports tubulin polymerization in T cells [33]. We used nocodazole, a drug well-known to disrupt microtubule assembly/disassembly, for the treatment of primary T cells. NSM2 deficient and nocodazole treated human primary T cells, both showed ATP accumulation within purified mitochondria, indicating that NSM2 and tubulin are involved in the transport of mitochondria ATP to the cytoplasm (Fig. 17). It is shown previously that nocodazole treatment and NSM2 deficiency enhance free depolymerized tubulin levels in the cytosol. Therefore, the accumulation of cytoplasmic tubulin, which interacts with VDAC1 in mitochondria membranes and blocks ATP transport to the cytosol, could be the possible mechanism explaining enhanced ATP levels within mitochondria of NSM2 deficient T cells.

In contrast, the total levels of ATP were not affected by nocodazole treatment, indicating that the regulation of ATP redistribution between mitochondria and cytoplasm is independent of tubulin dynamics. Nevertheless, the overall levels (Fig. 17) of ATP were significantly increased upon NSM2 inhibition/ablation in unstimulated $CD4^+$ T cells. The metabolic source for enhanced ATP production was investigated, and the results demonstrated that resting T cells are mainly dependent on mitochondria OXPHOS for ATP supply (Fig. 18) [158]. In contrast, the NSM2 ablated cells were affected equally by the treatments with oligomycin or 2-DG, which block the OXPHOS and glycolysis accordingly (Fig. 18) [159], [160], indicating the NSM2 deficient T cells upregulate glucose metabolism in the unstimulated state. The regulation of ATP/ADP levels in the cytoplasm is vital to keep the balance between the OXPHOS and glycolysis, and the low ATP/ADP ratio can promote glycolysis as an additional source for energy [161]. Possibly NSM2 deficient T cells accumulate ATP in mitochondria, and increased levels of cytoplasmic ADP lead to the upregulation of glycolysis in resting T

cells. In line with the hypothesis of a more glycolytic phenotype, we evaluated the glucose uptake of the cells, using 6-NDBG [162], a non-metabolized fluorescent glucose analog, by flow cytometry. The data confirmed that in the absence of NSM2 T cells increased the uptake of glucose analog, correlating with the rise of total ATP levels (Fig. 19). GLUT1 is the most abundant and most used glucose transporter in T cells due to its high affinity for glucose [163], [164]. The GLUT1 plasma membrane expression is regulated by vesicular trafficking and translocation to the cell surface of the cytoplasmic GLUT1 to support enhanced glucose demand upon TCR activation [165]. Our results demonstrated an up-regulation of GLUT1 on the cell surface accompanied by the increased total expression upon NSM2 genetic ablation by siRNA in T cells, supporting increased glucose uptake (Fig. 20). Notably, the absolute levels of GLUT1 were not increased upon pharmacological inhibition. The results possibly reflect the fact that the 2h time frame of the treatment with NSM2 inhibitor was not long enough to upregulate GLUT1 expression.

The previous data indicate a significant impact of the NSM2 absence on the basal glycolytic metabolism in resting $CD4^+$ T cells. The changes in the metabolic pathways can be analyzed by different tools, such as radiometric assay, metabolomics, or extracellular flux analysis [166]–[168]. From all the technics available, we favored the Seahorse extracellular flux analyzer (Seahorse XF) as it is a radioactive label-free technic, allowing the real-time measurements of the extracellular metabolites upon different treatments and stimuli. Another advantage is the possibility to measure the Oxygen Consumption Rates (OCR) and Extracellular Acidification Rates (ECAR) simultaneously, granting evaluation of the proportionate contribution of both energetic pathways [169].

ECAR measured in Seahorse glycolytic stress test was significantly higher in unstimulated $CD4^+$ T cells after NSM2 inhibition (Fig. 22). The glycolytic stress test

allows us to measure the key parameters of glycolytic flux. The non-glycolytic acidification was slightly but significantly enhanced in ES048 treated cells kept in medium without glucose, indicating that the tricarboxylic acid (TCA) cycle is more active in generating respiratory CO_2, which is converted to HCO_3^- and H^+. ECAR increase after glucose injection was significantly higher in NSM inhibited unstimulated cells, correlating with the increased capacity of cells to uptake and metabolize glucose. Importantly, the injection of oligomycin, a drug used to assess the maximum glycolytic capacity by blocking the mitochondria and forcing the cells to produce ATP only from glycolysis, did not improve the ECAR. This could be explained by the fact that quiescent and naïve T cells have rather low glycolytic flux, and it is already at the maximum after injection with saturated levels of glucose [170], [171]. Results described above support the hypothesis of increased glycolysis in resting NSM2 deficient T cells. The increased levels of non-glycolytic acidification in ES048 treated T cells indicate NSM dependent regulation of the TCA cycle, which can feed in mitochondrial ATP production by OXPHOS. Indeed, basal cellular respiration measured by oxidative phosphorylation (OCR) was enhanced after ES048 treatment (Fig. 23). One of the final products of glycolysis is pyruvate, which can be converted into lactate, or be imported to the mitochondria through the mitochondrial pyruvate carrier (MPC) or VDAC to feed the TCA cycle [172], [173]. Therefore, enhanced glycolysis can support an increase in basal respiration after pyruvate transport to the mitochondria of NSM2 deficient T cells. Further on, NSM2 inhibited T cells responded more vigorously in the mitochondria stress test. More than 50% of basal respiration was linked to ATP production in untreated cells, and this was significantly enhanced in ES048 treated cells. Similar, maximal respiration after challenge with Carbonyl cyanide-4-phenylhydrazone (FCCP) that interferes with the proton gradient in mitochondria, was increased in ES048 cells indicating highly “fit” mitochondria. Summarizing, the data reveal the important role of

NSM2 to control the basal metabolism of quiescent peripheral blood $CD4^+$ T cells, and its deficiency leads to the activated phenotype by increasing the uptake of glucose and ATP production.

6.2. NSM2 dampens early metabolic responses to antigenic stimulation of T-cells

Upon TCR/CD28 co-stimulation, naïve T cells initiate activation-dependent metabolic reprogramming to start the exit from quiescence [174]. In the first minutes after TCR engagement, T cells enhance aerobic glycolysis and OXPHOS to support the activation with energy [175], [176]. The results described above show the elevated basal glucose uptake and ATP production in NSM2 deficient $CD4^+$ T cells. Within the first minutes after α–CD3/CD28 co-stimulation, T cells increase glucose usage and mitochondrial respiration (Fig. 24). Remarkably, ES048 treated cells show significantly higher OCR and ECAR values within the first 2 hours of TCR/CD28 stimulation compared to untreated cells, indicating a more active initial response in the absence of NSM2 activity. It was shown that NSM2 is activated after TCR ligation alone or after co-stimulation with α-CD28 and the NSM2 deficiency leads to the hyper-responsiveness early after activation [28], [32]. The important role of NSM2 in modifying of plasma membrane lipids and amplifying of TCR signaling is established [33]. Results are indicating that lack of NSM2 activity increases the T cell energy requirements before and shortly after co-stimulation, resulting in enhanced metabolic activity early after stimulation resolving in a more “energetic” phenotype (Fig. 25).

When the ATP concentrations were measured, an increase of ATP levels was observed, reaching a maximum within the first 30 minutes of stimulation (Fig. 26). That correlated to the increase of ECAR/OCR after the injection of stimulatory antibodies.

This is associated with the initiation of the cellular growth phase, where the cells increase the global metabolism by rapid upregulation of ATP production and activation of metabolic pathways. [177], [178] The initial burst in ECAR is followed by an increased GLUT1 surface expression. The enhanced surface expression of GLUT1 and amino acid transporters is a part of the stimulation dependent metabolic reprogramming of activated T cells [52]. NSM ablated unstimulated T cells showed elevated GLUT1 expression on the surface even before stimulation, supporting fast and robust glycolytic response after stimulation of NSM2 inhibitor-treated cells.

6.3. NSM2 supports mitochondria functionality in stimulated CD4$^+$ T cells

T cell exit from quiescence is precisely regulated, and after co-stimulation, naïve T-cells fully complete the metabolic switch 16-24h after stimulation. Six steps can be distinguished during the time of T cell transition to activated state: cell growth, cell cycle entry from G0 to S phase, autocrine and paracrine IL-2 signaling, anabolic metabolism, nutrient uptake, and reprogramming of mitochondrial function. All these steps culminate in T cell clonal expansion and differentiation [174]. Several studies have reported the link between abnormal cellular metabolism and dysregulated resting state and exit from quiescence in T cells [57], [179]. The results presented above demonstrate that T cells treated with pharmacological NSM2 inhibitor ES048 have decreased mitochondria functionality after 24h of co-stimulation, as shown in figure 27. Similar, reduced mitochondria membrane potential and lower performance in mitochondria stress tests were measured in ΔNSM Jurkat (Fig. 28). Basal respiration, ATP production, and maximal respiration, parameters that were increased during NSM2 inhibition of unstimulated cells, were reduced about 12-25% in ES048 treated cells after 24 hours of stimulation. Börtlein et al. [33] demonstrate that ΔNSM Jurkats failed to release IL-2 after 48h stimulation with PMA/Ionomycin.

This could implicate reduced autocrine/paracrine IL-2 signaling affecting mitochondria functionality [40]. Prevention of ceramide accumulation by NSM2 inhibition could directly affect mitochondria activity and signaling [180]. Reduced plasma membrane ceramide levels in NSM2 deficient Jurkat cells prevent PKCζ membrane recruitment [139], proper microtubule cytoskeleton reorganization[33], and cholesterol ester (CE) accumulation [31], [181] events that could affect mitochondria performance in stimulated T cells.

Importantly, the proper and robust T cell activation needs precise coordination of TCR and CD28 co-stimulatory signaling to control the metabolic changes upon stimulation [178], [182], [183]. After 24h of TCR/CD28 co-stimulation, T cells increase ATP production to support the new energetic requirements needed for cell proliferation[137]. After TCR engagement, T cells switch the ATP production from mitochondrial to the glycolytic pathway and utilize the mitochondria mainly for the building of the metabolic blocks necessary for macromolecule synthesis. The glycolytic switch is advantageous to T cells because the products of glycolysis provide anabolic metabolites that can be used in different biosynthetic pathways [184]–[186]. NSM2 ablated cells were able to increase the ATP production upon long term stimulation, indicating that the cells are activated, but they produced 50% less ATP in comparison with CTRL cells. The ATP production in stimulated CTRL and NSM2 deficient T cells was provided mostly by the glycolytic pathway, as observed after 2-DG treatment (Fig. 34). Notably, there were no significant alterations in the glycolytic metabolism when analyzed by seahorse in primary ES048 treated $CD4^+$ T cells (Fig. 29) or ΔNSM Jurkat (Fig. 30). The upregulation of GLUT1 and an increase in the glucose uptake are indicators of the glycolytic switch [187]–[189]. However, when analyzed by FACS, the GLUT1 surface expression levels and glucose uptake were downregulated in NSM2 ablated/inhibited $CD4^+$ T cells (Fig. 31).

Additionally, T cells can upregulate other glucose transporters GLUT3 or GLUT4 to supply the uptake of glucose. The upregulation of glycolysis could explain why the glycolytic stress test does not show the difference at the same time the GLUT1 protein levels are low, and the uptake is also impaired.

In summary, diminished ATP production in stimulated NSM2 deficient T cells is instead reflecting mitochondria dysfunction at the intact glycolytic activity. The results demonstrate that NSM2 is important to sustain mitochondria functionality during T cell activation.

6.4. NSM2 maintains mTOR signaling pathway in TCR/CD28 stimulated T cells

mTORC1 is an evolutionary conserved ser/thr master kinase regulator for quiescence exit and activation of T cells. It integrates antigen receptor signaling and nutrient sensing [73], [190]–[192]. The results demonstrate fast and robust phosphorylation of mTORC1 and the downstream target of mTORC1 S6 within the first 30 min after TCR/CD28 stimulation of NSM2 deficient $CD4^+$ T cells (Fig. 36). Glucose levels are also known to regulated mTORC1 by shaping the activity of the negative regulator AMPK [193], [194]. In the absence of NSM2, T cells initially increase the glucose uptake and glycolytic activity (Fig. 24), correlating with the sufficient mTOR pathway activation. Results presented here demonstrate that NSM2 deficient T cells fail to sustain the mTOR pathway activity after 24h of co-stimulation (Fig. 36). Published studies show that IL-2 and IL-15 are important to assist the activation of mTOR [195], [196]. In contrast, NSM Jurkat cells are unable to produce IL-2 after unspecific phorbol-12-myristate-13-acetate (PMA) stimulation [124] It is not clear if TCR signal-dependent IL-2 production would be similar impaired in NSM2 deficient $CD4^+$ T cells.

The lipid composition of the plasma membrane, which is deregulated in NSM2 deficient T cells, is crucial for optimal TCR clustering and signaling [66], [67], and can be important to sustain mTOR activation. The accumulation of plasma membrane ceramides and CE was prevented, and intracellular cholesterol accumulation was enhanced in ΔNSM Jurkats, whereas TCR clustering was not disturbed in NSM2 deficient Jurkat cells [13]. There is no evidence that plasma membrane sphingolipids can directly affect the mTOR pathway. Similarly, the role of intracellular cholesterol accumulation in the regulation of mitochondria and lysosome-associated mTORC1 activity or transport is not known and should be investigated.

mTOR signaling is important to promote aerobic glycolysis [197]. The deregulation of mTOR activity influences T cell metabolic capacity and cell fate, due to the important role of regulating the gene expression of both glycolysis and OXPHOS. [58], [198]. In recent years, several pieces of evidence have established the role of mTORC1 as a central mitochondrial regulator affecting mitochondrial biogenesis, mitophagy, and fission and fusion processes [199], [200]. Published data show that mTOR co-interact with mitochondria and can be associated with the outer mitochondrial membrane. This association is so strong that when cells were treated with mitochondrial inhibitors, the activity of mTORC1 was decreased [201], *vice versa* when mTOR/raptor complex was inhibited with rapamycin or with RNAi the mitochondrial metabolism was affected negatively [202]. Results are shown above, and published data together suggest that ineffective mitochondrial performance observed in NSM2 inhibited CD4+ T cells after 24h co-stimulation could be associated with the deregulated mTORC1 signaling.

6.5. NSM2 regulates mitochondria biogenesis and membrane potential in Jurkat cells

Mitochondria are important organelles for the production of ATP in eukaryotic cells. Mitochondrial can quickly adapt to new conditions due to well-evolved communication with other cell compartments [203]. Mitochondria functionality is maintained through mitochondrial dynamics expressed as their fusion, fission, mobility, biogenesis, and degradation [106], [204]. Mitochondria supports T cell activation [205] by uptake of cytosolic calcium [206], ROS signaling [207], and mitochondria-derived ATP that act on purinergic receptors [208].

Using a lentiviral construct, we could create a cell line with mitochondria-targeted GFP to analyze the impact of NSM2 on mitochondrial biogenesis. Using a unique calculation tool, we were able to analyze mitochondria localization and measure their footprints expressed as area/mass of the mitochondria. Mitochondria distribution was not affected by ΔNSM cells. The massive T cell nucleus forces the mitochondria to accommodate together, giving the impression of clamped mitochondria. That is why it was not possible to speculate about the levels of fusion and fission in the T cell mitochondria. Remarkably, mitochondrial size (Fig. 40 and 41) and mitochondria membrane potential (Fig. 41) were significantly impaired in ΔNSM Jurkat cells correlating with the low functionality of mitochondria shown by stress test.

A cell line is a valuable tool to facilitate the visualization of mitochondria. It can be used to avoid the enormous variability of primary T cells isolated from healthy human donors. Still, it cannot accurately replicate the processes in primary cells [209]. Reduced mitochondria mass and potential were observed continuously in ΔNSM Jurkat cells. In contrast, using the MitoTracker dyes in primary $CD4^+$ T cells gave highly varying results. It showed a mild not significant tendency of lower mitochondria mass and

potential in NSM KD, or ES048 treated CD4+ T cells after TCR/CD28 stimulation (Fig. 43).

Nevertheless, analysis of the mitochondrial functionality by stress test in Seahorse metabolic flux analyzer showed significantly impaired mitochondria-related OCR after 24h co-stimulation (Fig. 27). As previously discussed, the mTOR pathway can regulate mitochondrial respiratory activities [210]. It can also adjust the expression of the mitochondrial electron transport chain (ETC) protein complexes I, II, and IV [211]. The aberrant mTORC1 activity affects mitochondria biogenesis. Data shown here suggest that the mitochondria in NSM2 deficient T cells have a functional defect in the ETC complex, indicated by the reduced mean fluorescence intensity of MitoTracker red. It is not clear if the ETC function is defective due to the impaired expression of ETC protein complexes. Voltage-dependent anion channel (VDAC) protein expression levels were similar in CTRL and NSM KD cells, suggesting functional deregulation in mitochondria ATP transport (Fig. 35).

The sphingolipid metabolism plays an important role in the cells, due to its highly compartmentalized nature. The well-known is the sphingolipid ceramide involved in the induction of apoptosis [152]. Ceramides form channels in the mitochondria membrane and regulate its function [212]. NSM2 is located at the inner leaflet of the plasma membrane [12], [13]. It is not known if the ceramide synthesized by NSM2 can be found in the mitochondria. Studies suggest that ceramides produced in the ER or plasma membrane can reach the mitochondria through the interaction between organelles and plasma membrane [14], [213]. Yu et al. [214] have shown that an increase in ceramide production through Ceramide Synthase (CerS) damages the respiratory chain in the mitochondria. ΔNSM Jurkats have less ceramide and increased levels of sphingomyelin in the plasma membrane[13]. It is not clear to what extent NSM2 regulated sphingolipids can directly affect mitochondria functions as there is no

evidence of the deregulated levels of sphingomyelin and ceramide in the mitochondria of NSM2 deficient T cells.

6.6. NSM2 activity supports T cell expansion

Energetic metabolism is a phenomenon that supports T cell activation and regulates T cell functions [215] and differentiation [216]. CD25/CD69 are known as early activation markers but can be found on the surface of stimulated T cell more than five days after the antigen encounter [217]. The results demonstrate that NSM2 absence did not affect the surface expression of CD25 and CD69 up to three days of co-stimulation (Fig. 44A). The sustained upregulation of the activation markers could be linked with an increase in cell-cell contact in the stimulatory plate [218]. The results suggest that the NSM KD T cell activation phase is not affected by impaired mitochondrial activity. Chang et al. [136] demonstrated that OXPHOS is needed to sustain the proliferation of activated T cells for at least two days after stimulation. NSM KD T cells showed reduced proliferation measured five days after TCR/CD28 stimulation (Fig. 45). The T-cell exhaustion is described as a state when T cells are incapable of proliferating or production of effector molecules [219]. Increased basal metabolic activity, enhanced early signaling, and reduced proliferative response are all phenomena observed in NSM deficient T cells and in literature are linked to the exhausted or aged T cells [220]. Taken together, the TCR signaling induced NSM2 activity coordinate the metabolic activity of quiescent and antigen engaged T cells, and its downregulation forces the T cells into an exhausted phenotype.

7. Conclusions

Data shown here reveal that sphingolipid metabolism at the plasma membrane inner leaflet communicates with cellular energy metabolism. NSM2 deficiency drives quiescent CD4^{+} T cells into a state more characteristic for exhausted immune cells with enhanced basal glycolytic activity. The absence of NSM2 promotes a hyperactive metabolic state in unstimulated CD4+ T cells yet fails to support sustained T cell responses upon antigenic stimulation.

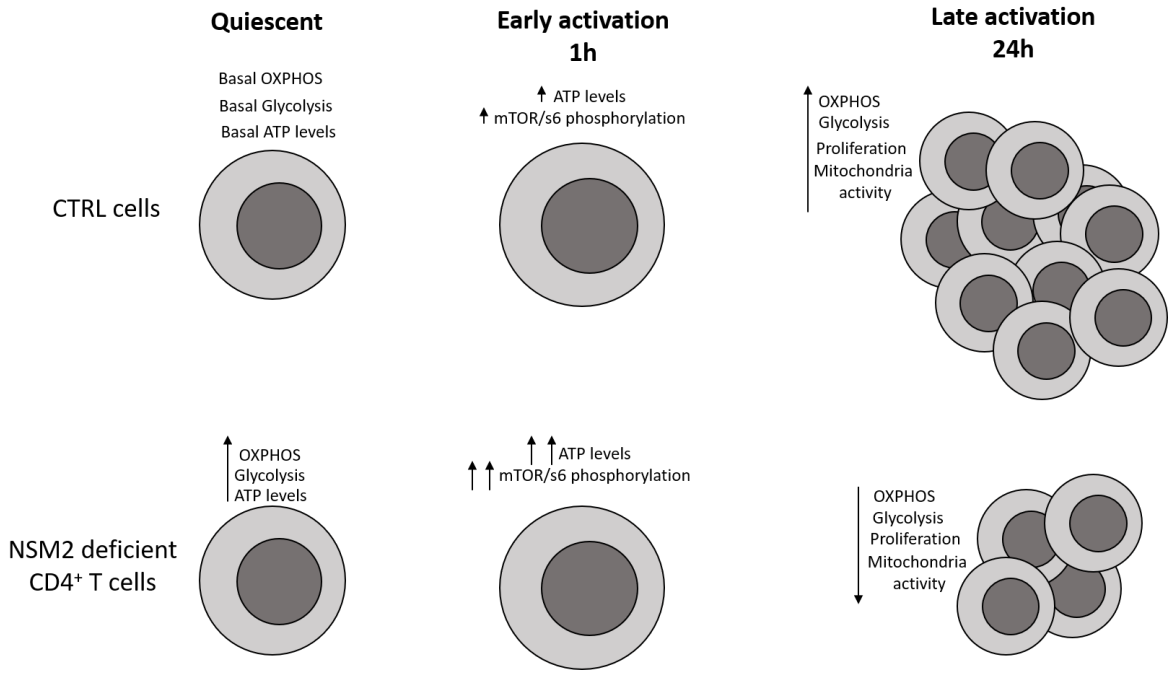

Figure 46. Graphical abstract of the main findings of the thesis.

8. References

[1] K. Simons and E. Ikonen, “Functional rafts in cell membranes,” *Nature*, vol. 387, no. 6633. Nature, pp. 569–572, 05-Jun-1997.

[2] Y. A. Hannun and L. M. Obeid, “Principles of bioactive lipid signalling: Lessons from sphingolipids,” *Nature Reviews Molecular Cell Biology*, vol. 9, no. 2. Nature Publishing Group, pp. 139–150, Feb-2008.

[3] C. R. Gault, L. M. Obeid, and Y. A. Hannun, “An overview of sphingolipid metabolism: From synthesis to breakdown,” *Advances in Experimental Medicine and Biology*, vol. 688. Adv Exp Med Biol, pp. 1–23, 2010.

[4] T. D. Mullen, Y. A. Hannun, and L. M. Obeid, “Ceramide synthases at the centre of sphingolipid metabolism and biology,” *Biochemical Journal*, vol. 441, no. 3. Biochem J, pp. 789–802, 01-Feb-2012.

[5] Y. Chen, Y. Liu, M. C. Sullards, and A. H. Merrill, “An introduction to sphingolipid metabolism and analysis by new technologies,” *NeuroMolecular Medicine*, vol. 12, no. 4. Neuromolecular Med, pp. 306–319, Dec-2010.

[6] K. Bocheńska and M. Gabig-Cimińska, “Unbalanced Sphingolipid Metabolism and Its Implications for the Pathogenesis of Psoriasis,” *Molecules*, vol. 25, no. 5, p. 1130, Mar. 2020.

[7] B. Liu, D. F. Hassler, G. K. Smith, K. Weaver, and Y. A. Hannun, “Purification and characterization of a membrane bound neutral pH optimum magnesium-dependent and phosphatidylserine-stimulated sphingomyelinase from rat brain,” *J. Biol. Chem.*, vol. 273, no. 51, pp. 34472–34479, Dec. 1998.

[8] S. Tomiuk, K. Hofmann, M. Nix, M. Zumbansen, and W. Stoffel, “Cloned mammalian neutral sphingomyelinase: Functions in sphingolipid signaling?,” *Proc. Natl. Acad. Sci. U. S. A.*, vol. 95, no. 7, pp. 3638–3643, Mar. 1998.

[9] O. Krut, K. Wiegmann, H. Kashkar, B. Yazdanpanah, and M. Krönke, “Novel tumor necrosis factor-responsive mammalian neutral sphingomyelinase-3 is a C-tail-anchored protein,” *J. Biol. Chem.*, vol. 281, no. 19, pp. 13784–13793, May 2006.

[10] K. Hofmann, S. Tomiuk, G. Wolff, and W. Stoffel, “Cloning and characterization of the mammalian brain-specific, Mg2+-dependent neutral sphingomyelinase,” *Proc. Natl. Acad. Sci. U. S. A.*, vol. 97, no. 11, pp. 5895–5900, May 2000.

[11] M. V Airola *et al.*, “Structure nSMase2 supporting info,” *Proc. Natl. Acad. Sci. U.*

S. A., vol. 114, no. 28, pp. E5549–E5558, Jul. 2017.

[12] M. Tani and Y. A. Hannun, “Analysis of membrane topology of neutral sphingomyelinase 2,” *FEBS Lett.*, vol. 581, no. 7, pp. 1323–1328, Apr. 2007.

[13] C. Börtlein, F. Schumacher, B. Kleuser, L. Dölken, and E. Avota, “Role of Neutral Sphingomyelinase-2 (NSM 2) in the Control of T Cell Plasma Membrane Lipid Composition and Cholesterol Homeostasis,” *Front. Cell Dev. Biol.*, vol. 7, Oct. 2019.

[14] H. Kitagaki *et al.*, “Isc1 regulates sphingolipid metabolism in yeast mitochondria,” *Biochim. Biophys. Acta - Biomembr.*, vol. 1768, no. 11, pp. 2849–2861, Nov. 2007.

[15] W. Stoffel, B. Jenke, B. Blöck, M. Zumbansen, and J. Koebke, “Neutral sphingomyelinase 2 (smpd3) in the control of postnatal growth and development,” *Proc. Natl. Acad. Sci. U. S. A.*, vol. 102, no. 12, pp. 4554–4559, Mar. 2005.

[16] I. Aubin *et al.*, “A deletion in the gene encoding sphingomyelin phosphodiesterase 3 (Smpd3) results in osteogenesis and dentinogenesis imperfecta in the mouse,” *Nat. Genet.*, vol. 37, no. 8, pp. 803–805, Aug. 2005.

[17] N. Marchesini, W. Osta, J. Bielawski, C. Luberto, L. M. Obeid, and Y. A. Hannun, “Role for mammalian neutral sphingomyelinase 2 in confluence-induced growth arrest of MCF7 cells,” *J. Biol. Chem.*, vol. 279, no. 24, pp. 25101–25111, Jun. 2004.

[18] N. Marchesini, C. Luberto, and Y. A. Hannun, “Biochemical properties of mammalian neutral sphingomyelinase2 and its role in sphingolipid metabolism,” *J. Biol. Chem.*, vol. 278, no. 16, pp. 13775–13783, Apr. 2003.

[19] J. Schulze *et al.*, “Osteolytic prostate cancer cells induce the expression of specific cytokines in bone-forming osteoblasts through a Stat3/5-dependent mechanism,” *Bone*, vol. 46, no. 2, pp. 524–533, Feb. 2010.

[20] W. J. Kim *et al.*, “Mutations in the neutral sphingomyelinase gene Smpd3 implicate the ceramide pathway in human leukemias,” *Blood*, vol. 111, no. 9, pp. 4716–4722, May 2008.

[21] M. Levy, S. S. Castillo, and T. Goldkorn, “nSMase2 activation and trafficking are modulated by oxidative stress to induce apoptosis,” *Biochem. Biophys. Res. Commun.*, vol. 344, no. 3, pp. 900–905, Jun. 2006.

[22] A. Cogolludo *et al.*, “Activation of neutral sphingomyelinase is involved in acute

hypoxic pulmonary vasoconstriction.," *Cardiovasc. Res.*, vol. 82, no. 2, pp. 296–302, May 2009.

[23] M. Nikolova-Karakashian, A. Karakashian, and K. Rutkute, "Role of neutral sphingomyelinases in aging and inflammation," *Subcell. Biochem.*, vol. 49, pp. 469–486, 2008.

[24] C. J. Clarke and Y. A. Hannun, "Neutral sphingomyelinases and nSMase2: bridging the gaps.," *Biochim. Biophys. Acta*, vol. 1758, no. 12, pp. 1893–901, Dec. 2006.

[25] C. J. Clarke, C. F. Snook, M. Tani, N. Matmati, N. Marchesini, and Y. A. Hannun, "The extended family of neutral sphingomyelinases," *Biochemistry*, vol. 45, no. 38, pp. 11247–11256, Sep. 2006.

[26] C. J. Clarke, T. G. Truong, and Y. A. Hannun, "Role for neutral sphingomyelinase-2 in tumor necrosis factor α-stimulated expression of vascular cell adhesion molecule-1 (VCAM) and intercellular adhesion molecule-1 (ICAM) in lung epithelial cells: p38 MAPK is an upstream regulator of nSMase2," *J. Biol. Chem.*, vol. 282, no. 2, pp. 1384–1396, Jan. 2007.

[27] C. J. Clarke and Y. A. Hannun, "Neutral sphingomyelinases and nSMase2: Bridging the gaps," *Biochim. Biophys. Acta - Biomembr.*, vol. 1758, no. 12, pp. 1893–1901, Dec. 2006.

[28] L. Tonnetti, M. C. Verí, E. Bonvini, and L. D'Adamio, "A role for neutral sphingomyelinase-mediated ceramide production in T cell receptor-induced apoptosis and mitogen-activated protein kinase-mediated signal transduction," *J. Exp. Med.*, vol. 189, no. 10, pp. 1581–1589, May 1999.

[29] B. X. Wu, C. J. Clarke, and Y. A. Hannun, "Mammalian neutral sphingomyelinases: Regulation and roles in cell signaling responses," *NeuroMolecular Medicine*, vol. 12, no. 4. Neuromolecular Med, pp. 320–330, Dec-2010.

[30] M. van Gijsel-Bonnello *et al.*, "Pantethine Alters Lipid Composition and Cholesterol Content of Membrane Rafts, With Down-Regulation of CXCL12-Induced T Cell Migration," *J. Cell. Physiol.*, vol. 230, no. 10, pp. 2415–2425, Oct. 2015.

[31] Megha and E. London, "Ceramide selectively displaces cholesterol from ordered lipid domains (rafts): Implications for lipid raft structure and function," *J. Biol. Chem.*, vol. 279, no. 11, pp. 9997–10004, Mar. 2004.

[32] N. Mueller, E. Avota, L. Collenburg, H. Grassmé, and S. Schneider-Schaulies, “Neutral Sphingomyelinase in Physiological and Measles Virus Induced T Cell Suppression,” *PLoS Pathog.*, vol. 10, no. 12, Dec. 2014.

[33] C. Börtlein *et al.*, “The neutral sphingomyelinase 2 is required to polarize and sustain T cell receptor signaling,” *Front. Immunol.*, vol. 9, no. APR, Apr. 2018.

[34] E. Avota, E. Gassert, and S. Schneider-Schaulies, “Measles virus-induced immunosuppression: From effectors to mechanisms,” *Medical Microbiology and Immunology*, vol. 199, no. 3. Med Microbiol Immunol, pp. 227–237, Aug-2010.

[35] L. A. J. O’Neill, R. J. Kishton, and J. Rathmell, “A guide to immunometabolism for immunologists,” *Nature Reviews Immunology*, vol. 16, no. 9. Nature Publishing Group, pp. 553–565, 25-Aug-2016.

[36] K. Murphy and C. Weaver, *Janeway’s Immunobiology*. W.W. Norton, 2016.

[37] R. M. Loftus and D. K. Finlay, “Immunometabolism: Cellular metabolism turns immune regulator,” *Journal of Biological Chemistry*, vol. 291, no. 1. American Society for Biochemistry and Molecular Biology Inc., pp. 1–10, 01-Jan-2016.

[38] M. O. Johnson, P. J. Siska, D. C. Contreras, and J. C. Rathmell, “Nutrients and the microenvironment to feed a T cell army,” *Seminars in Immunology*, vol. 28, no. 5. Academic Press, pp. 505–513, 01-Oct-2016.

[39] B. V. Park and F. Pan, “Metabolic regulation of T cell differentiation and function,” *Mol. Immunol.*, vol. 68, no. 2, pp. 497–506, Dec. 2015.

[40] N. D. L *et al.*, *Lehninger Principles of Biochemistry*. W. H. Freeman, 2005.

[41] G. R. Bantug, L. Galluzzi, G. Kroemer, and C. Hess, “The spectrum of T cell metabolism in health and disease,” *Nature Reviews Immunology*, vol. 18, no. 1. Nature Publishing Group, pp. 19–34, 01-Jan-2018.

[42] H. Hashimoto, O. McCallion, R. W. M. Kempkes, J. Hester, and F. Issa, “Distinct metabolic pathways mediate regulatory T cell differentiation and function,” *Immunology Letters*, vol. 223. Elsevier B.V., pp. 53–61, 01-Jul-2020.

[43] S. Zhang *et al.*, “ Newly Generated CD4 + T Cells Acquire Metabolic Quiescence after Thymic Egress ,” *J. Immunol.*, vol. 200, no. 3, pp. 1064–1077, Feb. 2018.

[44] K. A. Hogquist, Y. Xing, F.-C. Hsu, and V. S. Shapiro, “T Cell Adolescence: Maturation Events Beyond Positive Selection,” *J. Immunol.*, vol. 195, no. 4, pp. 1351–1357, Aug. 2015.

[45] M. GUPPY, E. GREINER, and K. BRAND, “The role of the Crabtree effect and an endogenous fuel in the energy metabolism of resting and proliferating

thymocytes," *Eur. J. Biochem.*, vol. 212, no. 1, pp. 95–99, Feb. 1993.

[46] M. F. Princiotta *et al.*, "Quantitating protein synthesis, degradation, and endogenous antigen processing," *Immunity*, vol. 18, no. 3, pp. 343–354, Mar. 2003.

[47] M. Papatriantafyllou, "T cells: MTOR lullabies for naive T cells," *Nature Reviews Immunology*, vol. 11, no. 9. pp. 572–573, Sep-2011.

[48] D. F. Tough and J. Sprent, "Life span of naive and memory t cells," *Stem Cells*, vol. 13, no. 3, pp. 242–249, 1995.

[49] M. Y. Kimura *et al.*, "IL-7 signaling must be intermittent, not continuous, during CD8 + T cell homeostasis to promote cell survival instead of cell death," *Nat. Immunol.*, vol. 14, no. 2, pp. 143–151, Feb. 2013.

[50] A. Mendoza *et al.*, "Lymphatic endothelial S1P promotes mitochondrial function and survival in naive T cells," *Nature*, vol. 546, no. 7656, pp. 158–161, Jun. 2017.

[51] Y. M. Kerdiles *et al.*, "Foxo1 links homing and survival of naive T cells by regulating L-selectin, CCR7 and interleukin 7 receptor," *Nat. Immunol.*, vol. 10, no. 2, pp. 176–184, Jan. 2009.

[52] A. N. Macintyre *et al.*, "The glucose transporter Glut1 is selectively essential for CD4 T cell activation and effector function," *Cell Metab.*, vol. 20, no. 1, pp. 61–72, Jul. 2014.

[53] C. T. Kuo, M. L. Veselits, and J. M. Leiden, "LKLF: A transcriptional regulator of single-positive T cell quiescence and survival," *Science (80-.).*, vol. 277, no. 5334, pp. 1986–1990, Sep. 1997.

[54] J. Wu and J. B. Lingrel, "KLF2 inhibits Jurkat T leukemia cell growth via upregulation of cyclin-dependent kinase inhibitor p21WAF1/CIP1," *Oncogene*, vol. 23, no. 49, pp. 8088–8096, Oct. 2004.

[55] A. F. Buckley, C. T. Kuo, and J. M. Leiden, "Transcription factor LKLF is sufficient to program T cell quiescence via a c-Myc-dependent pathway," *Nat. Immunol.*, vol. 2, no. 8, pp. 698–704, 2001.

[56] R. E. Haaland, W. Yu, and A. P. Rice, "Identification of LKLF-regulated genes in quiescent CD4 + T lymphocytes," *Mol. Immunol.*, vol. 42, no. 5, pp. 627–641, Mar. 2005.

[57] K. Yang, G. Neale, D. R. Green, W. He, and H. Chi, "The tumor suppressor Tsc1 enforces quiescence of naive T cells to promote immune homeostasis and function," *Nat. Immunol.*, vol. 12, no. 9, pp. 888–897, Sep. 2011.

[58] K. N. Pollizzi *et al.*, “mTORC1 and mTORC2 selectively regulate CD8^{+} T cell differentiation,” *J. Clin. Invest.*, vol. 125, no. 5, pp. 2090–2108, May 2015.

[59] T. F. O’Brien *et al.*, “Regulation of T-cell survival and mitochondrial homeostasis by TSC1,” *Eur. J. Immunol.*, vol. 41, no. 11, pp. 3361–3370, Nov. 2011.

[60] N. M. Chapman, M. R. Boothby, and H. Chi, “Metabolic coordination of T cell quiescence and activation,” *Nat. Rev. Immunol.*, vol. 20, no. January, 2020.

[61] H. Chen, T. Yang, L. Zhu, and Y. Zhao, “Cellular metabolism on T-cell development and function.,” *Int. Rev. Immunol.*, vol. 34, no. 1, pp. 19–33, Jan. 2015.

[62] S. Jiang and C. Dong, “A complex issue on CD4 $^{+}$ T-cell subsets,” *Immunol. Rev.*, vol. 252, no. 1, pp. 5–11, Mar. 2013.

[63] G. J. W. van der Windt and E. L. Pearce, “Metabolic switching and fuel choice during T-cell differentiation and memory development,” *Immunol. Rev.*, vol. 249, no. 1, pp. 27–42, Sep. 2012.

[64] Z. Chen, H. Zhang, W. Lu, and P. Huang, “Role of mitochondria-associated hexokinase II in cancer cell death induced by 3-bromopyruvate,” *Biochim. Biophys. Acta - Bioenerg.*, vol. 1787, no. 5, pp. 553–560, May 2009.

[65] S. Weinhouse, O. Warburg, D. Burk, and A. L. Schade, “On respiratory impairment in cancer cells,” *Science (80-.).*, vol. 124, no. 3215, pp. 267–272, 1956.

[66] E. F. Greiner, M. Guppy, and K. Brand, “Glucose is essential for proliferation and the glycolytic enzyme induction that provokes a transition to glycolytic energy production,” *J. Biol. Chem.*, vol. 269, no. 50, pp. 31484–31490, 1994.

[67] A. T. Waickman and J. D. Powell, “mTOR, metabolism, and the regulation of T-cell differentiation and function,” *Immunol. Rev.*, vol. 249, no. 1, pp. 43–58, Sep. 2012.

[68] C. M. Cham, G. Driessens, J. P. O’Keefe, and T. F. Gajewski, “Glucose deprivation inhibits multiple key gene expression events and effector functions in CD8+ T cells,” *Eur. J. Immunol.*, vol. 38, no. 9, pp. 2438–2450, Sep. 2008.

[69] Y. Cao, J. C. Rathmell, and A. N. Macintyre, “Metabolic reprogramming towards aerobic glycolysis correlates with greater proliferative ability and resistance to metabolic inhibition in CD8 versus CD4 T cells,” *PLoS One*, vol. 9, no. 8, Aug. 2014.

[70] M. Yano *et al.*, “Mitochondrial Dysfunction and Increased Reactive Oxygen

Species Impair Insulin Secretion in Sphingomyelin Synthase 1-null Mice," *J. Biol. Chem.*, vol. 286, no. 5, pp. 3992–4002, Feb. 2011.

[71] K. A. Frauwirth and C. B. Thompson, "Regulation of T Lymphocyte Metabolism," *J. Immunol.*, vol. 172, no. 8, pp. 4661–4665, Apr. 2004.

[72] K. A. Frauwirth and C. B. Thompson, "Activation and inhibition of lymphocytes by costimulation," *J. Clin. Invest.*, vol. 109, no. 3, pp. 295–299, Feb. 2002.

[73] R. J. Salmond, "mTOR regulation of glycolytic metabolism in T cells," *Frontiers in Cell and Developmental Biology*, vol. 6, no. SEP. Frontiers Media S.A., 25-Sep-2018.

[74] E. A. Greenfield, K. A. Nguyen, and V. K. Kuchroo, "CD28/B7 costimulation: A review," *Critical Reviews in Immunology*, vol. 18, no. 5. Begell House Inc., pp. 389–418, 1998.

[75] K. A. Frauwirth *et al.*, "The CD28 signaling pathway regulates glucose metabolism," *Immunity*, vol. 16, no. 6, pp. 769–777, 2002.

[76] S. R. Jacobs *et al.*, "Glucose Uptake Is Limiting in T Cell Activation and Requires CD28-Mediated Akt-Dependent and Independent Pathways," *J. Immunol.*, vol. 180, no. 7, pp. 4476–4486, Apr. 2008.

[77] N. Majewski *et al.*, "Hexokinase-mitochondria interaction mediated by Akt is required to inhibit apoptosis in the presence or absence of Bax and Bak," *Mol. Cell*, vol. 16, no. 5, pp. 819–830, Dec. 2004.

[78] K. Gottlob, N. Majewski, S. Kennedy, E. Kandel, R. B. Robey, and N. Hay, "Inhibition of early apoptotic events by Akt/PKB is dependent on the first committed step of glycolysis and mitochondrial hexokinase," *Genes Dev.*, vol. 15, no. 11, pp. 1406–1418, 2001.

[79] J. D. Powell, K. N. Pollizzi, E. B. Heikamp, and M. R. Horton, "Regulation of Immune Responses by mTOR," *Annu. Rev. Immunol.*, vol. 30, no. 1, pp. 39–68, Apr. 2012.

[80] M. Laplante and D. M. Sabatini, "MTOR signaling in growth control and disease," *Cell*, vol. 149, no. 2. Cell, pp. 274–293, 13-Apr-2012.

[81] L. V. Sinclair, J. Rolf, E. Emslie, Y. B. Shi, P. M. Taylor, and D. A. Cantrell, "Control of amino-acid transport by antigen receptors coordinates the metabolic reprogramming essential for T cell differentiation," *Nat. Immunol.*, vol. 14, no. 5, pp. 500–508, May 2013.

[82] K. N. Pollizzi *et al.*, "Asymmetric inheritance of mTORC1 kinase activity during

division dictates CD8+ T cell differentiation," *Nat. Immunol.*, vol. 17, no. 6, pp. 704–711, May 2016.

[83] K. Inoki, T. Zhu, and K. L. Guan, "TSC2 Mediates Cellular Energy Response to Control Cell Growth and Survival," *Cell*, vol. 115, no. 5, pp. 577–590, Nov. 2003.

[84] D. G. Hardie, F. A. Ross, and S. A. Hawley, "AMPK: A nutrient and energy sensor that maintains energy homeostasis," *Nature Reviews Molecular Cell Biology*, vol. 13, no. 4. Nat Rev Mol Cell Biol, pp. 251–262, Apr-2012.

[85] A. Mayer, S. Denanglaire, B. Viollet, O. Leo, and F. Andris, "AMP-activated protein kinase regulates lymphocyte responses to metabolic stress but is largely dispensable for immune cell development and function," *Eur. J. Immunol.*, vol. 38, no. 4, pp. 948–956, Apr. 2008.

[86] Y. Kim, Q. Lin, P. Glazer, and Z. Yun, "Hypoxic Tumor Microenvironment and Cancer Cell Differentiation," *Curr. Mol. Med.*, vol. 9, no. 4, pp. 425–434, Apr. 2009.

[87] Q. Lin and Z. Yun, "Impact of the hypoxic tumor microenvironment on the regulation of cancer stem cell characteristics," *Cancer Biology and Therapy*, vol. 9, no. 12. pp. 949–956, 15-Jun-2010.

[88] M. Linke, S. D. Fritsch, N. Sukhbaatar, M. Hengstschläger, and T. Weichhart, "mTORC1 and mTORC2 as regulators of cell metabolism in immunity," *FEBS Lett.*, vol. 591, no. 19, pp. 3089–3103, Oct. 2017.

[89] B. Alberts, "Molecular biology of the cell," 2018.

[90] D. B. Zorov, M. Juhaszova, and S. J. Sollott, "Mitochondrial reactive oxygen species (ROS) and ROS-induced ROS release," *Physiological Reviews*, vol. 94, no. 3. American Physiological Society, pp. 909–950, 01-Jul-2014.

[91] T. Pathak and M. Trebak, "Mitochondrial Ca2+ signaling," *Pharmacology and Therapeutics*, vol. 192. Elsevier Inc., pp. 112–123, 01-Dec-2018.

[92] B. T. Paul, D. H. Manz, F. M. Torti, and S. V. Torti, "Mitochondria and Iron: current questions," *Expert Review of Hematology*, vol. 10, no. 1. Taylor and Francis Ltd, pp. 65–79, 02-Jan-2017.

[93] N. Ishihara, Y. Eura, and K. Mihara, "Mitofusin 1 and 2 play distinct roles in mitochondrial fusion reactions via GTPase activity," *J. Cell Sci.*, vol. 117, no. 26, pp. 6535–6546, Dec. 2004.

[94] A. Santel, S. Frank, B. Gaume, M. Herrler, R. J. Youle, and M. T. Fuller, "Mitofusin-1 protein is a generally expressed mediator of mitochondrial fusion in

mammalian cells.,” *J. Cell Sci.*, vol. 116, no. Pt 13, pp. 2763–74, Jul. 2003.

[95] J. M. Adams and S. Cory, “The Bcl-2 apoptotic switch in cancer development and therapy,” *Oncogene*, vol. 26, no. 9. pp. 1324–1337, 26-Feb-2007.

[96] R. B. Seth, L. Sun, C. K. Ea, and Z. J. Chen, “Identification and characterization of MAVS, a mitochondrial antiviral signaling protein that activates NF-κB and IRF3,” *Cell*, vol. 122, no. 5, pp. 669–682, Sep. 2005.

[97] V. De Pinto, R. Benz, C. Caggese, and F. Palmieri, “Characterization of the mitochondrial porin from Drosophila melanogaster,” *BBA - Biomembr.*, vol. 987, no. 1, pp. 1–7, Dec. 1989.

[98] M. Colombini, “VDAC structure, selectivity, and dynamics,” *Biochimica et Biophysica Acta - Biomembranes*, vol. 1818, no. 6. Biochim Biophys Acta, pp. 1457–1465, Jun-2012.

[99] I. O. Mazunin, S. A. Levitskii, M. V. Patrushev, and P. A. Kamenski, “Mitochondrial matrix processes,” *Biochemistry (Moscow)*, vol. 80, no. 11. Maik Nauka Publishing / Springer SBM, pp. 1418–1428, 01-Nov-2015.

[100] K. E. Wellen and C. B. Thompson, “A two-way street: Reciprocal regulation of metabolism and signalling,” *Nature Reviews Molecular Cell Biology*, vol. 13, no. 4. Nat Rev Mol Cell Biol, pp. 270–276, Apr-2012.

[101] I. Martínez-Reyes and N. S. Chandel, “Mitochondrial TCA cycle metabolites control physiology and disease,” *Nature Communications*, vol. 11, no. 1. Nature Research, pp. 1–11, 01-Dec-2020.

[102] V. Eisner, M. Picard, and G. Hajnóczky, “Mitochondrial dynamics in adaptive and maladaptive cellular stress responses,” *Nature Cell Biology*, vol. 20, no. 7. Nature Publishing Group, pp. 755–765, 01-Jul-2018.

[103] L. Tilokani, S. Nagashima, V. Paupe, and J. Prudent, “Mitochondrial dynamics: Overview of molecular mechanisms,” *Essays in Biochemistry*, vol. 62, no. 3. Portland Press Ltd, pp. 341–360, 20-Jul-2018.

[104] K. Zhang, H. Li, and Z. Song, “Membrane depolarization activates the mitochondrial protease OMA1 by stimulating self-cleavage,” *EMBO Rep.*, vol. 15, no. 5, pp. 576–585, 2014.

[105] K. Trudeau, A. J. A. Molina, and S. Roy, “High glucose induces mitochondrial morphology and metabolic changes in retinal pericytes,” *Investig. Ophthalmol. Vis. Sci.*, vol. 52, no. 12, pp. 8657–8664, Nov. 2011.

[106] D. C. Chan, “Mitochondrial Fusion and Fission in Mammals,” *Annu. Rev. Cell*

Dev. Biol., vol. 22, no. 1, pp. 79–99, Nov. 2006.

[107] M. D. D. Buck *et al.*, “Mitochondrial Dynamics Controls T Cell Fate through Metabolic Programming,” *Cell*, vol. 166, no. 1, pp. 63–76, Jun. 2016.

[108] G. W. Dorn, “Evolving Concepts of Mitochondrial Dynamics,” *Annu. Rev. Physiol.*, vol. 81, no. 1, pp. 1–17, Feb. 2019.

[109] A. Y. Seo, A. M. Joseph, D. Dutta, J. C. Y. Hwang, J. P. Aris, and C. Leeuwenburgh, “New insights into the role of mitochondria in aging: Mitochondrial dynamics and more,” *Journal of Cell Science*, vol. 123, no. 15. The Company of Biologists Ltd, pp. 2533–2542, 01-Aug-2010.

[110] T. K. Rostovtseva, A. Komarov, S. M. Bezrukov, and M. Colombini, “VDAC channels differentiate between natural metabolites and synthetic molecules.,” *J. Membr. Biol.*, vol. 187, no. 2, pp. 147–56, May 2002.

[111] T. K. Rostovtseva and S. M. Bezrukov, “ATP transport through a single mitochondrial channel, VDAC, studied by current fluctuation analysis.,” *Biophys. J.*, vol. 74, no. 5, pp. 2365–73, May 1998.

[112] G. Báthori, M. Sahin-Tóth, A. Fonyó, and E. Ligeti, “Transport properties and inhibitor sensitivity of isolated and reconstituted porin differ from those of intact mitochondria,” *BBA - Biomembr.*, vol. 1145, no. 1, pp. 168–176, Jan. 1993.

[113] T. K. Rostovtseva and S. M. Bezrukov, “ATP transport through a single mitochondrial channel, VDAC, studied by current fluctuation analysis,” *Biophys. J.*, vol. 74, no. 5, pp. 2365–2373, 1998.

[114] S. Abu-Hamad, H. Zaid, A. Israelson, E. Nahon, and V. Shoshan-Barmatz, “Hexokinase-I protection against apoptotic cell death is mediated via interaction with the voltage-dependent anion channel-1: Mapping the site of binding,” *J. Biol. Chem.*, vol. 283, no. 19, pp. 13482–13490, May 2008.

[115] T. K. Rostovtseva *et al.*, “Tubulin binding blocks mitochondrial voltage-dependent anion channel and regulates respiration,” *Proc. Natl. Acad. Sci. U. S. A.*, vol. 105, no. 48, pp. 18746–18751, Dec. 2008.

[116] E. N. Maldonado, J. Patnaik, M. R. Mullins, and J. J. Lemasters, “Free tubulin modulates mitochondrial membrane potential in cancer cells,” *Cancer Res.*, vol. 70, no. 24, pp. 10192–10201, Dec. 2010.

[117] M. Carré *et al.*, “Tubulin is an inherent component of mitochondrial membranes that interacts with the voltage-dependent anion channel,” *J. Biol. Chem.*, vol. 277, no. 37, pp. 33664–33669, Sep. 2002.

[118] K. K. Arora and P. L. Pedersen, “Functional significance of mitochondrial bound hexokinase in tumor cell metabolism. Evidence for preferential phosphorylation of glucose by intramitochondrially generated ATP.,” *J. Biol. Chem.*, vol. 263, no. 33, pp. 17422–17428, Nov. 1988.

[119] M. G. Vander Heiden, N. S. Chandel, X. X. Li, P. T. Schumacker, M. Colombini, and C. B. Thompson, “Outer mitochondrial membrane permeability can regulate coupled respiration and cell survival,” *Proc. Natl. Acad. Sci. U. S. A.*, vol. 97, no. 9, pp. 4666–4671, Apr. 2000.

[120] I. Ramírez-Camacho *et al.*, “Role of sphingomyelinase in mitochondrial ceramide accumulation during reperfusion,” *Biochim. Biophys. Acta - Mol. Basis Dis.*, vol. 1862, no. 10, pp. 1955–1963, Oct. 2016.

[121] M. K. Verma *et al.*, “Inhibition of neutral sphingomyelinases in skeletal muscle attenuates fatty-acid induced defects in metabolism and stress,” *Springerplus*, vol. 3, no. 1, pp. 1–12, 2014.

[122] J. N. Kong *et al.*, “Novel function of ceramide for regulation of mitochondrial ATP release in astrocytes,” *J. Lipid Res.*, vol. 59, no. 3, pp. 488–506, 2018.

[123] A. Bai, E. Kokkotou, Y. Zheng, and S. C. Robson, “Role of acid sphingomyelinase bioactivity in human CD4+ T-cell activation and immune responses,” *Cell Death Dis.*, vol. 6, no. 7, Jul. 2015.

[124] L. Collenburg *et al.*, “The activity of the neutral sphingomyelinase is important in T cell recruitment and directional migration,” *Front. Immunol.*, vol. 8, no. AUG, Aug. 2017.

[125] B. L. Ibey *et al.*, “Plasma membrane permeabilization by trains of ultrashort electric pulses,” *Bioelectrochemistry*, vol. 79, no. 1, pp. 114–121, Aug. 2010.

[126] Q. Zheng and D. C. Chang, “High-efficiency gene transfection by in situ electroporation of cultured cells,” *BBA - Gene Struct. Expr.*, vol. 1088, no. 1, pp. 104–110, Jan. 1991.

[127] O. N. Pakhomova, B. W. Gregory, V. A. Khorokhorina, A. M. Bowman, S. Xiao, and A. G. Pakhomov, “Electroporation-induced electrosensitization,” *PLoS One*, vol. 6, no. 2, 2011.

[128] A. G. Pakhomov *et al.*, “Membrane permeabilization and cell damage by ultrashort electric field shocks,” *Arch. Biochem. Biophys.*, vol. 465, no. 1, pp. 109–118, Sep. 2007.

[129] M. Stacey *et al.*, “Differential effects in cells exposed to ultra-short, high intensity

electric fields: Cell survival, DNA damage, and cell cycle analysis," *Mutat. Res. - Genet. Toxicol. Environ. Mutagen.*, vol. 542, no. 1–2, pp. 65–75, Dec. 2003.

[130] A. J. Valente, L. A. Maddalena, E. L. Robb, F. Moradi, and J. A. Stuart, "A simple ImageJ macro tool for analyzing mitochondrial network morphology in mammalian cell culture," *Acta Histochem.*, vol. 119, no. 3, pp. 315–326, Apr. 2017.

[131] Y. Osipchuk and M. Cahalan, "Cell-to-cell spread of calcium signals mediated by ATP receptors in mast cells," *Nature*, vol. 359, no. 6392, pp. 241–244, 1992.

[132] G. Kroemer, L. Galluzzi, and C. Brenner, "Mitochondrial membrane permeabilization in cell death," *Physiological Reviews*, vol. 87, no. 1. pp. 99–163, Jan-2007.

[133] J. C. Rathmell, M. G. V. Heiden, M. H. Harris, K. A. Frauwirth, and C. B. Thompson, "In the absence of extrinsic signals, nutrient utilization by lymphocytes is insufficient to maintain either cell size or viability," *Mol. Cell*, vol. 6, no. 3, pp. 683–692, Sep. 2000.

[134] M. G. Moisescu, M. Radu, E. Kovacs, L. M. Mir, and T. Savopol, "Changes of cell electrical parameters induced by electroporation. A dielectrophoresis study," *Biochim. Biophys. Acta - Biomembr.*, vol. 1828, no. 2, pp. 365–372, Feb. 2013.

[135] A. V. Menk *et al.*, "Early TCR Signaling Induces Rapid Aerobic Glycolysis Enabling Distinct Acute T Cell Effector Functions," *Cell Rep.*, vol. 22, no. 6, pp. 1509–1521, Feb. 2018.

[136] C. H. Chang *et al.*, "Posttranscriptional control of T cell effector function by aerobic glycolysis," *Cell*, vol. 153, no. 6, p. 1239, Jun. 2013.

[137] G. Soto-Heredero, M. M. Gómez de las Heras, E. Gabandé-Rodríguez, J. Oller, and M. Mittelbrunn, "Glycolysis – a key player in the inflammatory response," *FEBS Journal*. Blackwell Publishing Ltd, 2020.

[138] L. Tonnetti, M. C. Verí, E. Bonvini, and L. D'Adamio, "A role for neutral sphingomyelinase-mediated ceramide production in T cell receptor-induced apoptosis and mitogen-activated protein kinase-mediated signal transduction," *J. Exp. Med.*, vol. 189, no. 10, pp. 1581–1589, May 1999.

[139] L. Collenburg, S. Schneider-Schaulies, and E. Avota, "The neutral sphingomyelinase 2 in T cell receptor signaling and polarity.," *Biol. Chem.*, vol. 399, no. 10, pp. 1147–1155, Sep. 2018.

[140] R. J. Deberardinis and N. S. Chandel, "We need to talk about the Warburg

effect,” *Nat. Metab.*

[141] J. B. Imboden, A. Weiss, and J. D. Stobo, “The antigen receptor on a human T cell line initiates activation by increasing cytoplasmic free calcium.,” *J. Immunol.*, vol. 134, no. 2, pp. 663–5, Feb. 1985.

[142] R. Chakrabarti, C. Y. Jung, T. P. Lee, H. Liu, and B. K. Mookerjee, “Changes in glucose transport and transporter isoforms during the activation of human peripheral blood lymphocytes by phytohemagglutinin.,” *J. Immunol.*, vol. 152, no. 6, pp. 2660–8, Mar. 1994.

[143] R. A. Gatenby and R. J. Gillies, “Why do cancers have high aerobic glycolysis?,” *Nature Reviews Cancer*, vol. 4, no. 11. Nat Rev Cancer, pp. 891–899, Nov-2004.

[144] K. S. Hamilton *et al.*, “T cell receptor-dependent activation of mTOR signaling in T cells is mediated by Carma1 and MALT1, but not Bcl10,” *Sci. Transl. Med.*, vol. 7, no. 329, Jun. 2014.

[145] S. Colombetti, V. Basso, D. L. Mueller, and A. Mondino, “Prolonged TCR/CD28 Engagement Drives IL-2-Independent T Cell Clonal Expansion through Signaling Mediated by the Mammalian Target of Rapamycin,” *J. Immunol.*, vol. 176, no. 5, pp. 2730–2738, 2006.

[146] A. T. Waickman and J. D. Powell, “Mammalian Target of Rapamycin Integrates Diverse Inputs To Guide the Outcome of Antigen Recognition in T Cells,” *J. Immunol.*, vol. 188, no. 10, pp. 4721–4729, 2012.

[147] H. Pelicano *et al.*, “Mitochondrial dysfunction in some triple-negative breast cancer cell lines: Role of mTOR pathway and therapeutic potential,” *Breast Cancer Res.*, vol. 16, no. 5, Sep. 2014.

[148] K. Yang *et al.*, “T Cell Exit from Quiescence and Differentiation into Th2 Cells Depend on Raptor-mTORC1-Mediated Metabolic Reprogramming,” *Immunity*, vol. 39, no. 6, pp. 1043–1056, Dec. 2013.

[149] L. Pangrazzi and B. Weinberger, “T cells, aging and senescence,” *Experimental Gerontology*, vol. 134. Elsevier Inc., p. 110887, 01-Jun-2020.

[150] Q. Jin, L. Agrawal, Z. VanHorn-Ali, and G. Alkhatib, “Infection of CD4+ T lymphocytes by the human T cell leukemia virus type 1 is mediated by the glucose transporter GLUT-1: Evidence using antibodies specific to the receptor’s large extracellular domain,” *Virology*, vol. 349, no. 1, pp. 184–196, May 2006.

[151] M. B. Mockler, M. J. Conroy, and J. Lysaght, “Targeting T cell immunometabolism for cancer immunotherapy; understanding the impact of the

tumor microenvironment," *Frontiers in Oncology*, vol. 4 MAY. Frontiers Research Foundation, 2014.

[152] G. A. Patwardhan, L. J. Beverly, and L. J. Siskind, "Sphingolipids and mitochondrial apoptosis," *J. Bioenerg. Biomembr.*, vol. 48, no. 2, pp. 153–168, Apr. 2016.

[153] S. Dadsena *et al.*, "Ceramides bind VDAC2 to trigger mitochondrial apoptosis," *Nat. Commun.*, vol. 10, no. 1, Dec. 2019.

[154] M. Colombini, "VDAC: The channel at the interface between mitochondria and the cytosol," *Molecular and Cellular Biochemistry*, vol. 256–257, no. 1–2. Mol Cell Biochem, pp. 107–115, Jan-2004.

[155] E. N. Maldonado, J. Patnaik, M. R. Mullins, and J. J. Lemasters, "Free tubulin modulates mitochondrial membrane potential in cancer cells," *Cancer Res.*, vol. 70, no. 24, pp. 10192–10201, Dec. 2010.

[156] J. N. Kong *et al.*, "Novel function of ceramide for regulation of mitochondrial ATP release in astrocytes," *J. Lipid Res.*, vol. 59, no. 3, pp. 488–506, 2018.

[157] E. Avota, M. N. de Lira, and S. Schneider-Schaulies, "Sphingomyelin Breakdown in T Cells: Role of Membrane Compartmentalization in T Cell Signaling and Interference by a Pathogen.," *Front. cell Dev. Biol.*, vol. 7, no. JULY, p. 152, 2019.

[158] L. A. Shchepina *et al.*, "Oligomycin, inhibitor of the F0 part of H+-ATP-synthase, suppresses the TNF-induced apoptosis," *Oncogene*, vol. 21, no. 53, pp. 8149–8157, Nov. 2002.

[159] J. LASZLO, B. LANDAU, K. WIGHT, and D. BURK, "The effect of glucose analogues on the metabolism of human leukemic cells.," *J. Natl. Cancer Inst.*, vol. 21, no. 3, pp. 475–483, Sep. 1958.

[160] J. LASZLO, S. R. HUMPHREYS, and A. GOLDIN, "Effects of glucose analogues (2-deoxy-D-glucose, 2-deoxy-D-galactose) on experimental tumors.," *J. Natl. Cancer Inst.*, vol. 24, pp. 267–281, Feb. 1960.

[161] W. D. Schwenke, S. Soboll, H. J. Seitz, and H. Sies, "Mitochondrial and cytosolic ATP/ADP ratios in rat liver in vivo.," *Biochem. J.*, vol. 200, no. 2, pp. 405–408, 1981.

[162] L. Speizer, R. Haugland, and H. Kutchai, "Asymmetric transport of a fluorescent glucose analogue by human erythrocytes," *BBA - Biomembr.*, vol. 815, no. 1, pp. 75–84, Apr. 1985.

[163] H. L. Wieman, J. A. Wofford, and J. C. Rathmell, “Cytokine stimulation promotes glucose uptake via phosphatidylinositol-3 kinase/Akt regulation of Glut1 activity and trafficking,” *Mol. Biol. Cell*, vol. 18, no. 4, pp. 1437–1446, Apr. 2007.

[164] J. A. Wofford, H. L. Wieman, S. R. Jacobs, Y. Zhao, and J. C. Rathmell, “IL-7 promotes Glut1 trafficking and glucose uptake via STAT5-mediated activation of Akt to support T-cell survival,” *Blood*, vol. 111, no. 4, pp. 2101–2111, Feb. 2008.

[165] R. C. Piper, L. J. Hess, and D. E. James, “Differential sorting of two glucose transporters expressed in insulin-sensitive cells,” *Am. J. Physiol. - Cell Physiol.*, vol. 260, no. 3 29-3, 1991.

[166] D. B. Kell, “Metabolomics and systems biology: Making sense of the soup,” *Current Opinion in Microbiology*, vol. 7, no. 3. Elsevier Current Trends, pp. 296–307, 01-Jun-2004.

[167] D. A. Ferrick, A. Neilson, and C. Beeson, “Advances in measuring cellular bioenergetics using extracellular flux,” *Drug Discovery Today*, vol. 13, no. 5–6. Elsevier Current Trends, pp. 268–274, 01-Mar-2008.

[168] D. C. Bradley and H. R. Kaslow, “Radiometric assays for glycerol, glucose, and glycogen,” *Anal. Biochem.*, vol. 180, no. 1, pp. 11–16, 1989.

[169] G. J. W. van der Windt, C. H. Chang, and E. L. Pearce, “Measuring bioenergetics in T cells using a seahorse extracellular flux analyzer,” *Curr. Protoc. Immunol.*, vol. 2016, pp. 3.16B.1-3.16B.14, 2016.

[170] M. D. Buck, D. O’Sullivan, and E. L. Pearce, “T cell metabolism drives immunity,” *J. Exp. Med.*, vol. 212, no. 9, pp. 1345–1360, 2015.

[171] E. L. Pearce and E. J. Pearce, “Metabolic pathways in immune cell activation and quiescence,” *Immunity*, vol. 38, no. 4. NIH Public Access, pp. 633–643, 18-Apr-2013.

[172] V. A. Gerriets *et al.*, “Metabolic programming and PDHK1 control CD4+ T cell subsets and inflammation,” *J. Clin. Invest.*, vol. 125, no. 1, pp. 194–207, Jan. 2015.

[173] K. S. McCommis and B. N. Finck, “Mitochondrial pyruvate transport: A historical perspective and future research directions,” *Biochemical Journal*, vol. 466, no. 3. Portland Press Ltd, pp. 443–454, 15-Mar-2015.

[174] N. M. Chapman and H. Chi, “Hallmarks of t-cell exit from quiescence,” *Cancer Immunol. Res.*, vol. 6, no. 5, pp. 502–508, May 2018.

[175] N. J. MacIver, R. D. Michalek, and J. C. Rathmell, “Metabolic Regulation of T

Lymphocytes," *Annu. Rev. Immunol.*, vol. 31, no. 1, pp. 259–283, Mar. 2013.

[176] L. A. Sena *et al.*, "Mitochondria Are Required for Antigen-Specific T Cell Activation through Reactive Oxygen Species Signaling," *Immunity*, vol. 38, no. 2, pp. 225–236, Feb. 2013.

[177] C. H. Patel and J. D. Powell, "Targeting T cell metabolism to regulate T cell activation, differentiation and function in disease," *Current Opinion in Immunology*, vol. 46. Elsevier Ltd, pp. 82–88, 01-Jun-2017.

[178] J. H. Esensten, Y. A. Helou, G. Chopra, A. Weiss, and J. A. Bluestone, "CD28 Costimulation: From Mechanism to Therapy," *Immunity*, vol. 44, no. 5. Cell Press, pp. 973–988, 17-May-2016.

[179] Q. Wu *et al.*, "The Tuberous Sclerosis Complex–Mammalian Target of Rapamycin Pathway Maintains the Quiescence and Survival of Naive T Cells," *J. Immunol.*, vol. 187, no. 3, pp. 1106–1112, 2011.

[180] A. Kogot-Levin and A. Saada, "Ceramide and the mitochondrial respiratory chain," *Biochimie*, vol. 100, no. 1. Elsevier, pp. 88–94, 01-May-2014.

[181] A. M. Campbell and S. H. P. Chan, "Mitochondrial membrane cholesterol, the voltage dependent anion channel (VDAC), and the Warburg effect," *J. Bioenerg. Biomembr.*, vol. 40, no. 3, pp. 193–197, Jun. 2008.

[182] K. Takase and T. Saito, "T cell activation," in *Ryumachi*, 1995, vol. 35, no. 5, pp. 853–861.

[183] K. Man and A. Kallies, "Synchronizing transcriptional control of T cell metabolism and function," *Nature Reviews Immunology*, vol. 15, no. 9. Nature Publishing Group, pp. 574–584, 25-Sep-2015.

[184] L. Araujo, P. Khim, H. Mkhikian, C. L. Mortales, and M. Demetriou, "Glycolysis and glutaminolysis cooperatively control T cell function by limiting metabolite supply to N-glycosylation," *Elife*, vol. 6, Jan. 2017.

[185] R. D. Michalek *et al.*, " Cutting Edge: Distinct Glycolytic and Lipid Oxidative Metabolic Programs Are Essential for Effector and Regulatory CD4 + T Cell Subsets ," *J. Immunol.*, vol. 186, no. 6, pp. 3299–3303, Mar. 2011.

[186] T. Wang, C. Marquardt, and J. Foker, "Aerobic glycolysis during lymphocyte proliferation," *Nature*, vol. 261, no. 5562, pp. 702–705, 1976.

[187] C. S. Palmer *et al.*, "Regulators of Glucose Metabolism in CD4+ and CD8+ T Cells," *International Reviews of Immunology*, vol. 35, no. 6. Taylor and Francis Ltd, pp. 477–488, 01-Nov-2016.

[188] M. K. Williamson *et al.*, “Upregulation of glucose uptake and hexokinase activity of primary human CD4+ T cells in response to infection with HIV-1,” *Viruses*, vol. 10, no. 3, Mar. 2018.

[189] C. Cammann *et al.*, “Early changes in the metabolic profile of activated CD8+ T cells,” *BMC Cell Biol.*, vol. 17, no. 1, p. 28, Dec. 2016.

[190] K. Araki *et al.*, “mTOR regulates memory CD8 T-cell differentiation,” *Nature*, vol. 460, no. 7251, pp. 108–112, Jul. 2009.

[191] A. Perl, “MTOR activation is a biomarker and a central pathway to autoimmune disorders, cancer, obesity, and aging,” *Ann. N. Y. Acad. Sci.*, vol. 1346, no. 1, pp. 33–44, 2015.

[192] R. J. Salmond and R. Zamoyska, “How does the mammalian target of rapamycin (mTOR) influence CD8 T cell differentiation?,” *Cell Cycle*, vol. 9, no. 15. Taylor and Francis Inc., pp. 3024–3029, 01-Aug-2010.

[193] K. Araki and R. Ahmed, “AMPK: a metabolic switch for CD8+ T-cell memory.,” *Eur. J. Immunol.*, vol. 43, no. 4, pp. 878–81, Apr. 2013.

[194] J. Rolf, M. Zarrouk, D. K. Finlay, M. Foretz, B. Viollet, and D. A. Cantrell, “AMPKα1: A glucose sensor that controls CD8 T-cell memory,” *Eur. J. Immunol.*, vol. 43, no. 4, pp. 889–896, Apr. 2013.

[195] G. H. Cornish, L. V. Sinclair, and D. A. Cantrell, “Differential regulation of T-cell growth by IL-2 and IL-15,” *Blood*, vol. 108, no. 2, pp. 600–608, Jul. 2006.

[196] J. P. Ray *et al.*, “The Interleukin-2-mTORc1 Kinase Axis Defines the Signaling, Differentiation, and Metabolism of T Helper 1 and Follicular B Helper T Cells,” *Immunity*, vol. 43, no. 4, pp. 690–702, Oct. 2015.

[197] L. Z. Shi *et al.*, “HIF1α-dependent glycolytic pathway orchestrates a metabolic checkpoint for the differentiation of TH17 and Treg cells,” *J. Exp. Med.*, vol. 208, no. 7, pp. 1367–1376, Jul. 2011.

[198] S. Shrestha, K. Yang, J. Wei, P. W. F. Karmaus, G. Neale, and H. Chi, “Tsc1 promotes the differentiation of memory CD8+T cells via orchestrating the transcriptional and metabolic programs,” *Proc. Natl. Acad. Sci. U. S. A.*, vol. 111, no. 41, pp. 14858–14863, Oct. 2014.

[199] P. M. Herst, C. Grasso, and M. V. Berridge, “Metabolic reprogramming of mitochondrial respiration in metastatic cancer,” *Cancer Metastasis Rev.*, vol. 37, no. 4, pp. 643–653, Dec. 2018.

[200] M. Leibovitch and I. Topisirovic, “Dysregulation of mRNA translation and energy

metabolism in cancer," *Advances in Biological Regulation*, vol. 67. Elsevier Ltd, pp. 30–39, 01-Jan-2018.

[201] B. N. Desai, B. R. Myers, and S. L. Schreiber, "FKBP12-rapamycin-associated protein associates with mitochondria and senses osmotic stress via mitochondrial dysfunction," *Proc. Natl. Acad. Sci. U. S. A.*, vol. 99, no. 7, pp. 4319–4324, Apr. 2002.

[202] S. M. Schieke *et al.*, "The mammalian target of rapamycin (mTOR) pathway regulates mitochondrial oxygen consumption and oxidative capacity," *J. Biol. Chem.*, vol. 281, no. 37, pp. 27643–27652, Sep. 2006.

[203] "Molecular Biology of the Cell, - Books - NCBI." [Online]. Available: https://www.ncbi.nlm.nih.gov/books/NBK21054/?term=Molecular Biology of the Cell%2C. [Accessed: 01-Jun-2020].

[204] B. Westermann, "Molecular machinery of mitochondrial fusion and fission," *Journal of Biological Chemistry*, vol. 283, no. 20. J Biol Chem, pp. 13501–13505, 16-May-2008.

[205] G. Desdín-Micó, G. Soto-Heredero, and M. Mittelbrunn, "Mitochondrial activity in T cells," *Mitochondrion*, vol. 41. Elsevier B.V., pp. 51–57, 01-Jul-2018.

[206] C. Schwindling, A. Quintana, E. Krause, and M. Hoth, "Mitochondria Positioning Controls Local Calcium Influx in T Cells," *J. Immunol.*, vol. 184, no. 1, pp. 184–190, Jan. 2010.

[207] M. M. Kamiński *et al.*, "Mitochondrial Reactive Oxygen Species Control T Cell Activation by Regulating IL-2 and IL-4 Expression: Mechanism of Ciprofloxacin-Mediated Immunosuppression," *J. Immunol.*, vol. 184, no. 9, pp. 4827–4841, May 2010.

[208] W. G. Junger, "Immune cell regulation by autocrine purinergic signalling," *Nature Reviews Immunology*, vol. 11, no. 3. Nat Rev Immunol, pp. 201–212, Mar-2011.

[209] G. Kaur and J. M. Dufour, "Cell lines," *Spermatogenesis*, vol. 2, no. 1, pp. 1–5, Jan. 2012.

[210] S. M. Schieke, J. P. McCoy, and T. Finkel, "Coordination of mitochondrial bioenergetics with G1 phase cell cycle progression," *Cell Cycle*, vol. 7, no. 12, pp. 1782–1787, Jun. 2008.

[211] C. K. Goo, H. Y. Lim, Q. S. Ho, H. P. Too, M. V. Clement, and K. P. Wong, "PTEN/Akt Signaling Controls Mitochondrial Respiratory Capacity through 4E-BP1," *PLoS One*, vol. 7, no. 9, Sep. 2012.

[212] L. J. Siskind, R. N. Kolesnick, and M. Colombini, “Ceramide channels increase the permeability of the mitochondrial outer membrane to small proteins.,” *J. Biol. Chem.*, vol. 277, no. 30, pp. 26796–803, Jul. 2002.

[213] V. Rajagopalan *et al.*, “Critical determinants of mitochondria-associated neutral sphingomyelinase (MA-nSMase) for mitochondrial localization,” *Biochim. Biophys. Acta - Gen. Subj.*, vol. 1850, no. 4, pp. 628–639, 2015.

[214] J. Yu *et al.*, “JNK3 signaling pathway activates ceramide synthase leading to mitochondrial dysfunction,” *J. Biol. Chem.*, vol. 282, no. 35, pp. 25940–25949, Aug. 2007.

[215] L. Almeida, M. Lochner, L. Berod, and T. Sparwasser, *Metabolic pathways in T cell activation and lineage differentiation*, vol. 28, no. 5. Academic Press, 2016, pp. 514–524.

[216] R. Wang and D. R. Green, “Metabolic checkpoints in activated T cells,” *Nature Immunology*, vol. 13, no. 10. Nat Immunol, pp. 907–915, Oct-2012.

[217] A. Johannisson, A. Thuvander, and I. L. Gadhasson, “Activation markers and cell proliferation as indicators of toxicity: A flow cytometric approach,” *Cell Biol. Toxicol.*, vol. 11, no. 6, pp. 355–366, Dec. 1995.

[218] F. Iannone, V. M. Corrigall, G. H. Kingsley, and G. S. Panayi, “Evidence for the continuous recruitment and activation of T cells into the joints of patients with rheumatoid arthritis.,” *Eur. J. Immunol.*, vol. 24, no. 11, pp. 2706–13, Nov. 1994.

[219] K. E. Pauken and E. J. Wherry, “Overcoming T cell exhaustion in infection and cancer,” *Trends in Immunology*, vol. 36, no. 4. Elsevier Ltd, pp. 265–276, 01-Apr-2015.

[220] A. Bratic and N. G. Larsson, “The role of mitochondria in aging,” *Journal of Clinical Investigation*, vol. 123, no. 3. J Clin Invest, pp. 951–957, 01-Mar-2013.

9. Appendix

List of figures

List of Tables

Abbreviations

Abbreviation	Definition
%	percent
×g	gravitational constant
°C	centigrade
2-DG	2-Deoxyglucose
4E-BPs	translational regulators 4E-binding proteins
AMPK	AMP-activated kinase
APS	ammonium persulfate
ASM	acid sphingomyelinase
ATP	adenosine triphosphate
ATV	antibiotic-Trypsin-Versene
BCL-2	B-cell lymphoma 2
BSA	bovine serum albumin
C1P	ceramide-1-phosphate
CaCl2	calcium chloride
Cas-9	CRISPR associated protein 9
CCR7	CC-chemokine receptor 7
CD	cluster of differentiation
cDNA	complementary DNA
CE	Cholesterol ester
Cer	ceramide
CerS	Ceramide Synthase
CFSE	carboxyfluorescein succinimidyl ester
CO_2	carbon dioxide
CPE	ceramide phosphoethanolamine
CRISPR	clustered regularly interspaced short palindromic repeats

CTRL	Jurkat T cells
$CuSO_4$	Copper Sulphate
DAPI	4',6-Diamidin-2-phenylindol
DEPTOR	DEP domain-containing mTOR-interacting protein
dH_2O	Distilled water
DMEM	Dulbecco's modified Eagle's medium
DMSO	Dimethyl sulfoxide
DNA	Deoxyribonucleic acid
Dr.	doctor
Drp1	dynamin-related protein 1
ECAR	extracellular acidification rate
EDTA	ethylenediaminetetraacetic acid
ER	endoplasmic reticulum
ETC	Electron Transport Chain
FACS	fluorescence-activated cell sorting
FAO	fatty acid oxidation
FCCP	Carbonyl cyanide-4-phenylhydrazone
FCS	fetal calf serum
FITC	fluorescein isothiocyanate
FSC	forward scatter
g	gram
Galβ1–10Cer	galactosylceramide
GAPDH	Glyceraldehyde 3-phosphate dehydrogenase
GFP	green fluorescent protein
GlcCer	glucosylceramide
GLUT	glucose transporter
GSH	glutathione

GTPases	guanosine triphosphatases
h	hour/hours
HEK	human embryonic kidney cell
HEPES	4-(2-hydroxyethyl)-1-piperazineethanesulfonic acid
HK	hexokinase
HMUPC	6-Hexadecanoylamino-4-methylumbelliferylphosphorylcholine
ICAM	intercellular adhesion molecule 1
IF	immunofluorescence
IFN I	interferon type I
Ig	immunoglobulin
IL	interleukin
IMM	inner mitochondrial membrane
KCl	potassium chloride
KD	knockdown
kDa	kilo Dalton
KLF2	Kruppel-like factor 2
LN	lymph node
M	molar
mA	milliampere
MACS	Magnetic-activated cell sorting
MAVS	mitochondrial antiviral signaling protein
MEM	minimal essential media
MFI	mean fluorescence intensity
Mfn-1 and Mfn-2	mitofusin1 and 2
MHC	major histocompatibility complex
MIM	mitochondria isolation media
min	minutes

mito-GFP	mitochondria-targeted GFP protein
MLST8	mammalian lethal with SEC13 protein 8
MPC	mitochondrial pyruvate carrier
mRNA	Messenger ribonucleic acid
mSIN1	mammalian stress-activated protein kinase interacting protein 1
mtDNA	mitochondrial DNA
mTOR	mammalian target of rapamycin
NaCl	sodium chloride
NaOH	sodium hydroxide
NBD	nitro-2-1,3-benzoxadiazol-4-yl
ng	nanogram
NSM	neutral sphingomyelinase
OCR	oxygen consumption rate
OMM	outer mitochondrial membrane
Opa1	optic atrophy 1
OXPHOS	oxidative phosphorylation
p	phosphorylated
PAGE	polyacrylamide gel electrophoresis
PBL	peripheral blood lymphocytes
PBMC	peripheral blood mononuclear cell
PBS	phosphate-buffered saline
PC-3	prostate cancer cell line
PEG	polyethylene glycol
PEI	polyethyleneimine
PFA	paraformaldehyde
PFK-2	phosphorylating phosphofructokinase-2
PI	propidium iodide

PI3	phosphoinositide 3
PI3K	phosphatidylinositol 3’-kinase
PLL	poly-L-lysin
PM	plasma membrane
PMA	phorbol-12-myristat-13-acetate
pmol	picomole
PRAS	proline rich Akt substrate
Prof.	professor
R/A	rotenone/antimycin A
RAPTOR	regulatory-associated protein of mTOR
RICTOR	rapamycin-insensitive companion of mTOR
RNA	ribonucleic acid
ROS	reactive oxygen species
rpm	revolutions per minute
RPMI	Roswell Park Memorial Institute
RT	room temperature
S1PR1	sphingosine-phosphate receptor 1
S6Ks	ribosomal protein S6 kinases
SDS	sodium-dodecylsulfat
siRNA	small interfering RNA
SL	sphingolipid
SM	sphingomyelin
SMase	sphingomyelinase
Sph	sphingosine
SphK	sphingosine kinase
SSC	side scatter
TCA	tricarboxylic acid

TCR	T cell receptor
Teff	T effector
TEMED	tetramethylethylenediamine
Th	T helper
TNF- α	Tumor necrosis factor
Treg	T regulatory
TSC	Tuberous Sclerosis Complex 2
VCAM	vascular cell adhesion molecule 1
VDAC	Voltage-Dependent Anion Channels
ΔNSM	CRISPR/Cas9 NSM KD Jurkat T cells
µg	microgram
µL	microliter
µm	micrometer

Affidavit

I hereby declare that my thesis entitled “The regulation of T cell metabolism by neutral sphingomyelinase 2” is the result of my work. I did not receive any help or support from commercial consultants. All sources and/or materials applied are listed and specified in the thesis.
Furthermore, I verify that this thesis has not yet been submitted as part of another examination process, neither in identical nor similar form.

Würzburg, 2020 _____

Maria Nathalia de Lira

Eidesstattliche Erklärung

Hiermit erkläre ich an Eides statt, die Dissertation „Die Regulation des T-Zell-Metabolismus durch neutrale Sphingomyelinase 2“ eigenständig, d.h. insbesondere selbständig und ohne Hilfe eines kommerziellen Promotionsberaters, angefertigt und keine anderen als die von mir angegebenen Quellen und Hilfsmittel verwendet zu haben.
Ich erkläre außerdem, dass die Dissertation weder in gleicher noch in ähnlicher Form bereits in einem anderen Prüfungsverfahren vorgelegen hat.

Würzburg, 2020 _____

Maria Nathalia de Lira

List of publications

Maria Nathalia De Lira, Sudha Janaki Raman, Almut Schulze, Sibylle Schneider Schaulies, Elita Avota - *Neutral sphingomyelinase-2 (NSM 2) controls T cell metabolic homeostasis and reprogramming during activation* – Frontiers in Molecular Biosciences – 2020

E. Avota, **M. de Lira,** S. Schneider-Schaulies - Sphingomyelin Breakdown in T Cells: Role of Membrane *Compartmentalization in T Cell Signaling and Interference by a Pathogen*. Frontiers in cell and developmental biology – 2019.

Congress participation

FEBS Special Meeting 2019 │ Sphingolipid Biology: Sphingolipids in Physiology and Pathology - *Role of NSM-2 in early and late TCR metabolic signaling and mitochondrial function* – Cascais – Portugal, 2019.

EUREKA! 2018 Symposium - *Role of NSM-2 in early and late TCR metabolic signaling – Würzburg, 2018.*

SphingoFOR 2123 – International Meeting - *Role of NSM-2 in early TCR metabolic signaling – Würzburg, 2017.*